Diagnosing and Treating Infectious Diseases and Antimicrobial Resistance Using Gold Nanoparticles

by

Mohamed Ahmed Abdou Mohamed

A thesis submitted in conformity with the requirements
for the degree of Doctor of Philosophy

Institute of Biomaterials and Biomedical Engineering
University of Toronto

Diagnosing and Treating Infectious Diseases and Antimicrobial Resistance Using Gold Nanoparticles

Mohamed Ahmed Abdou Mohamed

Doctor of Philosophy

Institute of Biomaterials and Biomedical Engineering
University of Toronto

2017

Abstract

The continued emergence of infectious diseases and the development of antimicrobial resistance represent a major global health challenge in the 21st century. Rapid and accurate diagnosis of infectious pathogens is vital for both the treatment and prevention of new forms of antimicrobial resistance. The current advances in nanotechnology have afforded the development of new simple and rapid diagnostic assays as well as novel therapeutic technologies. This thesis presents new and original work that exploits the physical and chemical properties of gold nanoparticles to diagnose and treat infectious diseases. The contributions to the field are two-folds. Earlier work was aimed at developing a rapid, sensitive and simple platform for the detection of infectious diseases and antimicrobial resistance, where signal readout could be observed with the naked eye. Second, the photo-thermal characteristics of gold nanoparticles were used to create a novel plasmonic thermogel that disinfected antimicrobial resistant bacteria in surgical wounds, preventing the use of a broad-spectrum antibiotic. It is anticipated that the contribution of this thesis will continue to advance the implementation of gold nanoparticles for the development of commercial diagnostics and therapeutics. Collectively, this work should improve the mitigation of infectious diseases and reduce the risk of the development of further antimicrobial resistance.

Acknowledgments

First, I would like to express my sincere gratitude and thanks to my supervisor Prof. Warren C. W. Chan for giving me the opportunity to join his lab and conduct my PhD research. I sincerely appreciate his guidance, patience, trust, and support over the years not only for my PhD studies but also to all aspects of my professional development.

I would also like to extend my sincere gratitude to my committee members Dr. Eli Sone and Dr. William Ryu for their valuable discussions and feedback, constructive criticism, and guidance during my committee meetings. I would also like to thank Dr. Ofer Levi for his discussions and guidance during my qualification exam.

I would like to thank Dr. Vahid Raeesi who worked with me side-by-side when I first joined the lab and for introducing me to the field of nanotechnology. Vahid has been always a best friend, I would really like to thank him for all the discussions that we have had.

I would like to thank Dr. Kyrylo Zagorovsky for his valuable discussions and getting me excited about the field of diagnostics and from whom I learned the MNAzyme assay. I would also like to thank my colleague Jisung Kim who worked with me side-by-side on the diagnostic projects. It was very exciting to work with Jisung and Kyrylo. I really enjoyed the troubleshooting and pushing our projects forward. It was one of the best collaborations I have ever had!

I would like to thank Dr. Justin Nodwell for giving me the opportuning to work in his lab and perform bacterial experiments and for providing the bacterial strains. I also would like to thank Dr. Jordan Feld and Dr. Samira Mubareka for providing the viral clinical samples.

I would like to thank Dr. Kate Banks for her valuable discussion and help with facilitating the animal experiments and manuscript revision, Dr. Patricia Turner for the histology analysis and Dr. Anu Rebbapragada for her valuable discussions.

I would also like to thank all members of Chan Lab for the friendship, great discussions during the weekly group meetings, idea sharing, events and all the funny moments that we have had.

Finally, I would like to thank the Egyptian government, Institute of Biomaterials and Biomedical Engieering, and University of Toronto for the funding and financial support.

Table of Contents

Table of Contents

List of Tables

List of Figures

List of Abbreviations

AR	Antibiotic resistance
AMR	Antimicrobial resistance
BLAST	Basic Local Alignment Search Tool
CDC	Center for Disease Control and Prevention
CTAB	Cetyl trimethylammonium bromide
CLSI	Clinical and Laboratory Standards Institute
CFU/ml	Colonies per milliliter
ELISA	Enzyme linked immunosorbent assay
GNPs	Gold nanoparticles
NRs	Gold nanorods
HBV	Hepatitis B virus
HCV	Hepatitis C virus
HIV	Human immunodeficiency virus
IDs	Infectious diseases
Flu	Influenza
iTPA	Isothermal target and signaling probe amplification
LFAs	Lateral flow assays
LAMP	Loop mediated isothermal amplification
MRSA	Methicillin resistant *S. aureus*
MIC	Minimum inhibitory concentration
MNAzyme	Multicomponent nucleic acid enzyme
MDR	Multi-drug resistant
NPs	Nanoparticles
NTC	No template control
NASBA	Nucleic acid sequence based amplification
PBS	Phosphate buffered saline
PTT	Photo-thermal therapy
POC	Point-of-care
PVCL	Poly vinyl caprolactam
PCR	Polymerase chain reaction
qPCR	Quantitative PCR
RPA	Recombinase polymerase amplification
rt	Reverse transcription
RCA	Rolling circle amplification
SARS	Severe acute respiratory syndrome
SPR	Surface plasmon resonance
TB	Tuberculosis
LOD	The limit of detection
tHDA	Thermophilic helicase dependent amplification
m-PEG-SH	Thiol terminated polyethylene glycol

TEM	Transmission electron microscope
WHO	World health organization

Chapter 1
Introduction

1.1 Infectious diseases

1.1.1 Prevalence of infectious diseases

Infectious diseases (IDs) are caused by different pathogenic organisms such as viruses, bacteria, parasites, and fungi[1]. There are more than 1,400 pathogenic organisms that cause diseases in humans, which range from simple to untreatable infections[2–5]. In 2015, the World Health Organization (WHO) has ranked IDs in the top 10 leading causes of deaths and years of life lost worldwide[6]. Annually, 6 million people die annually due to IDs such as lower respiratory infections, tuberculosis, and diarrheal diseases (Figure 1.1A). In high-income countries, deaths from IDs are mostly associated with respiratory infections[6] (Figure 1.1B). In low-income countries, the burden of IDs is considerably higher and deaths are mainly caused by respiratory infections, human immunodeficiency virus/acquired immune deficiency syndrome (HIV/AIDS), diarrheal diseases, and malaria and tuberculosis[6] (Figure 1.1C). Besides the mortality and years of life lost, IDs can result in economic burden from loss of productivity, money spent on treatment, and school and work absences[7,8]. Thus, the emergence and re-emergence of IDs will continue to be a major burden on the global public health. Over the next 25 years, IDs are expected to remain as the most common cause of mortality, particularly within low income countries[9].

The inability to combat IDs diseases in many cases is hindered by the lack of sensitive and easy-to-use diagnostic tests to detect early infections[10,11], and the lack of new effective therapeutics against antimicrobial resistant pathogens. Point-of-care (POC) diagnostics have the potential to improve the management of IDs, particularly in low-income countries where health-care infrastructure is weak, access to health-care providers is limited and timely medical care is a challenge[12–14]. POC diagnostics are simple, affordable, sensitive and specific tests that are conducted near the patients[11,12,15]. These tests can be used in different locations such as homes, community centers, clinics, peripheral laboratories and hospitals and has the ability to provide test results to health-care providers quickly[11–13,16]. Consequently, this can help to quarantine the infected individuals, thus, prevent the spread of the infections. Moreover, POC diagnostic tests can

help screen infectious pathogens for drug resistance, which facilitates the selection of optimal treatments. However, the rapid evolution and spread of antimicrobial resistance (AMR) among different pathogens render the currently available antimicrobials ineffective against these infections[17,18], necessitating the development of new therapeutics. Therefore, there is an urgent need to develop rapid and sensitive diagnostics and new alternative therapeutics to effectively control IDs and AMR.

The following sections will discuss the prevalence of some potential IDs and AMR, currently available methods for diagnosing IDs and AMR and their limitations, and finally introduce the nanotechnology as a potential solution to overcome the limitations of the current diagnostic tests and its implications in developing POC diagnostics and innovative therapeutics.

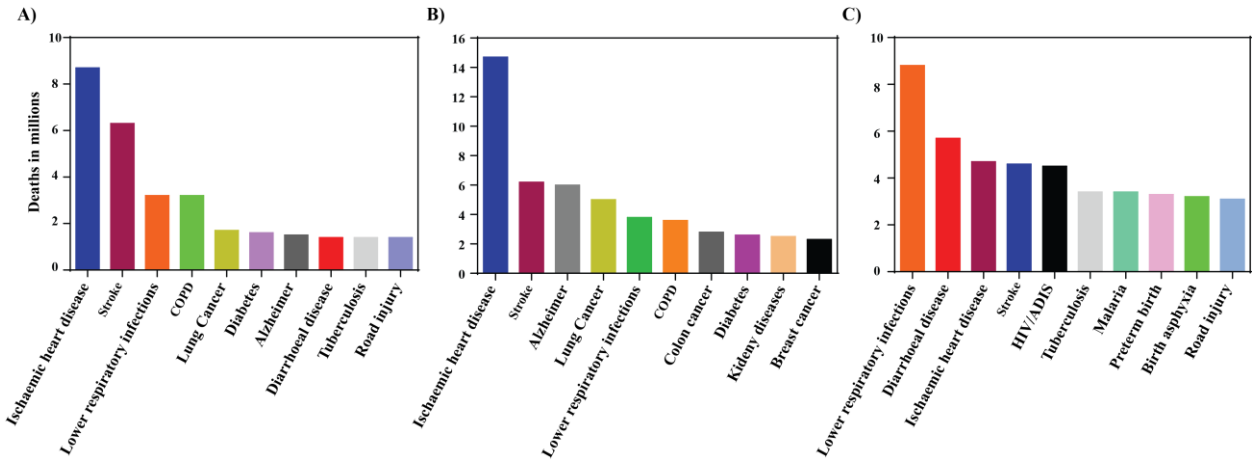

Figure 1.1. Prevalence of infectious diseases in 2015 according to WHO. A) Worldwide, B) Low-income countries and C) High-income countries. COPD = Chronic obstructive pulmonary disease. Adapted from Ref [6].

1.1.1.1 Respiratory tract infections

Respiratory tract infections are important leading causes of death worldwide[6,19,20]. Although viruses and bacteria both cause respiratory infections, viral infections remain the major contributors to this infection[19,21–23]. Although viruses such as syncytial virus, rhinovirus, coronavirus, and adenovirus can infect children and adults and cause mild to severe acute infections[19,22], influenza (Flu) viruses are considered the most frequent cause of respiratory infection with high morbidity and mortality[24,25] . Three types of Flu viruses infect humans are A, B, and C. FluA virus is the most common type that contributes to the most severe and acute

infections[26]. FluA is sub-divided into different serotypes based on the surface proteins: hemagglutinin (H) and neuraminidase (N) (H1through H18 and N1 through N11)[26]. Currently, FluA H1N1 and H3N2 are found in humans[26]. FluA outbreaks have occurred several centuries ago and resulted in significant number of deaths. Most FluA epidemics occur between January and March and in a typical endemic season, influenza results in about 200,000 hospitalizations and 36,000 deaths in United States[24]. The worst FluA pandemic in history occurred in 1918 in Spain (Spanish pandemic, H1N1) which resulted in about 675,000 deaths in United States and approximately 50 million worldwide[24,25]. After the SARS outbreak in 2003, various respiratory-associated viruses have emerged, including avian Flu and variant FluA H3N2 viruses[27]. In April 2009, there was another pandemic caused by H1N1 variant. This new 2009 H1N1 variant, known as the swine Flu virus, is different from the 1918 pandemic virus and has since replaced the 1918 H1N1[26]. The emergence of new virus sub-types render the current vaccines ineffective against them. Rapid and sensitive diagnostic assays that can detect and distinguish between different virus sub-types can help select the appropriate antiviral vaccine and hence, control the infections[28].

1.1.1.2 Blood-borne infections

Blood infection can be caused by many different pathogens, however, hepatitis B virus (HBV), hepatitis C virus (HCV) and HIV, known as blood-borne pathogens standard, are the main pathogens of concern[29]. The WHO estimated that 240 million people are chronically infected with HBV worldwide and about 686,000 people die every year[30]. About 5-10% of adults in sub-Saharan Africa and East Asia are chronically infected with HBV and about 2-5% in the Middle East and Indian sub-continent.

HCV is another blood-borne virus that causes acute and chronic infections in the liver[31]. HCV transmits mostly via transfusion of unscreened blood, re-use of syringes and inadequate sterilization of medical equipment[31]. Globally, HCV causes an estimate of 130-170 million infections and more than 350,000 deaths annually[31]. The prevalence of HCV is higher in low-income countries. In Africa, Middle East, many countries in Eastern Europe and South America the HCV burden is 3%[31–33]. Egypt shows the highest prevalence rate of HCV in the world with an estimate of 10%[33].

While the blood-borne pathogens HBV and HCV account for high rates of morbidity and mortality worldwide, HIV remains as the leading cause of death[34–36]. More than 95% of current HIV infections occur in low-income countries[34,35]. In 2009, the WHO estimated 68% of global HIV infections occur in Africa, of which 72% resulted is death. The high prevalence of blood-borne infections in developing countries is attributed to the lack of rapid POC diagnostics that can early detect these pathogens[37].

1.1.1.3 Wound and skin infections

Wound infection refers to the microbial invasion of the epidermis and subcutaneous tissues due to break or puncture of skin that induces either a local or systemic host response[38,39]. Wound infections can be categorized into two main infections: skin and soft tissue infections[39]. Skin harbors a wide variety of microbial flora that can produce infections[40]. However, community and hospital-acquired wound infections are more prevalent[39,41,42]. These infections account for a high rate of morbidity and economic burden worldwide[39,41,42]. In the emergency care settings, skin infections are one of the three most common diagnosed infections after chest and asthma[43]. The Nosocomial Infections National Surveillance Service reported that surgical wounds represent 10% of nosocomial infections in hospitals. Furthermore, in US, an estimate of 25% and 9% of nosocomial infections were attributed to surgical site infections among postoperative patients in US and UK respectively[41,44,45].

The ability of microbes to initiate wound or skin infection depends on many factors such microbial load per gram of tissue, cell and tissue adherence, toxins or enzymes production and the immune system host response, pH unbalance and moisture content[46,47]. For instance, when the bacterial load exceeds 10^5 organisms per gram of tissue, or when the immune system becomes suppressed, infection develops[48]. The increase of microbial load in wounds results in production of high amount of toxins and enzymes which can greatly endanger the wound and delay the healing process[48–50]. Furthermore, several risk factors such as diabetes mellitus, cirrhosis, neutropenia, animal contact, animal bite wounds and/or fresh water exposure can significantly potentiate the development of skin infections[40,43].

Bacteria are among the most common microbes that infect skin. Previous studies have reported that *Staphylococcus aureus*, *Pseudomonas aeruginosa*, *Escherichia coli*, *Streptococcus*

pyogens and *Enterococcus faecalis* are the most common bacterial pathogens that are associated with skin and wound infections[39,41–43,47,51]. These bacterial pathogens can colonize different anatomical structures depending on site-specific biochemical interactions and tissue-specific biofilm formation and cause several skin diseases such as abscesses, cellulitis, impetigo, erysipelas, foot ulcers, necrotizing fasciitis, skin-scaled staphylococcal syndrome, and streptococcal toxic shock syndrome[47,52,53]. In addition, infected wounds can be of great consequence on a patient's social and physical life due to excessive pain, anxiety, discomfort and high health-care costs[54]. Despite progress in wound management, it has been expected that wound infections will increase dramatically over the next several decades due to increase in the number of immunocompromised persons and continuous emergence of AMR[39,55].

1.1.2 Prevalence of antimicrobial resistance among infectious pathogens

AMR is defined as reduced susceptibility of infectious pathogens to the antimicrobial drugs leading to their infectiveness. Some microbes develop resistance to a single antibiotic, while others develop resistance to several antibiotics and are often referred to as multidrug-resistant (MDR) bacteria[56]. In some cases, microbes have become so resistant that no available antibiotics are effective against them. Among these microbes, viruses and bacteria are the most commonly known pathogens with increased rates of resistance[57].

1.1.2.1 Antimicrobial resistance in viruses

Antiviral drugs are some of the most important drugs that have been developed in the 20th century for treatment of viral infections[62,63]. The development of viral resistance to antiviral drugs is an increasing global concern[57]. In 2010, the WHO reported that 7% of people receiving HIV treatment in developing countries had drug-resistant HIV[57]. The resistance of FluA virus to the drug oseltamivir has also been reported during the FluA season in 2008-2009 worldwide[60]. Several factors contribute to viral resistance include: viral load, patient immune status and long-term exposure of viruses to antiviral drugs[59,61].

1.1.2.2 Antimicrobial resistance in bacteria

The most commonly known antimicrobials worldwide are antibiotics, which target bacterial associated infections [16]. Bacterial antibiotic resistance (AR) can be either intrinsic or

acquired. Intrinsic resistance occurs in bacteria due to naturally low permeability to antibiotics or due to the absence of the antibiotic target[62]. Acquired resistance on the other hand, involves transfer of the mobile resistance elements from resistant to non-resistant pathogens via vertical or horizontal gene transfer[62]. Bacteria have developed several resistance mechanisms such as efflux pumps, antibiotic-target modification, and enzymatic degradation of antibiotics[63–66]. These acquired mechanisms have reduced the effectiveness of the most currently available antibiotics.

Since the discovery of antibiotics in the 1930s , the estimated consumption has been more than 1 million tons worldwide[67]. The extensive and improper use of antibiotics has led to the emergence of AR among different pathogenic bacteria. Center for Disease and Control and Prevention (CDC) estimated that 2 million people are infected with AR bacteria each year, and of those 23,000 die due to these infections[16]. In many developing countries, there is a tremendous increase in the development and dissemination of AR. It has been estimated that the annual number of deaths associated with AR in developing countries will reach more than 5 million by 2050[68].

S. aureus is the well-known example that has always been a hassle for antibiotic therapy. The most prominent example is the methicillin-resistant *S. aureus* (MRSA). According to CDC the annual infection associated with MRSA in US hospitals increased from 40 to 60% between the years 1999 and 2005 with about 5,500 estimated number of deaths each year[69]. In 2014, the WHO estimated approximately 480,000 new cases of multidrug-resistant tuberculosis (MDR-TB) which is resistant to at least 4 of the core anti-TB drugs[57]. More recently, US reported the emergence of *E. coli* resistance to the last resort antibiotic, colistin, making the treatment against this bacteria very challenging[70].

The lack of POC diagnostic tests that can rapidly identify the infectious pathogens and their antibiotic susceptibility make it difficult for clinicians to prescribe the right drug to the right patient[71]. For example, for some diseases such as HIV and tuberculosis that requires long-term treatment using specific tailored drug regimens, patients are often tested for drug resistance before initiation of treatment[71]. Furthermore, due to the lack of rapid drug susceptibility tests for gonorrhea, doctors use antibiotics to which the fewest strains are resistant. This can potentially increase the AMR development against these drugs[71]. Therefore, the development of a rapid and sensitive POC diagnostic test has been called as an urgent need to guide the health-care providers

to give the appropriate treatment when needed. This will ultimately prevent the AMR spread and avoid risk of developing new resistance[71].

1.2 Current laboratories methods for detection of infectious diseases

There are four major methods that are currently used to detect infectious pathogens: microscopy, cell culture, and molecular and serological based tests. These methods can detect pathogens based on their morphology, metabolites produced, genomic signatures, antibodies produced by the patient in response to the infection, and pathogenic antigens.

1.2.1 Microscopy

Direct microscopic examination can be used in many different clinical settings to visualize microbes based on certain features such as shape, size and arrangement of microbial cells. Although, this technique is fast, it only provides qualitative results. Moreover, in many cases additional steps such as sample staining is needed in order to distinguish between different pathogen cells. For example, gram staining is important to distinguish between gram positive and gram negative bacteria. However, gram staining will not identify the pathogen to the species level. Also, this technique requires access to expensive microscopes and highly skilled personnel to provide an accurate identification of pathogens[72].

1.2.2 Culturing

Culturing is one of the most commonly used techniques that has been extensively used for identifications of microorganisms in laboratories. Some microorganisms can be cultured on artificial media (e.g. bacteria, yeast and fungi) while others (e.g. viruses) require a living host such as mammalian cells or living animals for culturing and isolation. Culturing can provide quantitative results when a specific volume of specimen is spread over the surface of agar media and the number of colonies per milliliter (CFU/ml) is calculated. This is a very common method for identification of bacterial pathogens associated with urinary tract infections. Although culturing can provide quantitative and accurate identification of pathogens up to the species level, it is time consuming (takes 24-72 hours). A follow up confirmatory test, and manual readout are also needed for accurate identification. Furthermore, some types of bacteria cannot be cultured in the laboratory, and therefore cannot be detected using this method[73,74].

1.2.3 Enzyme linked immunosorbent assay (ELISA)

ELISA uses the concept of antibody-antigen immunoreaction for detection of biomolecules such as proteins, antibodies and peptides. In a typical ELISA reaction, a specific antibody is immobilized on a surface and the antigen of interest is allowed to bind to the immobilized antibody. A primary antibody is then added to the captured antigen followed by an enzyme conjugated secondary antibody. The conjugated enzyme catalyzes the conversion of a chromogenic substrate into colored or fluorescent products, producing a positive result. ELISA has been used for the detection of many pathogens including viruses, parasites, and bacteria[75–82] with sensitivity ranging from fM to nM. Despite the higher sensitivity of ELISA tests, they are labor intensive, produce false positive results, require expensive antibody components and equipment for signal readout, and in many cases cannot distinguish between pathogen subtypes[28,75,83].

1.2.4 Lateral flow assays (LFAs)

LFAs are very simple and cost effective tests that are suitable for POC application. These assays are used as dipsticks or strips. LFAs can detect different pathogens via immunoreaction (antibody-antigen reaction) or via nucleic acid detection. Some LFAs use a suitable pH indicator that can induce color change in response to certain metabolites[84,85]. Since the introduction of the first LFAs in late 1960s for disease diagnosis, LFAs have been used for detection of many infections such as HIV, malaria, meningitis, Flu viruses, gonorrhea, TB and rubella[14,86–89]. Despite the simplicity and low cost of LFAs, they generally have low sensitivity (usually nM-pM range), and sometimes require a pre-enrichment or culturing[14,85,86,90–93] before testing, making the process time consuming and inefficient. In many cases more complex devices are necessary for accurate diagnosis[14,86].

1.2.5 Polymerase chain reaction (PCR)

Genetic-based assays have demonstrated higher detection sensitivity and specificity and they can be easily manipulated to detect many different pathogens. Unlike culturing, genetic-based assays do not require prolonged incubation times. Quantitative PCR (qPCR) is the most commonly used technique for quantitative detection of genetic elements of pathogens. This technique uses DNA polymerase enzymes and short DNA sequences know as primers to exponentially amplify and increase the concentration of specific detection targets while providing real-time detection.

Although qPCR is fast and sensitive, a major drawback is the need for large and expensive instruments which can be only operated by highly skilled personnel, limiting their utility in POC settings[94–96].

1.3 Current laboratories methods for detection of antimicrobial resistance

Extensive and improper use of antimicrobials have led to rapid evolution of AMR[16–18,97]. In particular, there is an emerging trend of MDR pathogens, which have acquired resistances to multiple drugs. Rapid, accurate and sensitive diagnostic approaches that can detect multiple AR determinants are needed to enable healthcare-providers to provide appropriate therapy and reduce the development of new resistance mechanisms [16,98–101]. Currently, there are two major laboratory techniques for the detection of AR: phenotypic culture-based tests which are mostly used for bacterial pathogens and genotypic tests which is commonly used for most pathogens.

1.3.1 Phenotypic assays

Phenotypic assays, such as broth dilution, agar dilution and gradient diffusion method (E-test)[98] are routinely used in clinical laboratories for determining bacterial susceptibility to antibiotics. Although phenotypic assays are cost effective, they are labor intensive and time consuming (usually take 24-72 hours for an accurate diagnosis), and require bulky instruments[98,99,102–104]. Moreover, phenotypic assays can only test susceptibility of aerobic bacteria and not applicable for other pathogens such as viruses.

Broth dilution method can be carried out either in macro-scale (test tubes) or micro-scale (96-well plate). This method involves preparation of different concentrations of antibiotics, followed by inoculation of bacteria and incubation for overnight. The tubes are then examined for the minimum inhibitory concentration (MIC), which is the minimum concentration at which there is no visible growth is observed. Although this method provides quantitative results, it is labor intensive, since each test requires manual preparations of the antibiotic solutions, and requires large space for incubation[98,105,106]. Many instruments have been developed to automate the broth dilution method. Use of instrumentation can provide test readouts without the need for manual readings. Currently, there are four commercial automated instruments approved by the FDA for use in the US: the MicroScanWalkAway (Siemens Healthcare Diagnostics), the BD Phoenix

Automated Microbiology System (BD Di- agnostics), the Vitek 2 System (bioMerieux) and, the Sensititre ARIS 2X (Trek Diagnostic Systems). Despite their simplicity, these instruments are bulky, expensive and only suitable for centralized laboratories[98].

E-test method on the other hand uses the principle of antibiotic gradients in the format of paper strips. The strips are applied onto the surface of the seeded agar plates. After overnight incubation, MIC is measured by the intersection of the lower part of the ellipse shaped growth inhibition area with the test strip[98]. This method is flexible because multiple E-test strips can be used simultaneously to test for multiple drugs. However, it is time consuming and becomes expensive when multiple strips are used[98]. In contrast, agar diffusion method uses paper antibiotic discs that contain fixed amounts of the antibiotic applied onto the surface of the seeded agar plates. After incubation overnight, the zones of growth inhibition around the antibiotic disc is measured and interpreted following the criteria listed by the Clinical and Laboratory Standards Institute (CLSI)[98,105,106]. This method is characterized by its simplicity, ease of interpretation, and flexibility for choosing antibiotic discs. However, the susceptibility of fastidious or slow growing bacteria cannot be accurately measured using this method[98,106].

1.3.2 Genotypic assays

Unlike phenotypic assays, genotypic tests can directly detect the presence of specific biomarkers (genes) such as AMR genes. Genotypic assays use inactivated or sterilized samples, thus providing improved safety[107]. Additionally, they are not affected by testing conditions, and are often used to confirm inconclusive phenotypic test results[108–111]. The gold standard technique for genetic detection is qPCR because it has high sensitivity. However, as mentioned previously, PCR is expensive, uses complex equipment, and requires highly skilled technicians, precluding its use in resource-limited areas.

1.4 Current needs to control infectious diseases and antimicrobial resistance

Despite the advances in antimicrobials and diagnostics since the 19th century, IDs remain a major global concern. Disease diagnosis represents an important key for successful disease control and management[12–14]. Some symptomatic infections can be managed without the need for diagnosis but this could potentially lead to overtreatment due to administration of inappropriate or

unnecessary treatment, and high risk of developing AMR (Figure 1.2). In some cases, one disease can be caused by different pathogens that produce the same symptoms. For instance, respiratory tract infection can be caused by FluA virus which produces respiratory symptoms that are clinically similar to those caused by streptococci, mycoplasmas or more than other many viruses[74]. As a result, an accurate and rapid identification of infectious pathogens is needed before initiation of treatment[12,74].

Development of POC diagnostic tests that can rapidly detect infectious pathogens and their susceptibility to antibiotics is therefore needed to help prevent the transmission of pathogens, and rule out the unnecessary prescription and use of antibiotics [71,112] (Figure 1.2). Consequently, this will help to administer the right drugs, conserve the currently available drugs, reduce health-care costs, and mitigate the risk of further AMR development[10,11,16,112,113]. The WHO has listed the ASSURED criteria that determine the characteristics of an ideal POC diagnostic test[11,12]. According to these criteria, a POC diagnostic assay should be simple (instrument-free), affordable, rapid, highly sensitive and specific, and user-friendly[11,12].

Another key aspect for successful disease management and control is delivering effective therapeutics. However, some microbial pathogens have already developed resistance to all the current available antibiotics, hence, the world might be moving to the post-antibiotic era[114]. Thus, there is an urgent need to develop new alternative therapeutics to combat these infections.

The tremendous progress in the field nanotechnology over the last 15 years has presented new era of innovation and technology development that can significantly improve the current diagnostic strategies and help develop new potential antimicrobial therapies. The next sections will discuss the properties of nanomaterials, with main focus on gold nanoparticles (GNPs) and their implications in developing POC diagnostics and photo-thermal based antimicrobial techniques.

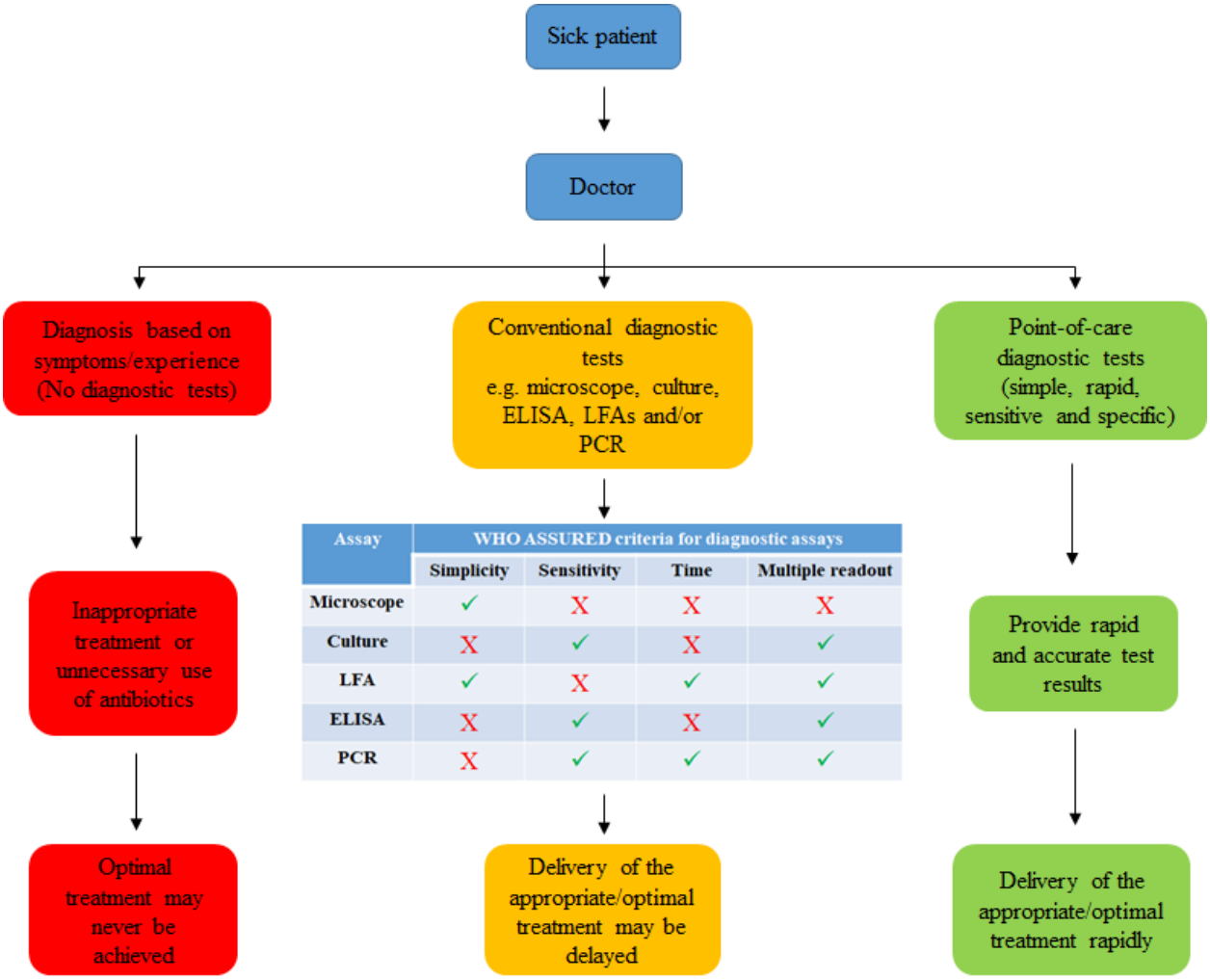

Assay	WHO ASSURED criteria for diagnostic assays			
	Simplicity	Sensitivity	Time	Multiple readout
Microscope	✓	X	X	X
Culture	X	✓	X	✓
LFA	✓	X	✓	✓
ELISA	X	✓	X	✓
PCR	X	✓	✓	✓

Figure 1.2. POC diagnostic tests optimize treatment. Non-diagnosed diseases can lead to selection of inappropriate drug, therefore, the optimal treatment may fail. Traditional diagnostic tests however, can help select the right drug, but they are often time consuming. On the other hand, POC diagnostic tests can provide rapid and accurate test results before initiation of empirical treatment thus, the optimal antimicrobial drug can be used.

1.5 Nanotechnology

Nanotechnology is defined as a branch of science that studies and manipulates materials or particles in the size range of 1-100 nm[115–117] (Figure 1.3). While nanotechnology was introduced by the Nobel Laureate Richard Feynman in 1959, who lectured "There is plenty room at the bottom", the use of colloidal gold has been recognized back to the middle ages[118]. The prime example is the gold staining of Romans glass cup "*Lycurgus cup"* from the 4th century. This glass cup exhibits a unique ruby red color when illuminated from inside, which was later revealed to be

due to gold and silver deposits (50-100 nm size)[119]. Although humans have benefited from nanostructures from centuries ago, the ability to produce and manipulate nanomaterials became only remarkable in the 20th century, particularly in the last 3 decades[120]. The recent advances in nanotechnology has impacted many fields including medicine, biophysics and biology and provided a new tool-kit for developing new diagnostics and therapeutic techniques[121,122].

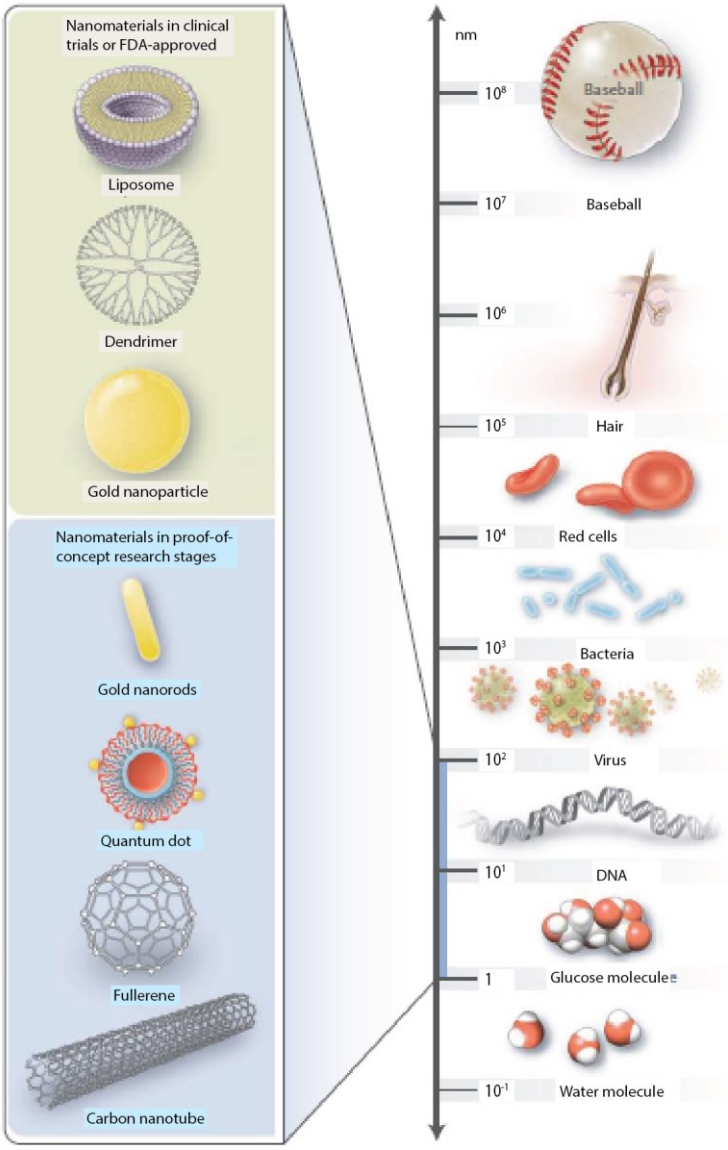

Figure 1.3. Schematic showing nanoscale and different nanomaterial types. The scale shows the size of nanomaterials in respect to size of different biological compartments. Reproduced with permission from ref [115]. Copyright 2010 Massachusetts Medical Society.

1.5.1 Properties of nanomaterials

Because nanomaterials possess a size range comparable to that of biological molecules, these materials are well suited for biomedical applications including therapeutics and biosensing. Unlike bulk materials, nanomaterials exhibit unique physical and chemical properties that depend on their size and shape. When the size of a bulk material is reduced to the nanoscale, its valance and conduction bands split into quantized energy levels leading to unique absorption and fluorescence properties[116,123]. In addition, at this size regime, the surface-to-volume ratio of the material increases because its atoms become located on the surface. For example, in a 1 cm cube of iron, the amount of surface atoms is 10^{-5} % which is significantly lower than that in a 1 nm cube in which all atoms would be a surface atom[118]. The higher surface-to-volume ratio of nanomaterials maximizes the surface available for interactions and functionalization with different chemical and biological agents[118,123].

Another unique property of nanoparticles (NPs) is their ability to confine and absorb photon energies in a phenomenon known as surface plasmon resonance (SPR). When nanoparticles are exposed to light energy, their conduction band electrons enter into a collective oscillation mode creating a dipole on the surface of NPs (Figure 1.4 A and B). When the frequency of incident light matches the frequency of the dipole formation, the photon's energy is then absorbed, producing a strong electromagnetic field. As a result, the radiative properties such as light absorption, fluorescence and scattering increase by orders of magnitude. On the other hand, the absorbed energy can also decay through non-radiative processes and produce heat via electron-hole recombination[118,121,123–125]. The SPR is size and shape dependent, therefore, metallic NPs such as gold and silver nanoparticles can be prepared with different size and shapes to produce different colors (Figure 1.4 C). For example, spherical gold nanoparticles (GNPs) have SPR around 520 nm which results in bright red color. Whereas, rod shape GNPs, known as gold nanorods (NRs), exhibit two SPR modes along longitudinal and transverse axes, giving rise to different colors depending on their aspect ratio[124]. Due to these unique properties, NPs hold a significant promise for developing simple and cost effective tools for disease diagnostics and treatment. In the following sections, the biomedical applications of GNPs (which were used in this thesis) in IDs diagnosis and therapy will be reviewed.

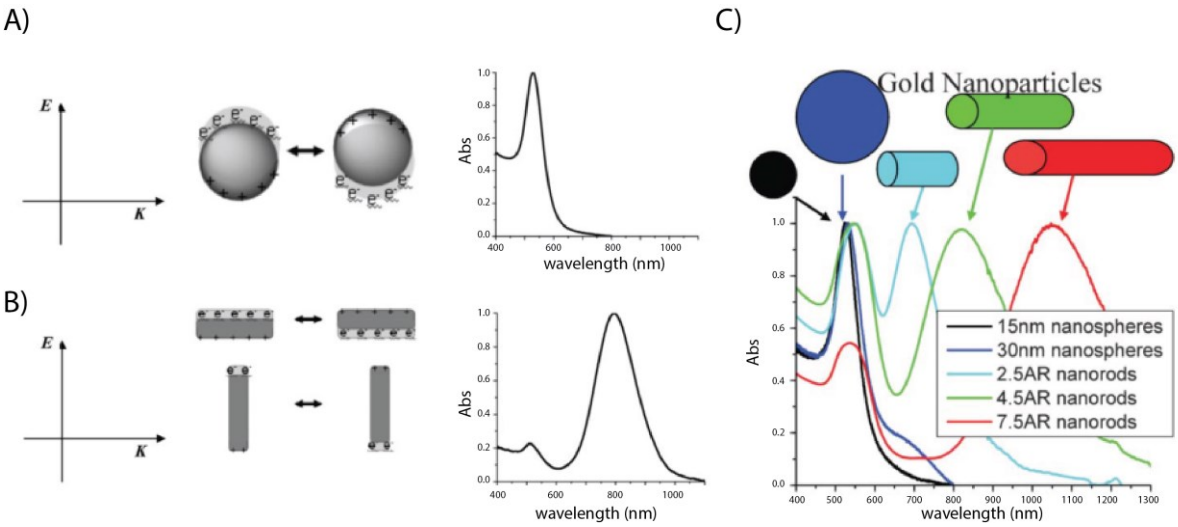

Figure 1.4. Interaction of light with gold nanoparticles. A) Gold nanospheres, B) Gold nanorods. Reproduced from Ref [123]. Copyright 2005 with permission from Royal Society of Chemistry. C) UV-Vis absorption spectra of different shapes and sizes of gold nanoparticles. The color of NPs changes in respect to size and shape due to SPR effect. Reproduced from Ref [116]. Copyright 2009 with permission from Wiley-VCH Verlag GmbH & Co. KGaA.

1.5.2 Gold nanoparticles based diagnostic assays

GNPs are among the most common type of NPs that have been extensively exploited in biomedical applications. This is because these NPs can be reproducibly synthesized and their surface can be easily functionalized with different biological molecules. The most common principle of GNPs in diagnosis is the color change in response to presence or absence of the analyte of interest. For instance, the surface of GNPs can be functionalized with antibodies, short oligonucleotides, aptamers and/or peptides to selectively detect specific targets. The binding between GNPs and target can alter the SPR enough to produce a visible color change that can be observed by naked eye (Figure 1.5). This makes GNPs very promising candidates in the field of biosensing[126–130]. GNPs have been used for pathogen diagnosis in the context of nucleic acid, proteins and whole-cell detection. Thus, GNPs have offered a broad spectrum of innovative approaches for rapid and sensitive detection of metals, proteins, nucleic acid and whole cells[131,132].

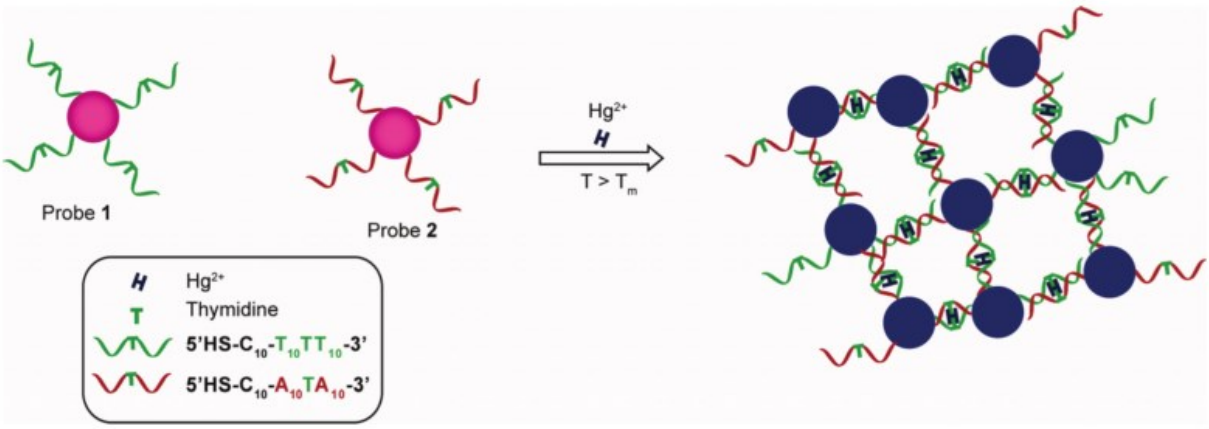

Figure 1.5. Illustration of the principle of GNPs sensing. DNA functionalized GNPs was used for colorimetric detection of heavy metals. The assay relies on thymidine-Hg^{+2}-thymidine coordination. The presence of Hg+3 causes GNP aggregation and as a result the color of GNPs shifts from red to blue. Reproduced from Ref [131]. Copyright 2012 with permission from American Chemical Society.

1.5.2.1 Gold nanoparticles for detection of whole cell

In this approach, GNPs were functionalized with aptamers or antibodies that can recognize specific targets on the surface of microbial cells[132]. This strategy has been demonstrated in the context of GNPs aggregation in response to the presence of pathogen. For aptamer conjugated GNPs, the aptamer desorbs from the surface of GNPs in response to presence of specific target and bind to it. The desorption of aptamer from the surface of GNPs results in de-stability and aggregation of GNPs in presence of high concentration of salts. This concept has been used for detection of *E. coli* and *Salmonella typhimurium*[133] (Figure 1.6). For antibody-conjugated GNPs, the aggregation of GNPs occurs via binding between the specific antigen on the surface of the cell and the GNP-attached antibody. This results in the aggregation of GNPs on the surface of microbial cells (Figure 1.7A and B), leading to a change in GNP size and thus a change in color. This concept is more common and has been applied for detection of various pathogens such as bacteria, viruses and protozoa (Table 1.1).

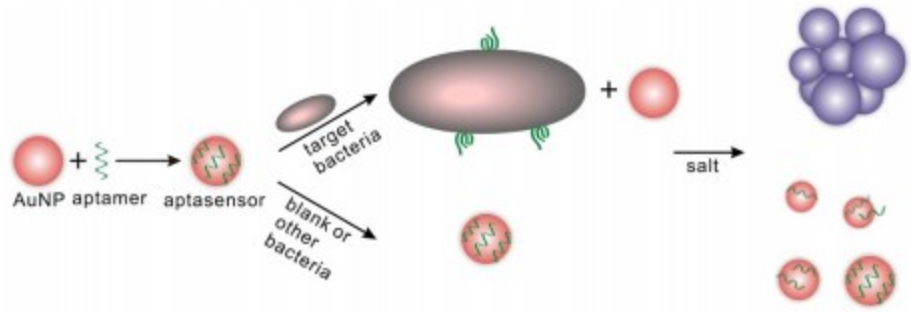

Figure 1.6. Schematic for detection of whole bacteria cells using aptamer conjugated GNPs. In the presence of target, the aptamer desorbs from the surface of GNPs which induce GNP aggregation in presence of high salt concentration. Reproduced with permission from Ref [133]. Copyright Wu et al.; licensee Springer. 2012.

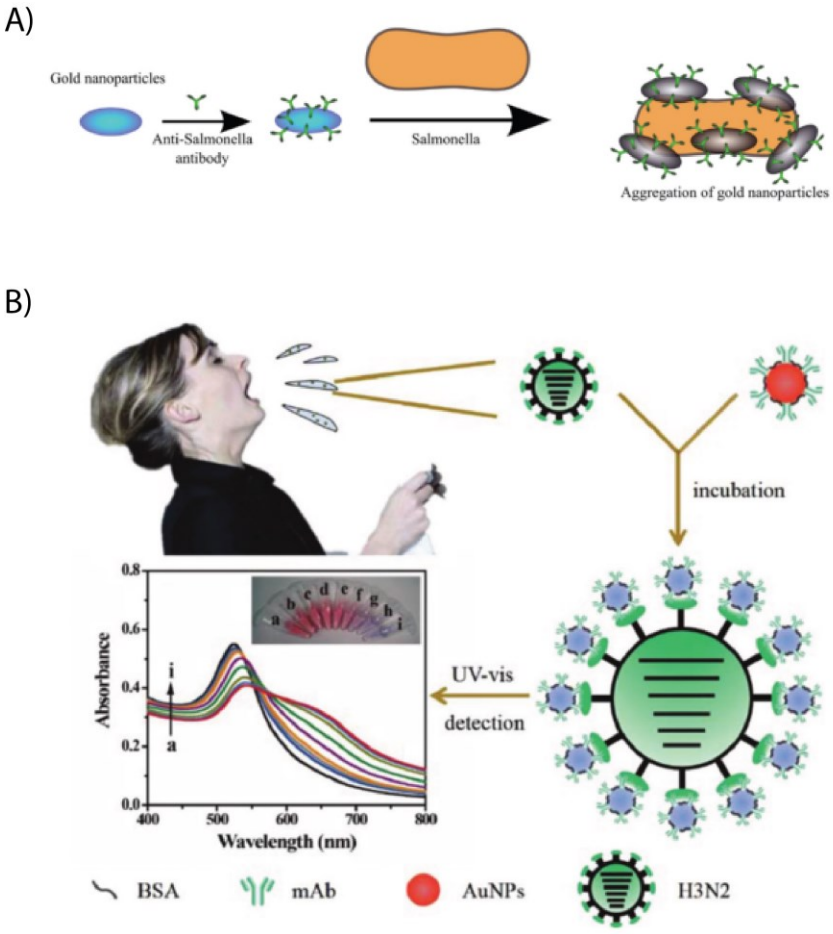

Figure 1.7. Schematic for detection of whole cell using antibody conjugated GNPs. A) Detection of bacteria. Reprinted from Ref [132]. Copyright 2015 with permission from Elsevier. B) Detection of viruses. GNPs aggregate on the surface of cell which shifts the SPR and changes the color from red to purple. Reproduced from Ref [134]. Copyright 2015 with permission from Royal Society of Chemistry.

Table 1.1. Protein conjugated gold nanoparticle for detection of different pathogens.

Pathogen	Purpose of study	Sample source	Assay time	Limit of detection	Reference
E. coli	Detection of pathogen	Culture	-	~10^2 CFU/ml	[132]
S. typhi	Detection of pathogen	Spiked blood	1 hr	~10^2 CFU/ml	[132,135]
S. aureus	Detection of pathogen	Spiked milk	40 min	~10^7 CFU/ml	[132,136]
FluA	Detection of pathogen	Culture	30 min	7.8 HAU	[134]
Dengue and west Nile viruses	Detection of pathogen	Culture	30 min	10 pfu/ml	[137]
Giardia lamblia cysts	Detection of pathogen	Culture	-	~10^2 cells/ml	[132,138]

1.5.2.2 Gold nanoparticles for detection of proteins produced by microbial cells.

In addition to whole cell detection, the concept of GNPs aggregation has also been applied for colorimetric detection of certain enzymes produced by pathogens. In this proof-of-concept approach, the aggregation of GNPs is driven by the free charged groups of the cleaved substrate. Therefore, when the pathogen produces the enzyme, it cleaves the substrate in the solution. This exposes the surface of GNPs to free reactive groups of the cleaved substrate, resulting in GNPs aggregation. This has been used for detecting human immunoglobulin A1 (IgA1) protease that is produced by *S. pneumonia*. When 20 nm citrate-GNPs and human IgA1 is added to the supernatant of *S. pneumonia* culture, the enzyme cleaves the IgA1, producing positively charged Fab regions that cross link negatively charged GNPs, leading to the aggregation of GNPs[132,139]. This approach has also been used for the detection of AR bacteria. For instance, the surface of 16 nm citrate-GNPs was conjugated with cephalosporin for detection of B-lactamase enzyme produced by B-lactam resistant bacteria such *as Enterococcus cloacae*, *E. coli* and *Bacillus cereus*[140,141].

1.5.2.3 Gold nanoparticles for detection of nucleic acids

As mentioned in section 1.2.5, nucleic acid based detection assays have demonstrated higher detection sensitivity and specificity and they can easily be modified to detect many different pathogens. Similar to whole cell and proteins detection, GNPs have also been used for colorimetric detection of nucleic acids. Two common detection strategies have been widely exploited: one probe and two probes strategies[132]. In the one probes strategy, the surface of GNPs is functionalized with one type of DNA probe that is complementary to the target DNA. High concentration of salt is then used to induce aggregation of GNPs. In the presence of the target DNA, the GNPs remain dispersed due to hybridization of target DNA with GNPs probe which stabilizes the GNPs and prevents their aggregation by salts. However, in the absence of target DNA, the GNPs aggregate due to high salt concentration, causing a color shift from red to blue[142,143] (Figure 1.8A and B). Whereas, the two probe strategy uses two different sets of GNPs which are prepared and mixed together. Each set is functionalized with different probes. The presence of the target cross-links the two sets of GNPs and causes their aggregation[144,145] (Figure 1.8 C). These strategies are suitable for POC testing since they are simple, rapid and instrument free. However, a major limitation of these assays is the low sensitivity (usually nM range). Thus, in order to improve the sensitivity of GNPs aggregation assays, an amplification step is required. Table 1.2 summarizes some of the studies employed GNPs for detection of unamplified nucleic acids.

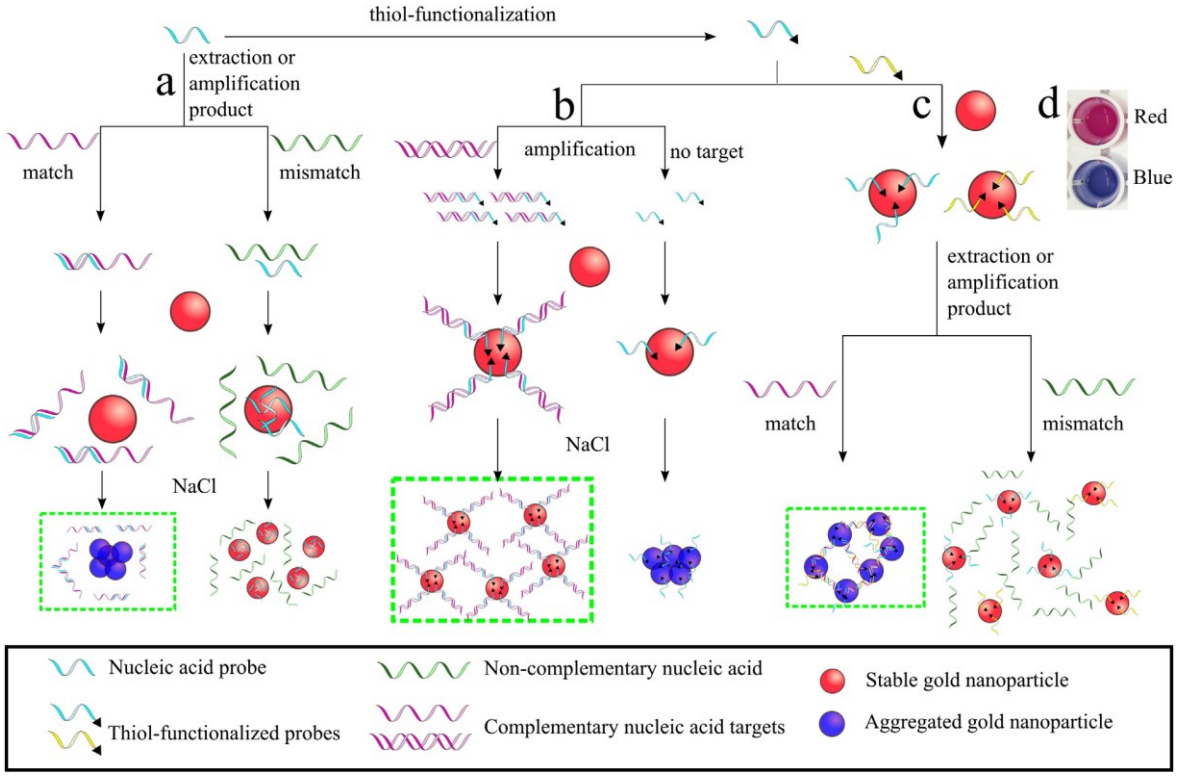

Figure 1.8. Schematic for different colorimetric detection of nucleic acids using GNPs. A) one probe (non-thiolated) strategy with citrate GNPs, b) one probe (thiolated) strategy with citrate GNPs, c) two probes (thiolated) with citrate GNPs, d) Image of aggregated (blue) and red (monodispersed) GNPs. Reprinted from Ref [132]. Copyright 2015 with permission from Elsevier.

Table 1.2. Amplification-free gold nanoparticle diagnostic assays for detection of nucleic acids.

Pathogen	Purpose of study	Assay time	Limit of detection	Reference
S. enterica	Detection of pathogen	~15 min	2.2 x 10^7 DNA copies/ml	[132,146]
HIV-1 and *Bacillus anthracis*	Detection of pathogen	30 min	6 x 10^{10} DNA copies/ml	[132,147]
Herpes virus and *Bartonella*	Detection of pathogen	~2 hr	1 x 10^{12} DNA copies/ml	[132,148]

1.5.2.3.1 Improving sensitivity of GNPs assays using DNAzyme

DNAzymes are classes of nucleic acid enzymes that cleave other nucleic acids with multiple turnovers and therefore, can introduce a linear amplification step. Integrating the plasmon coupling of GNPs with DNAzyme has been demonstrated to be a promising strategy to provide a

simple and fast colorimetric detection of genetic targets in POC settings[149]. The successful application of this technique was demonstrated in the detection of dengue virus nucleic acid. DNAzyme was attached to the surface of 15 nm GNPs, the catalytic activity of the DNAzyme was then triggered by addition of magnesium ions which cleaves the viral RNA. The cleaved RNA induces aggregation of GNPs in the presence of salt and heat[149]. Another example included the integration of multicomponent nucleic acid enzyme (MNAzyme)[149] which is a type of DNAzyme with GNPs aggregation assay. This system consists of a set of GNPs aggregated (blue color) by intact linker DNA, and MNAzyme components that are activated in the presence of target DNA or RNA to cleave the linker DNA, re-distributing GNPs to a monodispersed state, thus producing red color (Figure 1.9). Although MNAzyme improved the analytical sensitivity of the assay by 600 times[150], this improvement in sensitivity is still insufficient for the detection of most pathogens which requires significantly higher sensitivity. Therefore, the sensitivity of the MNAzyme-GNPs assay needs to be further improved. In addition, clinical testing is needed to verify the capability of this assay to detect different pathogens in clinical samples.

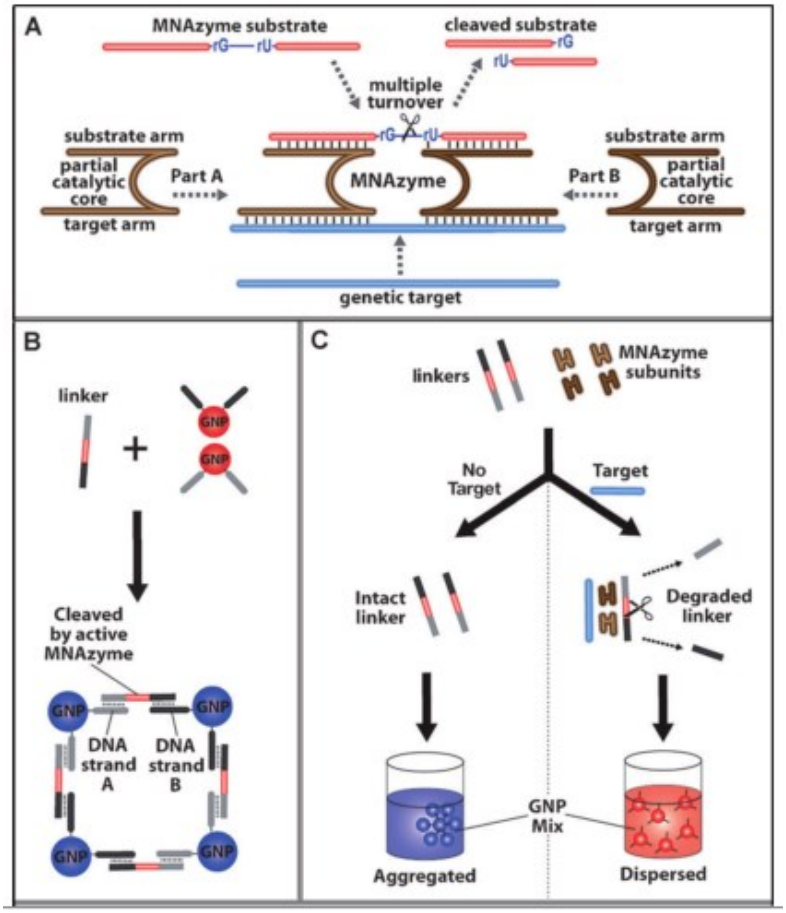

Figure 1.9. Schematic of MNAzyme-GNPs assay. A) Composition and catalytic activity of MNAzyme. MNAzyme is composed of two parts A and B, each of which contains substrate and target arms and a catalytic core. In the presence of target DNA, the addition of substrate activates MNAzyme which results in cleavage of multiple substrates. B and C) MNAzyme is activated by presence of target, which cleaves the linker DNA (substrate) rendering GNPs monodispersed. In absence of target the linker DNA remains intact due to inactive MNAzye hence, cause GNPs to aggregate. Reproduced from Ref [150]. Copyright 2013 with permission from Wiley-VCH Verlag GmbH & Co. KGaA, Weinheim.

1.5.2.3.2 Improving sensitivity of GNPs assays via amplification of nucleic acid

Amplification of target nucleic acids is another common method that has been implemented to improve the sensitivity of GNP assays (Table 1.3). In this format, the extracted DNA or RNA is first amplified to increase the concentration of nucleic acids prior to GNPs assays. Although the implementation of PCR improved the sensitivity of GNPs aggregation assays, PCR is limited by high costs and the need for bulky thermocycler. To overcome the limitations of PCR, isothermal amplification techniques have been developed and implemented into GNPs assays.

Unlike PCR, isothermal amplification techniques amplify nucleic acids at a constant temperature without the need for thermal cycling. Isothermal amplification techniques that have been incorporated into GNPs assays are rolling circle amplification (RCA), loop mediated isothermal amplification (LAMP), thermophilic helicase dependent amplification (tHDA), isothermal target and signaling probe amplification (iTPA), and nucleic acid sequence based amplification (NASBA). Taking into account the limitations associated with these techniques, the utilization of these isothermal techniques in POC settings becomes very challenging. For example, RCA can only amplify circular DNA or plasmids, and if linear DNA is used, there is a need to circularize it which adds more complexity [132,151]. LAMP and tHDA require pre-denaturation step (95 ºC), and they operate at high constant temperature (~60 ºC) [152,153].

Recombinase polymerase amplification (RPA) is an isothermal amplification technique that operates at constant temperature (37 ºC) using the same primer designs as PCR, without the need for pre-denaturation step. It has similar sensitivity to PCR, and can be done within 30 minutes. Figure 1.10 describes the RPA process: RPA uses a recombinase enzyme that bind to the forward and reverse primers, facilitated by ATP. Once the nucleoprotein is formed, it scans the double stranded DNA and at homologous sites the nucleoprotein structure creates, D-loop like structures to allow primers to bind to the single stranded DNA. The DNA polymerase then binds to the primers at 3' end and starts the extension, producing a complementary DNA strand [154]. Owing to its advantages, RPA provides a simple and rapid amplification method that can be potentially used for developing highly sensitive POC diagnostic assays.

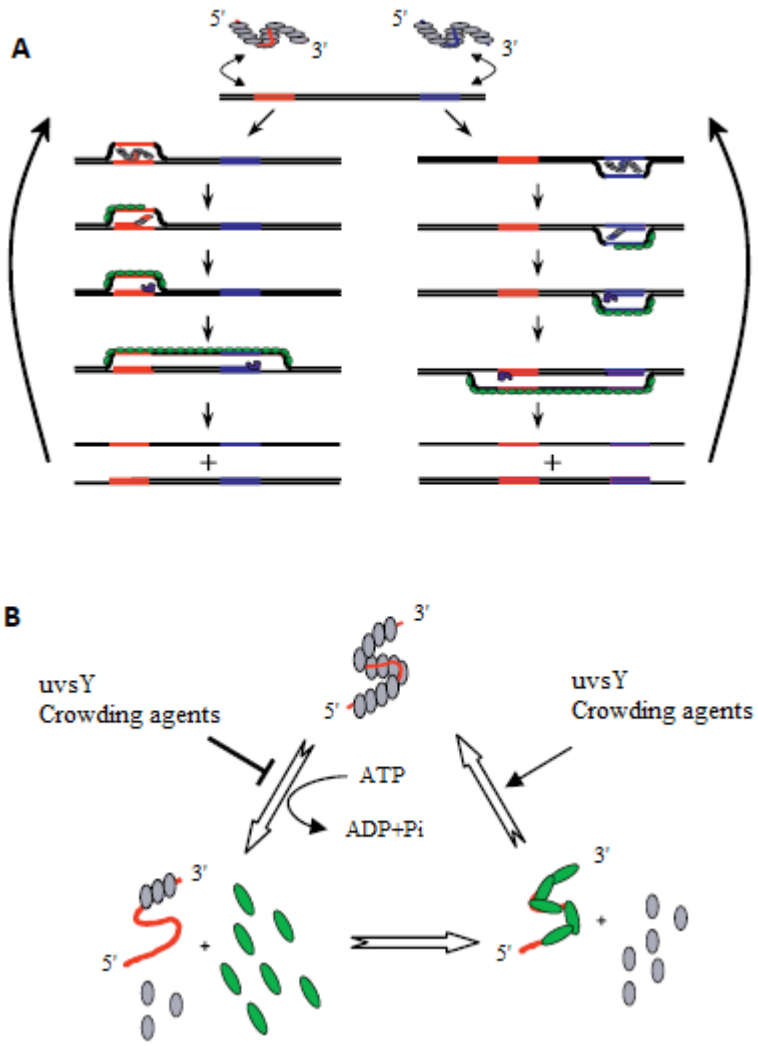

Figure 1.10. Recombinase polymerase amplification. A) The process of amplification. Recombinase protein binds to the primers and scans DNA target for homologous sequence which allows binding of primers. Primers are then extended by DNA polymerase to form new complementary strand. B) The formation of nucleoprotein complex which is mediated by ATP. Reproduced with permission from Ref [154]. Copyright 2006 Piepenburg et al.

Table 1.3. Amplification-based gold nanoparticle diagnostic assays for detection of nucleic acids.

Organism	Sample source	Purpose of study	Amplification method	Time	Limit of detection	Reference
S. aureus	Blood, urine, wound swabs, respiratory samples, pus and body fluids	Detection of pathogen and methicillin resistance	PCR	~1.5 hr	-	[142]
Chlamydia trachomatis	Urine	Detection of pathogen	iTPA	1.5-2 hrs	$5x10^3$ DNA copies/ml	[144]
S. typhimurium	Culture	Detection of pathogen	NASBA	~2.5 hr	-	[155]
InflA virus	Nucleic acid	Detection of pathogen	RT-PCR	2.5 hr	3.2×10^{11} RNA copies/ml	[132,156]
Lieshmania major	Skin biobsy	Detection of pathogen	NASBA	~1.5 hr	-	[157]
HIV-1 and *Troponema pallidum*	Serum	Detection of pathogen	PCR	~ 6 hr	10^4 DNA copies/ml	[132,158]
InflA H1N1 virus	Nucleic acid	Detection of pathogen	RCA	3 hr	6.02×10^8 DNA copies/ml	[132,151]
Neisseria gonorrhoeae, T. pallidum, HBV *and Plasmodium flaciparum*	Synthetic targets	Detection of pathogen	MNAzyme	1.5-2 hrs	~10^{10} DNA copies/ml	[150]
Dengue virus	Nucleic acid	Detection of pathogen	DNAzyme	5 min post extraction	2.2×10^7 RNA copies/ ml	[149]
M. tuberculosis	Culture	rifampin resistance	PCR	~2.5-3 hr	-	[159]
M. tuberculosis	Culture	rifampin resistance	LAMP	~ 1.5 hr	-	[152]
Helicobacter pylori	Gastric biobsy	Detection of pathogen	tHDA	~ 1 hr	10^4 CFU/ml	[153]

1.5.3 Photo-thermal therapy using gold nanoparticles for treating Infectious disease and antimicrobial resistance

As mentioned previously, the successful control of IDs and AMR not only requires accurate diagnosis but also delivery of effective treatments. Nonetheless, the diagnosis of MDR pathogens in some cases might be inadequate for infection control, particularly if the available antibiotics are ineffective. Furthermore, the decreased trend in producing new antibiotics drives the world to the pot-antibiotic era[114,160]. This necessitates the development of new alternative therapeutics that can target and destroy various microbes with minimal risk of developing AR.

Heat has shown to destroy microbial cells by means of physical destruction via disruption of cell membrane, fatty acid melting, and protein/enzymes denaturation[161]. Since most of microbes comprise of the same cell membrane structure, mainly of protein and fatty acids, heat can be effective against wide range of different microbes. However, one challenge in using heat to treat microbial infections is to accurately and selectively deliver the desired amount of heat to the infected area without damaging the healthy tissue. The conventional thermal techniques such as ultrasound, microwaves, and radiofrequency have been used for cancer treatment. Taking into account the inability of these techniques to focus heat into small areas, limited energy penetration depth, poor tissue heat transfer, need for designing sophisticated heat applicators, and risk of harming healthy tissue, it will be very challenging to use these systems for microbial cell disinfection[162]. Therefore, there is a need to develop convenient techniques that have the ability to control heat delivery at small scales.

Inorganic nanoparticles, GNPs in particular, can generate heat upon light exposure. When the frequency of incident light matches the SPR absorption peak, GNPs can then produce heat via non-radiative decay. A monochromatic light source, typically a laser light, with SPR matching wavelength is used for this purpose. In this process, the excited hot electrons transfer their energy to the lattice upon relaxation. This process is followed by phonon-phonon interaction in which the lattice energy is dissipated to the surrounding medium, resulting in local heating around the nanoparticles. This process is known as photo-thermal therapy (PTT)[118,121,123–125]. The amount of heat generated by GNPs can be controlled by either changing laser power or concertation of GNPs in the medium. Hence, GNPs can provide fine control and homogenous distribution of heat compared to the conventional heating probes[162]. Additionally, the surface of GNPs can be

functionalized with targeting ligands such as antibodies to specifically target diseased cells which minimizes undesired off target effect.

PTT using GNPs has been demonstrated in many biomedical application including tumor ablation, disease diagnosis and controlled drug release[115,117,163–167]. Previous studies have also demonstrated that PTT can be used to kill AR bacteria *in vitro*[168–173]. The first demonstration of PTT for microbial cell killing *in vitro* was reported by Zharov et al[174]. In this study, spherical GNPs were functionalized with monoclonal antibody that targets protein A on the surface of *S. aureus* (gram-positive). The bacterial killing was achieved after incubation of GNPs with *S. aureus* followed by laser irradiation[174]. In another study by Norman et al, the PTT using antibody conjugated NRs have been shown to selectively kill MDR *P. aeruginosa* (gram-negative) *in vitro* [168]. The selective PTT killing of *salmonella sp* (gram negative) using anti-salmonella antibody conjugated GNPs have been demonstrated by incubating these particles with *E. coli* bacteria. No antibacterial effect was observed against *E. coli* whereas, 97% of bacterial death was achieved against *salmonella sp*, which indicates that the PTT is highly selective[170]. These studies illustrate the potential of GNPs-PTT as a versatile technique that can be used to kill various types of bacteria and thus treat different types of infections. Although these are promising results, further research is required to test the efficacy and the safety of this technique *in vivo*.

1.6 Thesis overview

This thesis therefore builds on the development of GNPs-based techniques for diagnosing and treating IDs and AMR. The facile synthesis of different shapes and sizes of GNPs, as well as their unique physicochemical properties have enabled the development of robust yet rapid and simple platforms for diagnosing and treating IDs and AMR. However, current GNPs-based diagnostic assays are limited by low diagnostic sensitivity and the lack of clinical validation. Additionally, the GNPs-based PTT techniques are hindered by lack of proper design that would facilitate their translation from *in vitro* to *in vivo* to treat microbial infections associated with AMR. Therefore, the objectives of this thesis are to: i) develop a simple and ultra-sensitive nano-diagnostic assay for the detection of IDs in clinical samples, ii) demonstrate the ability of the developed nano-diagnostic assay to detect MDR by detecting multiple AMR biomarkers in parallel, and iii) develop a novel PTT platform using a combination of NRs and a thermo-

responsive polymer (*i.e.* plasmonic thermogel) for the treatment of AMR infections *in vivo*. These platforms are demonstrated in chapters 2, 3 and 4.

Chapter 2 investigates the incorporation of RPA into MNAzyme-GNPs system to develop a sensitive, rapid, and instrument-free diagnostic assay for POC testing. The integration of RPA into MNAzyme-GNPs assay was assessed by measuring the analytical sensitivity of the assay with and without RPA. The capability of the assay for detecting two viral pathogens HBV and FluA (which represent diagnosis of both DNA and RNA viruses) using patient samples was investigated by measuring the clinical sensitivity and specificity levels.

Chapter 3 demonstrates the detection of MDR in bacteria using a parallel MNAzyme-GNPs assay combined with a multiplexed RPA format. Three AR bacterial isolates were screened to demonstrate the ability of the assay to detect multiple AR genes without cross-reactivity.

Chapter 4 describes the development of a versatile plasmonic thermogel that consists of a thermally sensitive polymer and NRs for photo-thermal killing of AR bacteria. The antimicrobial activity of the proposed technique against AR bacteria was assessed *in vitro*. An infected excisional wound was used as an *in vivo* model to test the ability of the technique to disinfect wounds contaminated with AR bacteria. Further, the safety of the technique on skin tissues and wound healing was assessed.

Chapter 5 concludes the achievements illustrated in the thesis and highlights potential future work and vision.

1.7 Author contributions

Chapter 1. Introduction.

***Mohamed Mohamed*:** performed the literature survey and wrote the introduction. The chapter was revised by Prof. Warren Chan.

Chapter 2. Colorimetric amplification system for point-of-care clinical diagnosis of viral infections.

***Mohamed Mohamed*:** helped with study design, developed the DNA sequences for MNAzyme and GNPs probes, synthesized and characterized the GNPs, carried out the MNAzyme-GNPs experiments, and processed the TLC images using ImageJ, analyzed the data and generated the figures.

Jisung Kim: initiated the idea of integrating RPA into MNAzyme-GNPs, developed the DNA sequences of primers and blocking strands, carried out the RPA experiments and post-RPA purification, gel electrophoresis, carried out the denaturation and blocking strand steps, helped with the figures design and wrote the manuscript which was revised by all authors.

Dr. Kyrylo Zagorovsky: initiated the idea of integrating RPA into MNAzyme-GNPs, helped with developing the DNA sequences for MNAzyme and GNPs probes.

***Abdullah Syed*:** developed the ImageJ macro to process TLC photographs.

Dr. Jordan Feld and Dr. Samira Mubareka: provided us with the extracted DNA and RNA from clinical samples

Dr. Warren Chan: provided expertise, guidance, contributed to the study design and revised the chapter.

This chapter has been adapted from the following paper (in the final stage of preparation):

> Kim J*, **Mohamed MAA***, Zagorovsky K, Feld J, Mubareka S, Chan WCW. Colorimetric amplification system for point-of-care clinical diagnosis of viral infections. *Manuscript in preparation*. (* these authors contributed equally).

Chapter 3. Colorimetric screening of antibiotic resistance using nucleic acid enzymes and gold nanoparticles**.**

Mohamed Mohamed: initiated the idea of the project, did the literature study to select the bacterial model and AR genes, performed all the bioinformatics analysis to select gene target sequences, deigned all primers, blocking strands, MNAzymes and GNPs probe sequences, developed and optimized the multiplex RPA reactions, carried out the denaturation and blocking strand steps, performed DNA extraction from bacterial cells, carried out MNAzyme-GNPs and antibiotic

susceptibility test experiments, processed the TLC images using ImageJ, analyzed the data, generated the final figures, and wrote the manuscript which was revised by all authors.

Jisung Kim: preformed the singleplex and multiplex RPA for the AR genes, post-RPA purification, gel electrophoresis, carried out the denaturation and blocking strand steps, helped with study design, figures generation, and data analysis.

Dr. Kyrylo Zagorovsky: helped with the initiation of the project idea, synthesized the GNPs and carried out the PCR experiments.

Dr. Warren Chan: provided expertise, guidance, contributed to the study design and revised the chapter.

This chapter has been adapted from the following paper (in the final stage of preparation):

> **Mohamed MAA***, Kim J*, Zagorovsky J, Chan WCW. Colorimetric screening of antibiotic resistance using nucleic acid enzymes and gold nanoparticles. *Manuscript in preparation*. (* these authors contributed equally).

Chapter 4. A versatile plasmonic thermogel for disinfection of antimicrobial resistant bacteria.

***Mohamed Mohamed*:** synthesized and characterized NRs, developed temperature profiles, carried out all the in vitro testing of PTT against bacteria, designed the initial animal experiments, wrote the animal protocol, carried out the in vivo experiments, analyzed the data and generated the final figures.

Dr. Vahid Raeesi: initiated the idea of using PVCL as dispersion media for NRs, developed and provided the protocols for synthesis and characterization of NRs, sat up the laser system, helped with thermal analysis experiments, helped with the initial design of the animal experiments, contributed to data analysis and wrote the first draft of the manuscript which was followed by Mohamed Mohamed and then revised by all authors.

Mr. Rainer Deguzman: performed all wound surgeries.

Dr. Kate Banks: helped with the initial design of the animal experiment, choosing the animal model, collected the skin samples for histology analysis.

Dr. Patricia Turner**:** preformed all the histology analysis for the study.

Dr. Anu Rebbapragada**:** provided expertise, guidance, and helped with the initiation of the study.

Dr. Warren Chan: initiated the idea of using PVCL, provided expertise, guidance, contributed to the study design and revised the chapter.

This chapter has been adapted from the following paper:

> **Mohamed MAA***, Raeesi V*, Turner P, Rebbapragada A, Banks K, Chan WCW (2016). A versatile plasmonic thermogel for disinfection of antimicrobial resistant bacteria. *Biomaterials*. 97:154-163.

Chapter 2
Colorimetric amplification system for point-of-care clinical diagnosis of viral infections

2.1 Introduction

As mentioned in section 1.2, the current diagnostic approaches to combat the spread of IDs such as microscopy, culture, LFA, and ELISA are hindered by lack of sufficient simplicity of use, sensitivity and specificity, precluding their use at POC settings. On the other hand, PCR, the gold standard technique for detection of genetic elements offers higher detection sensitivity and specificity. However, PCR requires an expensive equipment and skilled technicians limiting its use in low-income countries[95]. As a result, there has been an increasing demand for developing rapid, cost-effective and sensitive POC diagnostic tests[11,175,176]. This will allow the health-care providers to make their treatment decisions in a time effective manner by removing the need to send the samples to centralized laboratories[11].

Unlike fluorescence and electrochemical-based diagnostic assays, colorimetric based assays do not require an instrument for signal readout, which make them ideal for POC testing. As discussed in section 1.5.2, GNPs are ideal candidates for developing colorimetric based assays. However, these assays are limited by low sensitivity. The integration of MNAzyme into GNPs-based assays has been demonstrated to be a promising strategy to improve the sensitivity of these assays[150]. MNAzyme-GNPs system consists of a set of GNPs aggregated by intact linker DNA, and MNAzyme components that are activated in the presence of target DNA to cleave the linker DNA, re-distributing GNPs to a monodispersed state. The switch of GNPs from aggregated to monodispersed state shifts the absorbance to a shorter wavelength, and correspondingly alters the solution color from dark purple to red[150]. The inclusion of MNAzyme was demonstrated to provide multiple turnovers of catalytic activity and improve the analytical sensitivity of GNPs based colorimetric assays by 600 times which corresponds to $10^7 – 10^9$ DNA copies/μL when synthetic DNA targets were used [150]. However, the limit of detection (LOD) requirement for clinical diagnosis of many viral diseases such as HBV, HCV, HIV, and FluA is much lower (10^3-10^4 DNA copies/μL). Therefore, the analytical sensitivity of the MNAzyme-GNPs assay needs to be further improved by a very significant factor. In a recent study, similar improvement in analytical sensitivity has already implemented quantitatively in the context of quantum dot barcode assay[177].

This involved introduction of RPA step to pre-amplify viral DNA prior to the fluorescence-based detection step. Therefore, the goal of this chapter was to integrate RPA into MNAzyme-GNP assay to: i) improve the analytical sensitivity of the assay and ii) establish the clinical validation of the assay by screening clinical specimens in a blinded-experiment and measuring clinical sensitivity and specificity levels. RPA was used for nucleic acid amplification because it is simple to use and it operates at a constant low temperature (37~40 °C), which removes the difficulty of using an expensive thermocycler as in PCR and can be performed within 30 min[154].

2.2 Materials and Methods

2.2.1 Infectious pathogens

Two viral pathogens were chosen for this study, HBV and FluA, to represent diagnosis of both DNA and RNA viruses. HBV represents one of the major blood borne and sexually transmitted infections while FluA represents one of the major viral respiratory infections.

2.2.2 Selection of target regions and design of primers, blocking strands, MNAzyme and GNPs probe.

The genetic sequences of HBV DNA and FluA RNA were obtained from the national center for biotechnology information (https://www.ncbi.nlm.nih.gov). The nucleic acid sequences were screened using Basic Local Alignment Search Tool (BLAST) (https://www.ncbi.nlm.nih.gov) to select the most conserved region. New primers were designed for each conserved region using primerQuest Tool from Integrated DNA Technologies, Inc., (https://www.idtdna.com/Primerquest/Home/Index) to produce amplicon sizes of 100bp for HBV virus and 242bp for FluA virus. Same bioinformatics tools were used to develop specific blocking strands, MNAzymes and GNPs probes.

2.2.3 Synthesis and conjugation of 13nm GNPs

13 nm GNPs were synthesized using citrate reduction method, pioneered by the Chan group. Solution containing 98 mL of water and 1 mL of 1% $HAuCl_4$ were brought to a rapid boil in aqua regia (30 mL HCl, 10 mL nitric acid) prewashed 250 mL flask on a benchtop stir plate (set to 300°C). 1 mL of 33 mg/mL of sodium citrate tribasic solution was then quickly added, and solution kept heated and stirring for another 10 min, then cooled on ice. NPs size and

monodispersity (PDI < 0.1 accepted) were measured by dynamic light scattering. Tween-20 was then added to a final concentration of 0.01% (v/v) and NPs were concentrated by centrifugation at 12,000g for 35 min. NPs concentration was measured by UV-vis spectroscopy at λ=520 nm (extinction coefficient 2.33×10^8 M^{-1} cm^{-1}), then adjusted to 100 nM using 0.01% (v/v) Tween-20 solution. To functionalize NPs surface with thiolated DNA (DNA-SH), 100 μL of 100 nM GNPs were mixed with 100 μL of DNA strand (2.5 μM for GNPs probe 1 and 10 μM for GNPs probe 2), 40 μL 0.1% (v/v) Tween-20 and 60 μL water. Solution was incubated for 5 min at room temperature. 100 μL of 100 mM trisodium citrate (pH 3) buffer was then added, and mixture further incubated for 30 min at room temperature to allow DNA to adsorb onto GNPs. NPs surface was then backfilled with polyethylene glycol (PEG) by adding 50 μL of 2 mM 1000 kDa methoxy and thiol terminated polyethylene glycol (m-PEG-SH) and incubated for 30 min at 60°C. NPs were washed by 3X centrifugation at 16,000g for 35 min, re-suspended in 0.01% (v/v) Tween-20 solution, and concentration was adjusted to 11 nM.

2.2.4 Extraction of DNA and RNA from Clinical Specimens

DNA samples for HBV test were extracted from serum of patients and healthy subjects. Serum samples were collected by venipuncture in a Vacutainer, which were stood upright for 0.5 to 1 hour, spun in a refrigerated centrifuge, aliquoted and stored at -80 °C until later use. DNA was extracted from the aliquots using Chemagic Viral DNA/RNA Kit (PerkinElmer). RNA samples for FluA test were extracted from mid-turbinate nasal from patients presenting with febrile respiratory illness at a tertiary acute care center. Samples (200 μL) were extracted with EZ1 XL or EZ1 virus mini kit version 2 (Qiagen), eluted in 60 μL and stored at -80 °C.

2.2.5 RPA and rt-RPA, and Purification

RPA was performed using the TwistAmp Basic kit (TwistDx), forward and reverse primer pairs (Bio Basic Inc.), and extracted DNA samples. HPLC-purified primers were purchased, and prepared at a concentration of 100 pmol/μL in TE buffer, diluted to 10 pmol/μL aliquots, and stored at 4 °C until later use. For measurement of analytical sensitivity, a premix solution containing 2.4 μL of each forward and reverse primers (10 pmol/μL), 29.5 μL of rehydration buffer, 12.2 μL of nuclease-free water, and 2.5 μL of magnesium acetate (280 mM), and 1 μL of the serially diluted DNA samples (10^{-1} to 10^{10} copies/μL) was prepared to make a total volume of

50 μL. For the negative controls, 1 μL of nuclease-free water was added instead of extracted DNA. For measurement of clinical sensitivity and specificity, the premix solution contained 9.2 μL of nuclease-free water and 4 μL of the extracted DNA, and NTCs included 4 μL of nuclease-free water instead of extracted DNA. This solution was then transferred to a tube containing the lyophilized enzyme pellet, mixed and incubated at 37 °C for 30 min.

Reverse transcription (rt-RPA) was performed using the TwistAmp Basic RT kit (TwistDx), forward and reverse primer pairs (Bio Basic Inc.), RNAse Inhibitor (BioShop Canada Inc.), and extracted RNA samples. A premix solution containing 2.6 μL of forward primer, 3.0 μL of reverse primer, 29.5 μL of rehydration buffer, 1.4 μL of nuclease-free water, 1 μL of RNAse inhibitor (40 units/μL), and 2.5 μL of magnesium acetate (280 mM), and 10 μL of extracted RNA was prepared to make a total volume of 50 μL. For NTCs, 10 μL of nuclease-free water was added instead of extracted RNA. This solution was then transferred to a tube containing the lyophilized enzyme pellet, mixed and incubated at 40 °C for 30 min.

RPA and rt-RPA products were then purified using EZ-10 spin column DNA gel extraction kit (Bio Basic Inc.), eluted into 50 μL, visualized by agarose gel electrophoresis, and stored at 4 °C until later use.

2.2.6 Denaturation and Blocking of Amplicons

For the measurement of analytical sensitivity, 1 μL of purified RPA product, 2 μL of blocking strands mix (final concentration of 50 pmol/μL for each strand) and 2 μL of TE buffer were mixed, incubated at 95 °C for 10 min, and incubated for 10 min at 40 °C. For the measurement of HBV clinical sensitivity and specificity, 2 μL of purified RPA product, 4 μL of blocking strands mix (final concentration of 50 pmol/μL for each strand) and 4 μL of TE buffer were mixed, incubated at 95 °C for 10 min, and incubated for 10 min at 40 °C. For the measurement of FluA clinical sensitivity and specificity, 5 μL of purified rt-RPA product and 2 μL blocking strands mix (final concentration of 50 pmol/μL for each strand) were mixed, incubated at 95 °C for 10 min, and incubated for 10 min at 40 °C

For the chemical denaturation, 1 μL of RPA product, 2 μL of blocking strands mix (final concentration of 50 pmol/μL for each strand), and 1 μL of NaOH (0.1 M) were mixed, incubated at room temperature for 5 min, and neutralized by adding 1 μL HCL (0.1 M).

2.2.7 MNAzyme-GNP Assay

For the measurement of analytical sensitivity of HBV and FluA, 4 μL of blocked RPA amplicons of HBV or FluA samples were mixed with 1 μL of 10X MNAzyme buffer (0.1 M Tris-HCl, 0.5 M KCl, pH 8.3), 1 μL of 300 mM MgCl2, 1 μL of HBV or FluA MNAzyme (4 μM) 1 μL of 1 μM of linker for HBV or 1 uL of 0.7 μM of linker for FluA and 2 μL of water. For negative control, 5 μL of elution buffer and blocking strands mix were used. The mixture was incubated at 50 °C for 1 hour. After incubation, 10 μL of GNPs probe mixture was then added to the samples and negative control and incubated at 50 °C for 20 min to allow aggregation of GNPs. 3 μL of sample were then deposited on the surface of TLC plate. The remaining of the sample was measured using UV-vis spectrophotometer to record the peak absorbance wavelength. For the measurement of HBV and FluA clinical sensitivity and specificity, the same method mentioned above was used except that 6 μL of the blocked RPA amplicons were used for both HBV and FluA.

2.2.8 Quantification of RPA and rt-RPA products

The plasmid of known concentration (725 ng/μL) was serially diluted to make the following concentrations: 10, 5, 2.5, 1.25, 0.625, 0.312, 0.156 and 0 ng/μL. 6 μL of the DNA samples were mixed with 114 μL of SYBR Green (1X) to develop the standard curves, and measure the fluorescence signal of RPA or rt-RPA products. The fluorescence signals were measured using BMG Labtech plate reader. To calculate the concentration of RPA or rt-RPA products, the fluorescence signal of the sample was fitted into the equation of the line obtained from the standard curves. For instance, for HBV RPA product that was used to measure the analytical sensitivity, fluorescence signal of 123151 a.u. was fitted into the equation (y=19383x-991.5) to obtain the x-value of 6.4 ng/μL. This number was divided by the molecular weight of the amplicon (60586.25 g/mol for HBV and 149568.76 g/mol for FluA) to obtain the molar concentration and number of copies per μL.

2.2.9 Statistical analysis

Data were statistically analyzed using GraphPad Prism 6 and Microsoft Excel 2013. The student t-test was used for hypothesis testing between data pairs.

2.3 Results and Discussion

2.3.1 Synthesis and characterization of GNPs

13 nm GNPs was chosen in this work due to their ease of synthesis and functionalization, and reproducibility. UV-Vis spectrophotometer revealed that GNPs had a distinct absorbance peak around at 518 nm (Figure 2.1A). Further, the size of GNPs was confirmed by TEM (Figure 2.1B). After characterization, the surface of GNPs was modified with DNA-SH and then backfilled with m-PEG-SH to stabilize the GNPs. The DNA-GNPs were characterized using UV-vis spectrophotometry and gel electrophoresis. As shown in Figure 2.1A after surface modification, GNPs exhibited a peak shift by 5 nm with absorbance maxima at 523 nm. Additionally, the gel electrophoresis data revealed that DNA-GNPs migrated faster in the gel compared to citrate capped GNPs which were prone to aggregation, thus migrated slower (Figure 2.1C).

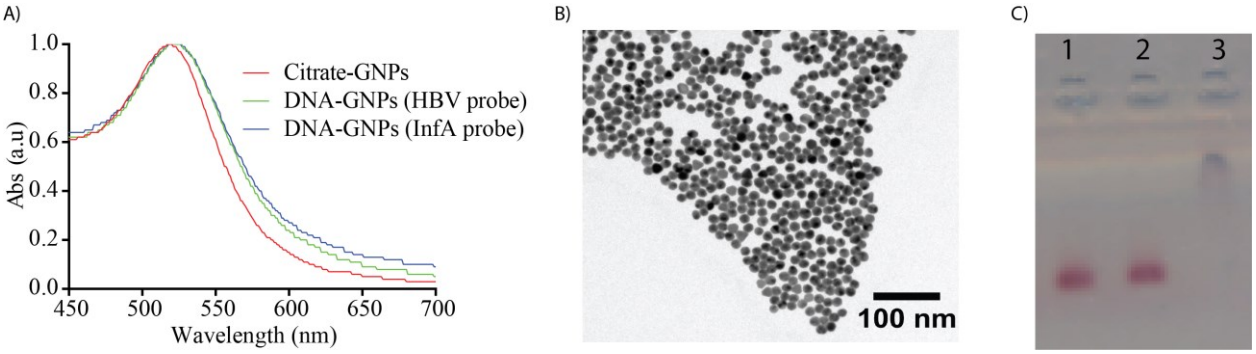

Figure 2.1. Characterization of GNPs. A) UV-vis spectrophotometry for citrate capped GNPs and DNA functionalized GNPs. After surface modification, the absorbance peak shifts by 5 nm. B) TEM image shows the shape and size of the GNPs. C) Gel electrophoresis image for 1) DNA-GNPs (HBV probe), 2) DNA-GNPs (FluA probe) and 3) citrate GNPs.

2.3.2 Colorimetric Amplification System

Figure 2.2 demonstrates the schematic of the colorimetric amplification system. Extracted viral DNA or RNA from a patient's serum (HBV) or nasal swab (FluA) was first amplified via RPA or RPA rt-RPA respectively. Purified amplification products were then thermally denatured,

and hybridized with blocking oligonucleotides to prevent re-hybridization with anti-sense strands. Such blocking strategy was proven to be effective in preventing re-hybridization of sense-strand of target DNA with its anti-sense strand, allowing hybridization with any other available DNA probes[178], and was confirmed to be an essential step in obtaining positive signals in our assay (Figure 2.3). Blocked amplicons were then mixed with MNAzyme and linker DNA, where the binding of the MNAzyme to amplicons activate the cleavage of linker DNA. Lastly, the reaction mixture was incubated with GNPs functionalized with DNA probes that were designed to hybridize with linker DNA. In the presence of target DNA, degraded linker fails to crosslink GNPs, leaving the particles monodispersed in the solution. This in turn results in a red color solution. In the absence of target, intact linker crosslinks GNPs resulting in a dark purple color. DNA sequences of primers, blocking oligonucleotides, MNAzyme, linker DNA and GNP probes for HBV and FluA are summarized in Table 2.1.

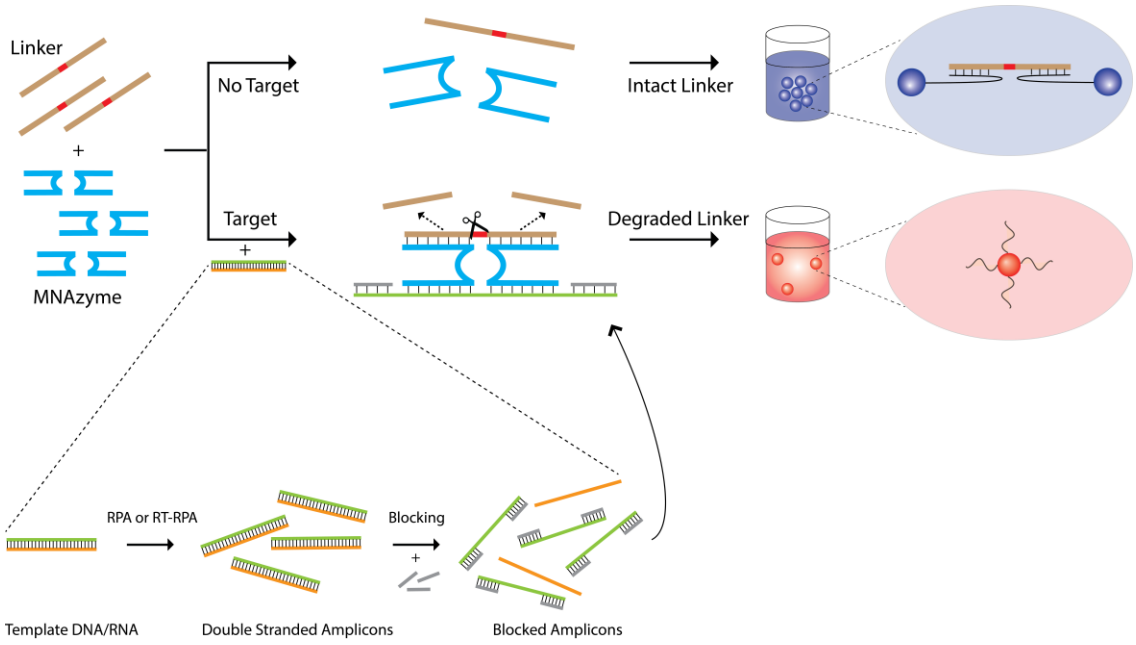

Figure 2.2. Schematic of colorimetric amplification system. Viral DNA or RNA is amplified via RPA or rt-RPA respectively followed by thermal denaturation and blocking of amplicons from re-hybridization. MNAzymes are activated by blocked amplicons, which cleave the linker DNA, distributing GNPs into a mono-dispersed state. GNPs aggregate with intact linkers in the absence of target DNA.

Table 2.1. List of DNA sequences.

	HBV (5' to 3')	FluA (5' to 3')
Forward Primer	TGTT GACAAGAATC CTCACAATAC CACAGAGTC	ATGAGYCTTY TAACCGAGGT CGAAACG
Reverse Primer	CGAA TTTTGGCCAG GACACACGGG TGTTCC	TGGACAAANC GTCTACGCTG CAG
Target	TGTT GACAAGAATC CTCACAATAC CACAGAGTCT AGACTCGTGG TGGACTTCTC TCAATTTTCT AGGGGGAACA CCCGTGTGTC CTGGCCAAAA TTCG	ATGAG TCTTCTAACC GAGGTCGAAA CGTACGTTCT CTCTATCATC CCGTCAGGCC CCCTCAAAGC CGAGATCGCG CAGAAACTTG AAGATGTCTT TGCAGGAAAG AACAC**C**GATC T**C**GAGGCTCT CATGGA**G**TGG CTAAAGACAA GACCAATCCT GTCACCTCTG ACTAAAGGGA TTTTGGGATT TGTATTCACG CTCACCGTGC CCAGTGAGCG AGGACTGCAG CGTAGACGCT TTGTCCA
Blocking Strand #1	TGTG GTATTGTGAG GATTCTTGTC AACA	CTTTCCTGCA AAGACATCTT CAAGTTTCTG CGCGATCTCG GCTTTGAGGG
Blocking Strand #2	CGAA TTTTGGCCAG GACACACGGG TGTTC	GGCCTGACGG GATGATAGAG AGAACGTACG TTTCGACCTC GGTTAGAAGA CTCAT
Blocking Strand #3	NA	TGGACAA AGCGTCTACG CTGCAGTCCT CGCTCACTGG GCACGGTGAG
Blocking Strand #4		CGTGAATACA AATCCCAAAA TCCCTTTAGT CAGAGGTGAC AGGATTGGT
MNAzyme Left arm	GACACAAAGAAGGCTAGCTGTCCACCA CGAGTCTAGACTC	CAAGATCGCTAGGCTAGCTGAGAGCCTC AAGATCTGTGTT
MNAzyme Right arm	CCCCTAGAAAATTGAGAGAAACAACGA TCTCTACGACT	CTTGTCTTTAGCCATTCCAT ACAACGAATAGTGTCACA
Linker DNA	GCGTCCCTCCTCGTATAGTCGTAGAGAR GRUTCTTTGTGTCTTCATACAATTGCACT	CGTCGCACTCACTCGTTGTGACACTATR GRUAGCGATCTTGTTGACTGTAAGCCAC C
GNPs probe 1	SS—AAAAAAAAAATACGAGGAGGGACGC	HS--AAAAAAAAAACGAGTGAGTGCGACG
GNPs probe 2	AGTGCAATTGTATGAAAAAAAAAAA--SS	GGTGGCTTACAGTCAAAAAAAAAAA--SH

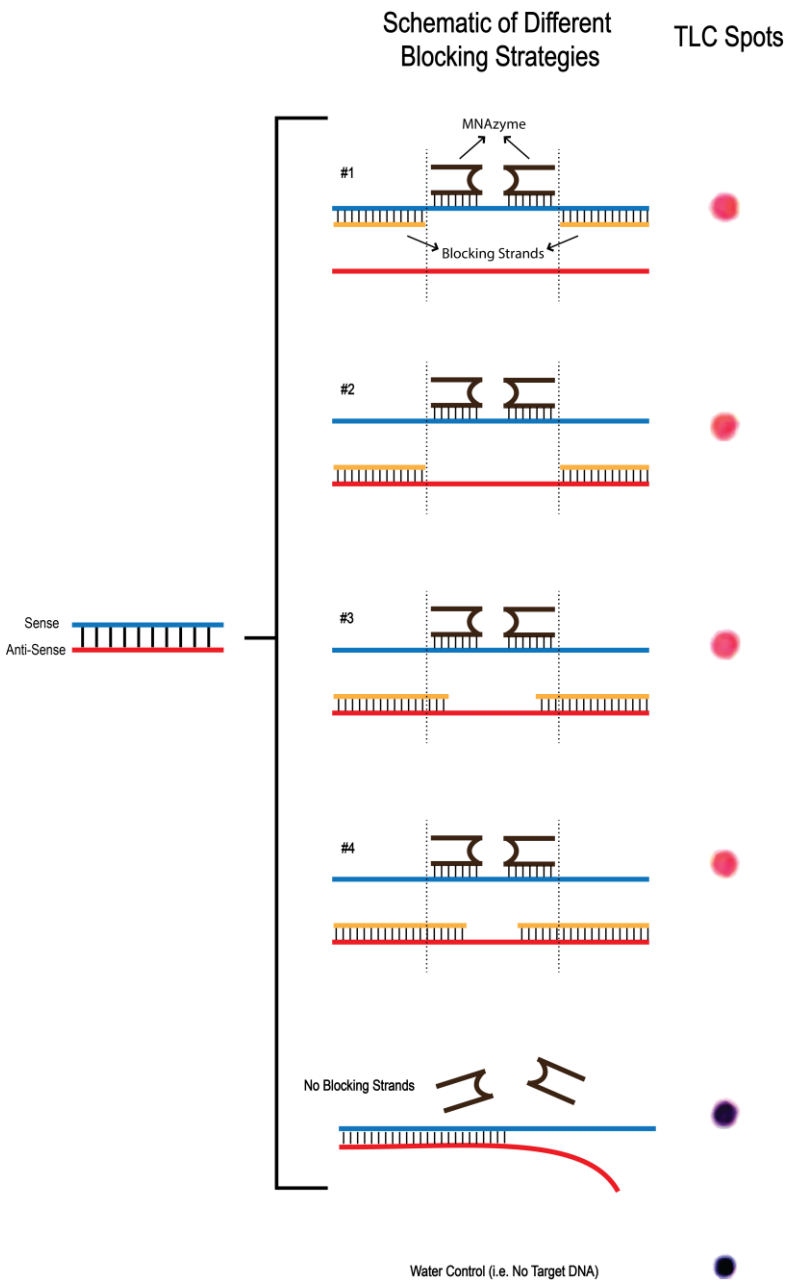

Figure 2.3. Schematic of blocking strategies and TLC spot images. Four blocking strategies were investigated and compared to the absence of blocking strands or target DNA: #1. 30 bp blocking strands hybridize to sense strand of the amplicon, #2. 30bp blocking strands hybridize to anti-sense of the amplicon, #3. 35 bp blocking strands hybridize to anti-sense strand of the amplicon, #4. 40 bp blocking strands hybridize to anti-sense strand of the amplicon.

2.3.3 Analytical Sensitivity

The analytical sensitivity of the assay was first compared with and without the incorporation of RPA for HBV and FluA genetic targets (Figure 2.4). To make 10^{10} and 10^{11} copies/μL target DNA samples for HBV and FluA, DNA and RNA extracted from clinical specimens (Sample# 41 in Table 2.2, and Sample# 40 in Table 2.3) were first amplified using RPA and rt-RPA respectively, and the concentrations were measured by mixing with SYBR Green and developing standard curves with a plasmid of known concentration (Figure 2.5). For instance, the post-RPA HBV DNA concentration was measured to be 6.4 ng/μL (Figure 2.5A), which is equal to $6.4x10^{10}$ copies/μL. Compared to the initial HBV DNA concentration in the RPA mixture ($=1.8x10^{4}$ copies/μL), this corresponds to an increase in the DNA concentration by 6-orders of magnitude. The amplification products were then serially diluted from 10^{10} to 10^{-1} copies/μL for HBV and 10^{11} to 10^{-1} copies/μL for FluA. The serially diluted samples were either directly denatured and blocked, or re-amplified via RPA, denatured and blocked prior to mixing with the assay components. After running MNAzyme-GNP assay, 3μL of the samples were deposited on a thin-layer chromatography (TLC) plate, and the peak absorbance wavelength of the solution was measured with a spectrometer to confirm the TLC plate result.

The inclusion of the additional amplification step demonstrated a significant improvement in the analytical sensitivity of the assay for both genetic targets. In the case of HBV detection, the TLC image reveals a shift in the spot color from dark purple to red at 10^{4} DNA copies/reaction with RPA, and 10^{10} DNA copies/reaction without RPA (Figure 2.4A). This corresponds to an enhancement in the detection limit by 6-orders of magnitude, and matches the amount of increase in the DNA concentration after RPA. Quantitatively, statistically significant difference ($P<0.001$) was measured in the peak absorbance wavelength at greater than or equal to 10^{4} DNA copies with RPA, and 10^{10} DNA copies without RPA when compared to the negative controls. In the case of FluA detection, there was an even greater enhancement in the analytical sensitivity. TLC image reveals a shift in the spot color at 10^{3} DNA copies/reaction with RPA, and 10^{11} DNA copies/reaction without RPA (Figure 2.4 B), which corresponds to an improvement in the detection limit by 8-orders of magnitude. Partially dispersed particles at 10^{3} DNA copies with RPA are qualitatively seen on the plate with a red ring surrounding the black spot image, and confirmed to have a statistically significant difference ($p<0.05$) in the peak absorbance wavelength when

compared to the negative control. The difference in the improvement of analytical sensitivities between HBV and FluA tests may be due to several factors. First, RPA efficiency can be hampered by the number and distribution of sequence mismatches as a result of genetic mutations at the primer binding sites, or due to primer-dependent artifacts[179]. Also, the catalytic activity of MNAzyme and aggregation of GNPs are dependent on the genetic sequences of amplicon and linker DNA respectively. These factors may account for the variance in the detection limits between HBV and FluA targets.

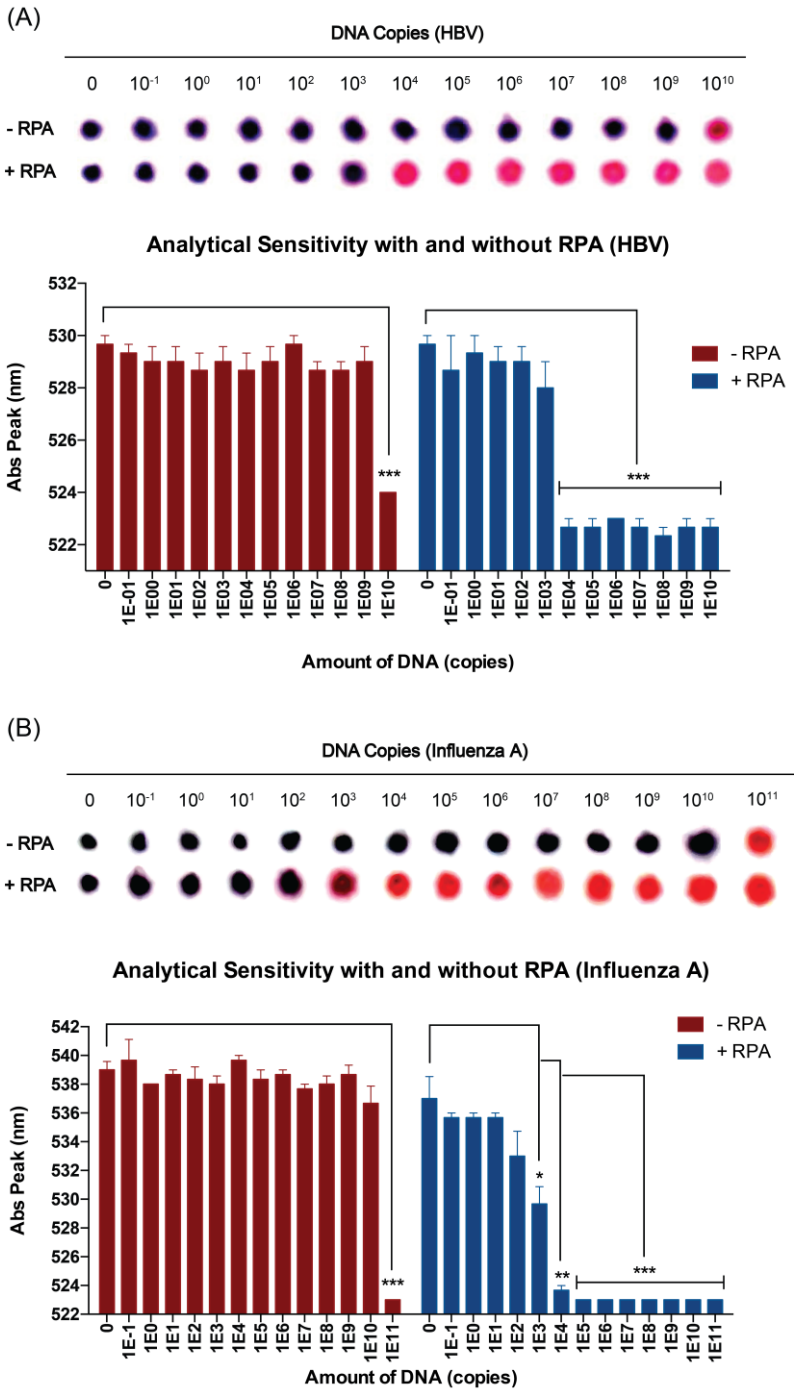

Figure 2.4. Analytical sensitivity with and without RPA. Varying amount of (A) HBV and (B) FluA DNA was amplified via RPA and detected with MNAzyme-GNPs assay. Spot images represent colorimetric readout on a TLC plate after adjusting for brightness and contrast on ImageJ. DNA copies refer to the amount of DNA per reaction. Bar graphs represent the wavelength of the absorbance peak. Error bars represent standard error of the mean from experimental triplicates. All statistics were calculated on excel using a two-tailed unpaired T-test assuming two-sample equal variance (*$p<0.05$, **$p<0.01$, and ***$p<0.001$).

Table 2.2. List of HBV samples.

Sample #	Serology			Genotype	HBV DNA (copies/μL)	Treatment History
	Core Ab	sAg	eAg			
Negative Samples						
1	-	-	-	N/A	N/A	N/A
2	-	-	-	N/A	N/A	N/A
3	-	-	-	N/A	N/A	N/A
4	-	-	-	N/A	N/A	N/A
5	-	-	-	N/A	N/A	N/A
6	+	-	-	N/A	N/A	N/A
7	+	-	U/A	N/A	N/A	N/A
8	+	-	-	N/A	N/A	N/A
9	+	-	U/A	N/A	N/A	N/A
10	+	-	-	N/A	N/A	N/A
11	+	+	-	U/A	Not Detectable	*On Treatment*
12	+	+	-	U/A	Not Detectable	*On Treatment*
13	+	+	-	U/A	Not Detectable	*On Treatment*
14	+	+	-	U/A	Not Detectable	*On Treatment*
15	+	+	-	U/A	Not Detectable	*On Treatment*
16	+	+	-	U/A	Not Detectable	*On Treatment*
17	+	+	-	U/A	Not Detectable	*On Treatment*
18	+	+	-	U/A	Not Detectable	*On Treatment*
19	+	+	+	U/A	Not Detectable	*On Treatment*
20	+	+	-	U/A	Not Detectable	*On Treatment*
21	+	+	-	U/A	Not Detectable	*On Treatment*
Positive Samples						
22	+	+	-	C	1.30E+02	Naive
23	+	+	-	C	2.00E+02	Naive
24	+	+	+	B	2.13E+02	Naive
25	+	+	+	A	2.58E+02	*On Treatment*
26	+	+	+	U/A	4.01E+02	Naive
27	+	+	+	U/A	1.84E+03	Naive
28	+	+	+	U/A	1.92E+03	Naive
29	+	+	+	U/A	2.61E+03	Naive
30	+	+	-	D	3.59E+03	Naive
31	+	+	+	A	3.72E+03	*Previous Treatment*
32	+	+	-	B	7.94E+03	Naive
33	+	+	+	U/A	1.66E+04	*On Treatment*
34	+	+	+	U/A	2.17E+04	*On Treatment*
35	+	+	+	U/A	3.58E+04	Naive
36	+	+	-	U/A	4.75E+04	*On Treatment*
37	+	+	+	U/A	5.37E+04	Naive
38	+	+	+	U/A	7.68E+04	Naive
39	+	+	-	U/A	9.66E+04	*On Treatment*
40	+	+	+	E	1.73E+05	Naive
41	+	+	+	B	2.27E+05	Naive

42	+	+	+	B	2.70E+05	Naive
43	+	+	+	D	3.62E+05	Naive
44	+	+	+	B	4.22E+05	Naive
45	+	+	+	E	4.87E+05	Naive
46	+	+	+	U/A	7.45E+05	Naive
47	+	+	+	B	9.84E+05	Previous Treatment
48	+	+	+	U/A	9.89E+05	Naive
49	+	+	+	B	9.89E+05	Naive
50	+	+	+	U/A	9.89E+05	Previous Treatment
51	+	+	-	B	1.20E+06	Naive
52	+	+	-	B	1.38E+06	*On Treatment*
53	+	+	+	B	1.92E+06	Naive
54	+	+	+	B	2.95E+06	Naive
55	+	+	-	C	3.19E+06	*On Treatment*
56	+	+	+	B	3.86E+05	Naive

Table 2.3. List of FluA samples.

Sample #	Virus	Year	FluA RNA (copies/µL)	RVP Fast MFI	
				Matrix	H3
Negative Samples					
1	ENR	U/A	N/A	N/A	N/A
2	ENR	U/A	N/A	N/A	N/A
3	ENR	U/A	N/A	N/A	N/A
4	HPMV	U/A	N/A	N/A	N/A
5	ENR	U/A	N/A	N/A	N/A
6	ENR	U/A	N/A	N/A	N/A
7	ENR	U/A	N/A	N/A	N/A
8	HPMV	U/A	N/A	N/A	N/A
9	ENR	U/A	N/A	N/A	N/A
10	PIV4	U/A	N/A	N/A	N/A
11	RSV	2014	N/A	N/A	N/A
12	ENR	2016	N/A	N/A	N/A
13	ENR	2016	N/A	N/A	N/A
14	RSV	2015	N/A	N/A	N/A
15	NEG	2016	N/A	N/A	N/A
16	NEG	2016	N/A	N/A	N/A
17	NEG	2016	N/A	N/A	N/A
18	RSV	2015	N/A	N/A	N/A
19	RSV	2015	N/A	N/A	N/A
20	ENR	2016	N/A	N/A	N/A
Positive Samples					
22	H3N2	2014	3.35E+04	2.87E+03	3.54E+03
23	H3N2	U/A	3.28E+05	2.49E+03	6.60E+02
24	H3N2	2015	7.83E+04	2.45E+03	1.80E+03
25	H3N2	2015	1.32E+05	2.87E+03	2.90E+03

26	H3N2	2015	5.04E+05	3.07E+03	3.92E+03
27	H3N2	2015	3.99E+03	2.61E+03	3.47E+02
28	H3N2	2015	2.11E+05	2.67E+03	2.70E+03
29	H3N2	2016	9.24E+05	1.75E+03	2.22E+03
30	H3N2	2016	4.80E+06	2.06E+03	1.99E+03
31	H3N2	2016	3.51E+06	2.40E+03	2.58E+03
32	H3N2	2016	1.21E+05	2.31E+03	8.58E+02
33	H3N2	2016	6.99E+04	2.44E+03	3.83E+02
34	H3N2	2016	3.31E+05	2.32E+03	1.57E+03
35	H3N2	2016	3.14E+06	2.45E+03	2.79E+03
36	H3N2	2016	4.69E+05	2.52E+03	1.70E+03
37	H3N2	2016	7.37E+05	2.20E+03	2.31E+03
38	H3N2	2016	1.75E+06	2.17E+03	1.19E+03
39	H3N2	2016	9.04E+05	6.03E+03	3.39E+03
40	H3N2	2016	U/A	2.06E+03	1.99E+03
41	H3N2	2016	U/A	2.52E+03	1.70E+03
42	H3N2	2016	U/A	2.20E+03	2.31E+03
43	H3N2	2016	U/A	2.45E+03	2.79E+03
44	H3N2	2016	U/A	2.17E+03	1.19E+03
45	H3N2	2016	2.49E+05	2.98E+03	1.36E+03
46	H3N2	2015	1.91E+05	2.93E+03	3.56E+03
47	H3N2	2015	2.60E+04	2.68E+03	1.24E+03
48	H3N2	2016	1.73E+06	2.04E+03	2.15E+03
49	H3N2	2016	7.66E+05	2.27E+03	1.79E+03

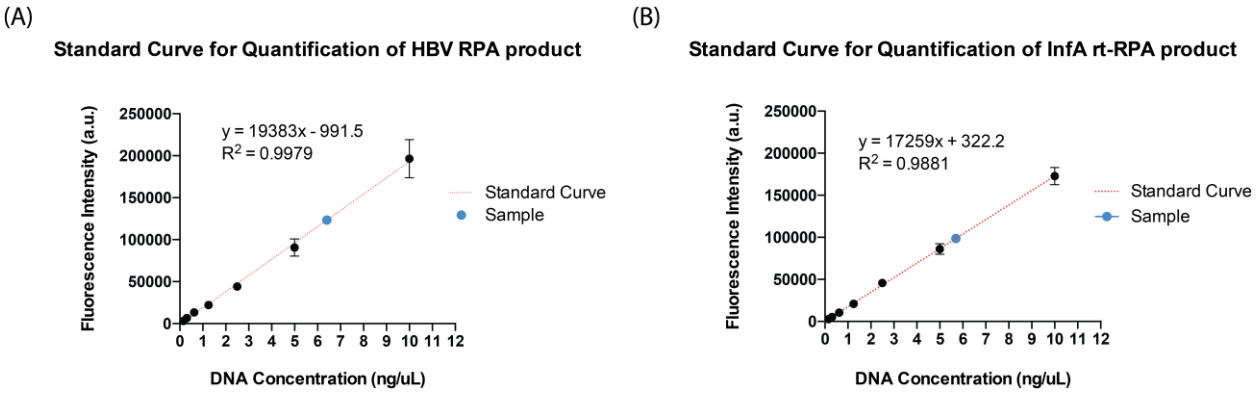

Figure 2.5.Quantification of RPA and rt-RPA products. Standard curves developed for the quantification (A) HBV RPA and (B) FluA rt-RPA products. Serially diluted plasmid of known concentration was mixed with SYBR Green (1X), and the fluorescence signal was measured using a plate reader. The fluorescence intensity of FluA rt-RPA sample was obtained from 18 times diluted concentration because the full concentration generated intensity level that is beyond the standard curve range. Error bars represent standard error of the mean from experimental triplicates

2.3.4 Clinical Sensitivity and Specificity

Next, the clinical sensitivity and specificity of the colorimetric amplification system was measured by screening clinical specimens in a blinded-experiment. The evaluation of emerging diagnostic technologies using clinical metrics is an important step in the translation of bench-side research work to clinical applications[180]. Clinical sensitivity and specificity indicate the degree of true-positive and true-negative rates compared to a reference diagnostic test respectively, and can directly influence the diagnostic decisions of healthcare providers [113,181]. HBV samples of various genotypes (A-E) and viral loads ($1x10^2$ to $3x10^6$ copies/μL) were selected to represent different spectrum of the disease (Table 2.2). For FluA test, H_3N_2 subtype was chosen with the viral loads ranging from $4x10^3$ to $5x10^6$ copies/μL (Table 2.3). For testing HBV, a total of 56 clinical samples (21 negative and 35 positive) were collected from Toronto Western Hospital Liver Clinic, and the presence of the infection was confirmed according to current clinical procedures by testing for HBV surface antigen (sAg), anti-hepatitis B core antibody (Core Ab), and HBV DNA (COBAS Amplicor HBV Monitor Test or COBAS AmpliPrep/COBAS TaqMan HBV Test v2.0). For FluA test, a total of 48 clinical samples (20 negative and 28 positive) were collected from Sunnybrook Health Sciences Centre, and tested for FluA RNA using the Luminex xTAG Respiratory Viral Panel Fast test. Extracted viral DNA and RNA from clinical specimens were amplified via RPA and rt-RPA respectively. Purified, denatured and blocked amplicons were then incubated with the MNAzyme assay components, transferred to GNP solutions, and spotted on a TLC plate. Detection of HBV viral DNA achieved a clinical sensitivity of 91.4% (95% CI, 75.8-97.8%), and a specificity of 95.2% (95% CI, 74.1-99.8%) (Figure 2.6A). FluA test achieved a clinical sensitivity of 92.9% (95% CI, 75.0-98.8%), and a specificity of 100.0% (95% CI, 80.0-100.0%) (Figure 2.6B). Two types of negative controls were used in these experiments to ensure correct interpretation of our diagnostic results. The first control was EBS control composed of elution buffer of DNA purification kit and blocking strands. This control was mixed with MNAzyme assay components and transferred to GNP solutions to confirm proper aggregation of GNPs with inactive MNAzyme and intact linker DNA. The second control was no template control (NTC), which replaced viral DNA or RNA with water in RPA or rt-RPA reactions to ensure that there is no target nucleic acid contamination in the reagents. These two controls confirmed that the positive signals are obtained by the selective activation of MNAzyme with amplicons, and not due to improper aggregation of

GNPs or contamination in RPA or rt-RPA reactions. The false-negative results (sample# 23-25 for HBV, and 27 and 47 for FluA) may be caused by genetic mutations that are prevalent in viral genomes hampering MNAzyme binding sites. The false positive results (sample#12 for HBV) may be attributed to the ability of RPA to tolerate the presence of 5-9 mismatches in the primers binding site[182]. Bioinformatics analysis on sequence variability can alleviate these problems by allowing the design of better degenerate primers and MNAzyme components that can tolerate few genetic mutations.

2.4 Conclusion

In conclusion, the work presented herein describes the integration of RPA into MNAzyme-GNP assay for POC diagnosis of viral infections. The incorporation of RPA improved the analytical sensitivity of the assay by 6-orders of magnitude for the detection of HBV, and by 8-orders of magnitude for the detection of FluA. Over 90% clinical sensitivity and 95% clinical specificity were measured when clinical specimens were screened using our colorimetric amplification system in a blinded manner. This system is well-suited for rapid, cost-effective and sensitive diagnosis of viral diseases in POC settings since the entire assay can be performed within 2 hours, does not require expensive equipment, and can detect as low as 10^3 copies of genetic materials. Although MNAzyme was incubated with amplicons and linker DNA for 1 hour in the experiments, the assay performance was also investigated at shorter incubation periods, and demonstrated that the assay can produce the same level of positive signals with 10 min of MNAzyme incubation (Figure 2.7). Hence, the entire assay can potentially be performed within 1 hour (30 min of RPA, 10 min of MNAzyme, and 20 min of GNP aggregation steps).

Chemical denaturation method will be incorporated in the near future to replace the thermal denaturation of amplification products. The denaturation of double-stranded RPA products was examined using NaOH [183], which was proven to be as effective as thermal denaturation method for generating single-stranded DNA that can hybridize with blocking oligonucleotides to prevent re-hybridization with anti-sense strands (Figure 2.8). This strategy will be useful in resource-limited settings where heating devices are unavailable for thermal denaturation of amplicons. Lastly, a field-testing with larger sample size is required to fully assess the capability of diagnosing patients in POC settings

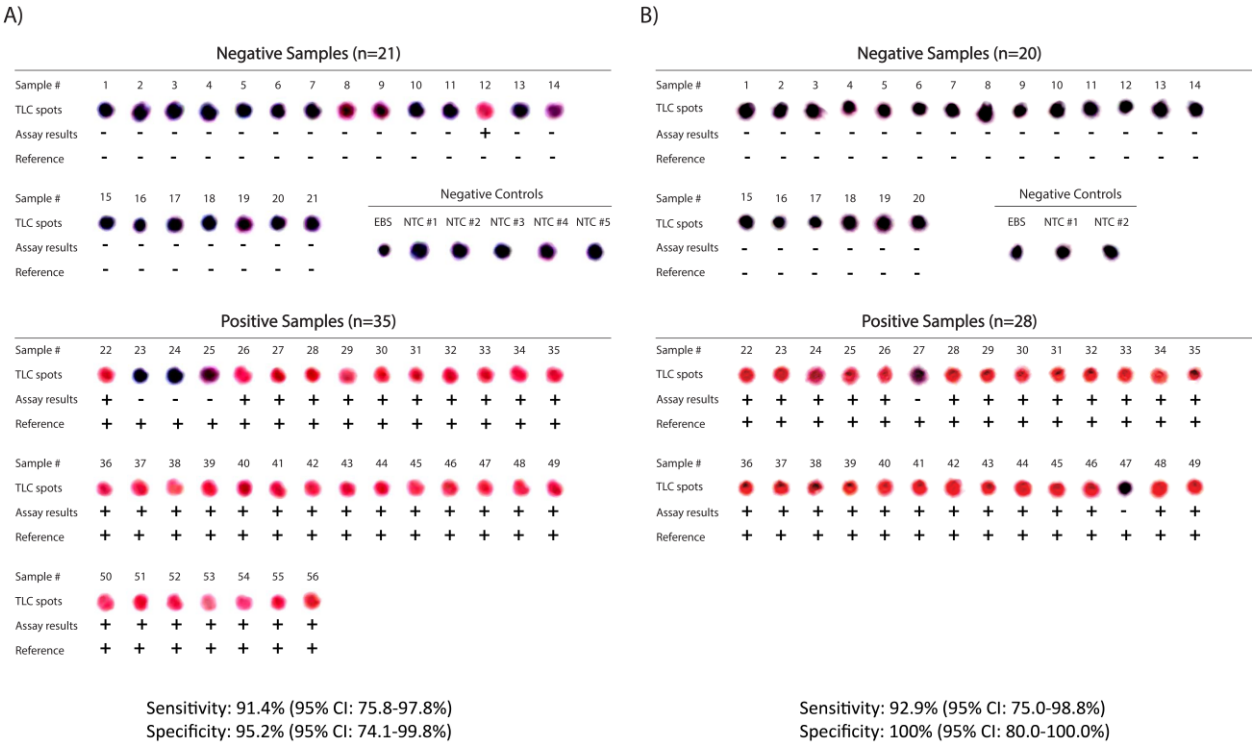

Figure 2.6.Clinical sensitivity and specificity measurements. Colorimetric readout of clinical samples on a TLC plate after adjusting for brightness and contrast on ImageJ for detection of (A) HBV viral DNA, and (B) FluA viral RNA. "EBS" refers to elution buffer blocking strands control, which was used to test the aggregation of GNPs. "NTC" refers to no template control, which was used to test contamination in RPA. "Reference" row indicates the diagnostic results from standard clinical tests. 95% confidence intervals were determined using the online calculator (http://vassarstats.net/clin1.html).

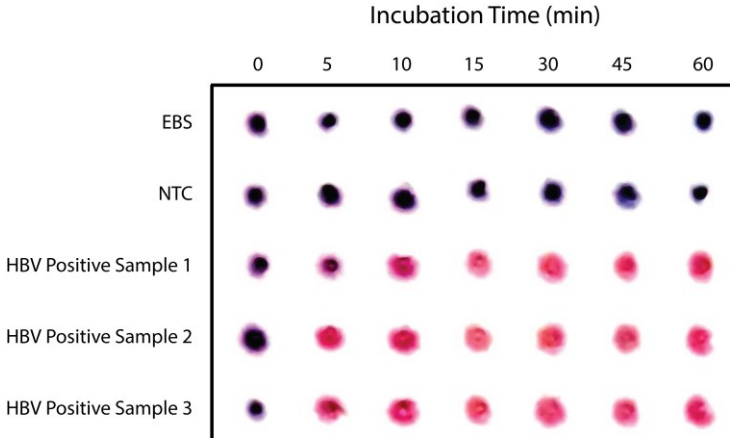

Figure 2.7. Shortening MNAzyme incubation time. Different MNAzyme incubation time periods (0, 5, 10, 15, 30, 45 and 60 min) were investigated with 3 HBV-positive samples. MNAzyme activation was effective down to 10 minutes of incubation.

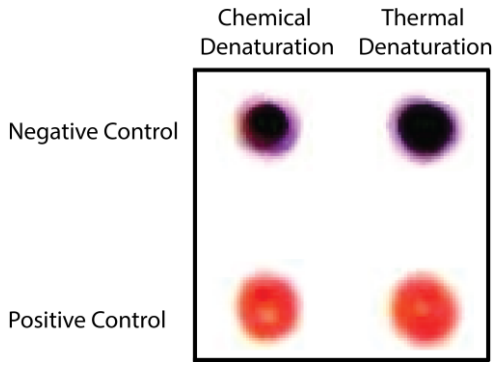

Figure 2.8. Chemical vs. thermal denaturation of RPA products. RPA products mixed with blocking oligonucleotides were denatured either chemically by incubating with NaOH or thermally by incubating at 95 °C.

Chapter 3
Colorimetric screening of antibiotic resistance using nucleic acid enzymes and gold nanoparticles

3.1 Introduction

Extensive and improper use of antibiotics have led to rapid evolution of AR[16–18,97]. In particular, there is an emerging trend of MDR pathogens, which have acquired resistances to multiple antibiotics. Rapid, accurate and sensitive diagnostic approaches that can detect multiple AR determinants are needed to enable healthcare-providers to provide appropriate therapy and reduce the development of new resistance mechanisms[16,98–100,107]. These techniques should be simple, instrument-free and adaptable for use in remote locations and in countries with limited resources where screening for AR is inadequate[112]. Currently, the two major laboratory techniques for detection of AR are phenotypic culture-based tests and genotypic tests. Although phenotypic culture methods such as agar diffusion, microdilution, or selective chromogenic media are cost-effective, they take 24-72 hours for an accurate diagnosis[98,99,102–104]. In addition, pathogens that carry AR genes can appear as phenotypically antibiotic sensitive due to the lack of gene expression or the decreased potency of the antibiotic, producing false-negative results[184–187]. This lack of resistance gene expression or the decreased potency of the antibiotic can be influenced by several environmental factors such as temperature, pH and NaCl content of the culture medium, and therefore the results might not represent actual bacterial resistance in human host[188,189]. In contrast, genotypic tests can directly detect the presence of AR genes, are not affected by testing conditions, and are often used to confirm inconclusive phenotypic test results[108–111] (Figure 3.1). Another advantage of these genotypic tests includes the improved safety, since they can be carried out using inactivated or sterilized samples [107]. The gold standard technique for genetic detection is qPCR. However, qPCR is expensive, uses complex equipment, and requires highly skilled technicians, precluding its use in resource-limited areas. To overcome the limitations associated with the current screening technologies for AR, there has been an effort to develop molecular technologies for screening AR such as microfluidic culture based techniques and nanomaterial-based nucleic acid assays[142,154,159,190–194]. However, these techniques are either phenotypic, have insufficient sensitivity, focus on detection of only a single AR determinant, or still rely on PCR for amplification of target DNA.

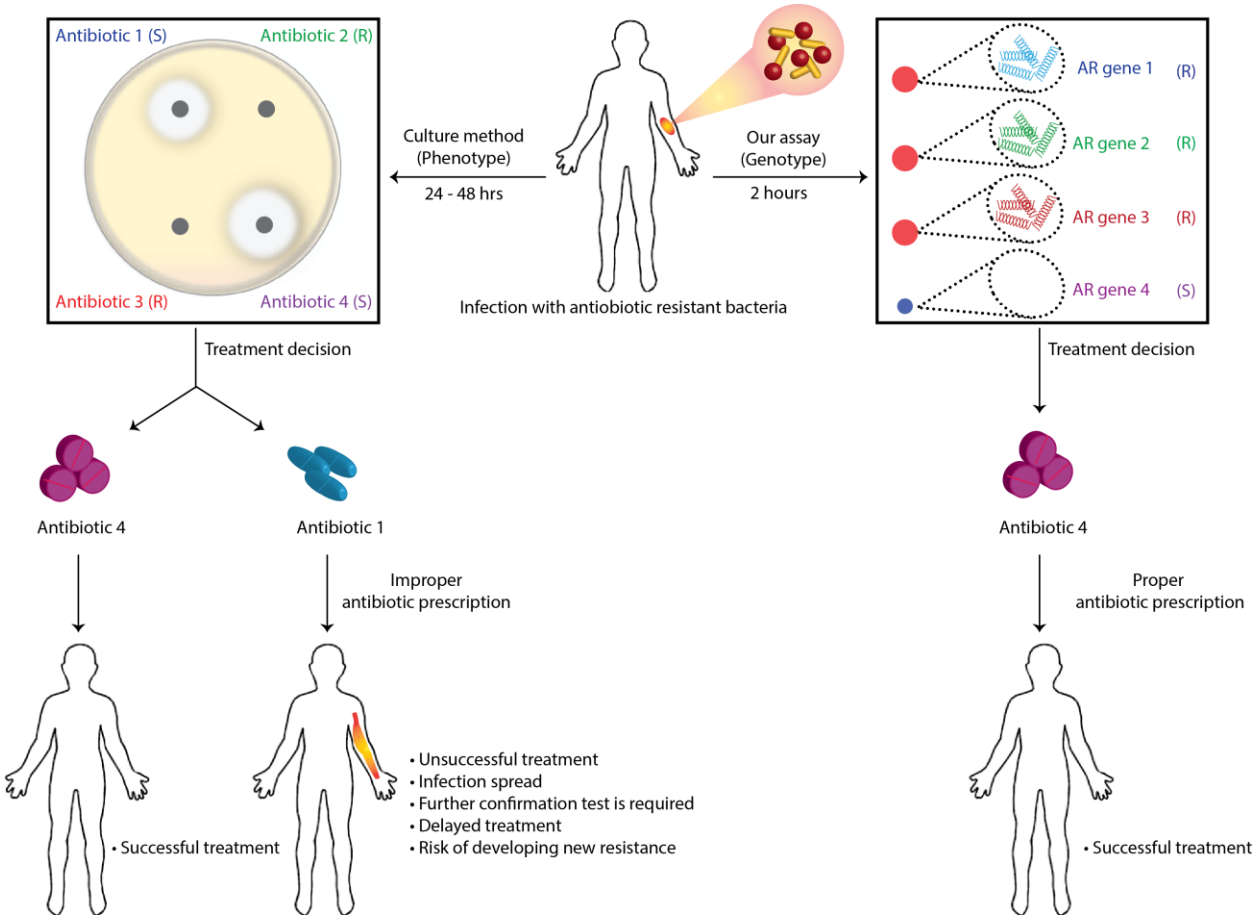

Figure 3.1. Utility of MNAzyme-GNPs assay. Utility of the MNAzyme-GNPs assay for AR identification and impact on treatment decision. Lack of gene expression can lead to the sensitivity of bacteria to antibiotic 1. This in effect can lead to increased risk of improper antibiotic prescription. On the other hand, MNAzyme-GNPs assay which is genotype based assay can detect AR genes directly and lead to proper antibiotic prescription.

This chapter describes development of an instrument-free and highly sensitive diagnostic assay that is capable of detecting and profiling multiple AR determinants. The assay was developed to detect 10 different genes responsible for resistance to 5 major antibiotics with detection limits of 10^2-10^3 CFU/ml of MRSA bacteria, which is the most common antibiotic resistant pathogen[195,196]. This was done via simultaneous amplification of AR genes using multiplex RPA and MNAzyme formats, followed by parallel colorimetric detection using different GNPs probes. This assay presents a method for simple and cost effective clinical detection and profiling of antibiotic resistance in bacterial pathogens, which can be easily adapted to both centralized and remote testing locations.

3.2 Material and Methods

3.2.1 Bacteria strains

Three different *S. aureus* strains were used in this study: *S. aureus* ATCC BAA-44 (MRSA-44), *S. aureus* ATCC BAA-41 (MRSA-41) and *S. aureus* ATCC 29213 (MSSA). MRSA was chosen in this study because it is one of the most common invasive antibiotic resistant pathogens acquired in hospital and is commonly associated with skin and soft tissue infection [195]. Moreover, MRSA strains have evolved and disseminated in the past 40 years causing serious hospital infections worldwide and accounted for 20-25% mortality rate in US [195–198].

3.2.2 Design of Antibiotic resistance genes target regions, primers and MNAzyme constructs.

Ten different antibiotic resistance genes that represent five different families of antibiotics were selected for this study. The genes were selected based on their common presence in *S. aureus* strains. The gene sequences were obtained from AR genes database (https://ardb.cbcb.umd.edu) and the national center for biotechnology information (https://www.ncbi.nlm.nih.gov). Then the gene sequences were screened using BLAST (https://www.ncbi.nlm.nih.gov) to select the most conserved region. New primers were then designed for each conserved region using primerQuest Tool from Integrated DNA Technologies, Inc. (https://www.idtdna.com/Primerquest/Home/Index) to produce amplicon sizes of 100bp (*mecA* and *balZ*), 125bp (*vanA* and *vanB*), 150bp (*tetK* and *tetM*), 201bp (*ermC*) and 219 (*ermA*) bp. The cross reactivity of all primers was examined using OligoAnalyzer 3.1 from Integrated DNA Technologies, Inc. (https://www.idtdna.com/calc/analyzer). Same bioinformatics tools were used to develop blocking strands, MNAzymes and GNPs probes All DNA oligonucleotides were purchased from Biobasic Canada Inc.

3.2.3 Synthesis and surface modification of gold nanoparticles

Solution containing 98 mL of water and 1 mL of 1% $HAuCl_4$ was brought to a rapid boil in aqua regia (30 mL HCl, 10 mL nitric acid) prewashed 250 mL flask on a benchtop stir plate (set to 300°C). 1 mL of 33 mg/mL of sodium citrate tribasic solution was then quickly added, and solution kept heated and stirring for another 10 min, then cooled on ice. NPs size and monodispersity (PDI < 0.1 accepted) were measured by dynamic light scattering. Tween-20 was

then added to a final concentration of 0.01% (v/v) and NPs concentrated by centrifugation at 12,000g for 35 min. NPs concentration was measured by UV-vis spectroscopy at λ=520 nm (extinction coefficient 2.33×10^8 M^{-1} cm^{-1}), then adjusting to 100 nM using 0.01% (v/v) Tween-20 solution. To functionalize NPs surface with thiolated DNA, 100 µL of 100 nM GNPs were mixed with 100 µL of DNA strand (2.5 µM for GNPs probe 1 and 10 µM for GNPs probe 2), 40 µL 0.1% (v/v) Tween-20 and 60 µL water. Solution was incubated for 5 min at room temperature, 100 µL of 100 mM trisodium citrate (pH 3) buffer was then added, and mixture further incubated for 30 min at room temperature to allow DNA to adsorb onto GNPs. NPs surface was then backfilled with PEG by adding 50 µL of 2 mM 1000 kDa m-PEG-SH and incubating for 30 min at 60°C. NPs were washed by 3X centrifugation at 16,000g for 45 min, re-suspended in 0.01% (v/v) Tween-20 solution, and concentration adjusted to 11 nM.

3.2.4 DNA extraction from bacterial cells

DNA was extracted from bacterial cells using DNA commercial extraction kits (GeneJET Genomic DNA Purification kit, ThermoFisher Scientific Inc.). For sensitivity curve, the number of freshly grown cells was adjusted to 10^7 CFU/ml and serially diluted to 10^0 CFU/ml in LB media. Cells were centrifuged at 5000g for 10 min. The supernant was removed and the cells were re-suspended in 160 µL of lysis buffer (2x TE, 1.2% triton x-100) followed by 10 µL of lysostaphine (Sigma Aldrich) and 10 µL of 20mg/ml lysozyme (Bioshop Canada). The cells were incubated at 37 ºC for 30 min. After incubation, 200 µL of lysis solution (kit component) were added and the mixture was incubated at 56 ºC for 30 min. The mixture was treated with 20 µL of proteinase K and 20 µL of RNAse. 400 µL of 50% ethanol was added and the mixture was transferred to the spin column for purification. The purified DNA was then eluted in 50 µL and stored at 4ºC for further use. For multiplex reaction, the DNA was extracted from bacterial cells at concertation of 10^5 CFU/ml and purified following the same procedure.

3.2.5 RPA

RPA was performed using the TwistAmp Basic kit (TwistDx), forward and reverse primers (Bio Basic Inc.), and target DNA samples. HPLC-purified primers were prepared at a concentration of 100 pmol/µL in TE buffer, diluted to 10 pmol/µL aliquots, and stored at 4 °C until later use. For the measurement of analytical sensitivity using synthetic DNA targets, a premix

solution containing 2.4 µL of each forward and reverse primers (10 pmol/µL), 29.5 µL of rehydration buffer, 12.2 µL of nuclease-free water, 2.5 µL of magnesium acetate (280 mM), and 1 µL of serially diluted DNA samples (10^0 to 10^{11} copies/µL) was prepared to make a total volume of 50 µL. For NTCs, 1 µL of TE buffer was added instead of target DNA. This solution was transferred to a tube containing the lyophilized enzyme pellet, mixed and incubated at 37 ºC for 30 min.

For singleplex screening of AR genes from bacteria, DNA was extracted from 10^7 CFU/mL MRSA-44, MRSA-41 and MSSA isolates. A premix solution containing 2.4 µL of each forward and reverse primers (10 pmol/µL), 29.5 µL of rehydration buffer, 12.2 µL of nuclease-free water, 2.5 µL of magnesium acetate (280 mM), and 1 µL of extracted DNA was prepared to make a total volume of 50 µL. For the NTCs, 1 µL of water was added instead of extracted DNA. This solution was transferred to a tube containing the lyophilized enzyme pellet, mixed and incubated at 37 ºC for 30 min.

For the measurement of analytical sensitivity using AR genes extracted from bacterial isolate (MRSA-44), a similar premix solution was prepared using 3.2 µL of nuclease-free water and 10 µL of extracted DNA from serially diluted bacteria (10^7-10^0 CFU/mL). For the NTCs, 10 µL of solution extracted from the media without bacteria was added instead of extracted DNA. This solution was then transferred to a tube containing the lyophilized enzyme pellet, mixed and incubated at 37 °C for 30 min.

For cross-reactivity test of the first multiplexed RPA group, a premix solution containing 7 µL of *blaZ* forward and reverse primer mix (5 pmol/µL per primer), 8 µL of *vanA* primer mix (5 pmol/µL per primer), 2.5 µL of *tetK* primer mix (5 pmol/µL per primer), 13 µL of *aph3iiia* primer mix (5 pmol/µL per primer), 3.5 µL of *ermA* primer mix (5 pmol/µL per primer), 145 µL of rehydration buffer, 53.5 µL of nuclease-free water, and 12.5 µL of magnesium acetate (280 mM) was prepared to make a total volume of 245 µL The premix solution was then mixed with a target mix containing 1 µL of *blaZ* (10^5 copies/µL), 1 µL of *vanA* (10^5 copies/µL), 1 µL of *tetK* (10^5 copes/µL), 1 µL of *aph3iiia* (10^5 copies/µL), and 1 µL of *ermA* (10^5 copies/µL) synthetic target DNA for "All" condition, or 1 µL of one of the five genes plus 4 µL of nuclease-free water to

make a final volume of 250 μL. NTC condition contained 5 μL of nuclease-free water instead of target DNA. For screening clinical isolates, a similar premix solution was prepared using 8.5 μL of nuclease-free water and 50 μL of DNA extracted from bacteria (10^5 CFU/mL). NTC contained 50 μL of water instead of extracted DNA. This solution was then transferred to a tube containing 5 lyophilized enzyme pellets, mixed, and incubated at 37 °C for 30 min.

For cross-reactivity test of the second multiplexed RPA group, a premix solution containing 4.8 μL of *mecA* forward and reverse primer mix (5 pmol/μL per primer), 4.8 μL of *vanB* primer mix (5 pmol/μL per primer), 3.5 μL of *tetM* primer mix (5 pmol/μL per primer), 4 μL of *acc6* primer mix (5 pmol/μL per primer), 3.6 μL of *ermC* primer mix (5 pmol/μL per primer), 118 μL of rehydration buffer, 45.5 μL of nuclease-free water, and 10 μL of magnesium acetate (280 mM) was prepared to make a total volume of 194.2 μL The premix solution was then mixed with a target mix containing 1 μL of *mecA* (10^5 copies/μL), 1 μL of *vanB* (10^5 copies/μL), 1 μL of *tetM* (10^5 copies/μL), 1 μL of *acc6* (10^5 copies/μL), and 1 μL of *ermC* (10^5 copies/μL) synthetic target DNA for "All" condition, or 1 μL of one of the five genes plus 4 μL of nuclease-free water to make a final volume of 199.2 μL. NTC condition contained 5 μL of nuclease-free water instead of target DNA. For screening clinical isolates, a similar premix solution was prepared using 50 μL of DNA extracted from bacteria (10^5 CFU/mL) without nuclease-free water. NTC contained 50 μL of water instead of extracted DNA. This solution was then transferred to a tube containing 4 lyophilized enzyme pellets, mixed, and incubated at 37 °C for 30 min. RPA products were then purified using EZ-10 spin column DNA gel extraction kit (Bio Basic Inc.), eluted to 50 μL, visualized by agarose gel electrophoresis (135 V, 3% agarose gel, 30-45 minutes), and stored at 4 °C until later use. Low molecular weight DNA ladder (New England Biolabls) was used.

3.2.6 Denaturation and Blocking of RPA products

For the measurement of analytical sensitivity using synthetic DNA targets and DNA extracted from clinical isolates, and singleplex screening of bacterial strains, 1 μL of purified RPA product or elution buffer (negative control), 2 μL of blocking strand mix (final concentration of 50 pmol/μL for each strand), and 1 μL of NaOH (0.1 M) were mixed, incubated at room temperature for 5 min, and neutralized by adding 1 μL of HCl (0.1 M) to the solution mix.

For cross-reactivity test and screening clinical isolates of the first multiplexed RPA group, 12 μL of purified RPA product, 1 μL of 5 blocking strands mix (20 pmole/μL of each strand mix), and 2.5 μL of NaOH (0.1M) were mixed, incubated at room temperature for 5 min, and neutralized by adding 2.5 μL of HCL (0.1M) to the solution mix.

For cross-reactivity test and screening clinical isolates of the second multiplexed RPA group, 6 μL of purified RPA product, 6 μL of 5 blocking strands mix (24 pmole/μL each strand mix), and 3 μL of NaOH (0.1M) were mixed, incubated at room temperature for 5 min, and neutralized by adding 3 μL of HCL (0.1M) to the solution mix.

3.2.7 MNAzyme-GNPs assay

For the measurement of analytical sensitivity of synthetic DNA targets and DNA extracted from clinical isolates, and singleplex screening of bacterial strains, 5 μL of blocked RPA amplicons of each gene or elution buffer was mixed with 1 μL of 10X MNAzyme buffer (0.1 M Tris-HCl, 0.5 M KCl, pH 8.3), 1 μL of 300 mM MgCl2, 1 μL of MNAzyme (4 μM), 1 μL of 1 μM of Linker DNA and 1μL of water. The mixture was incubated at 50 ºC for 1 hour. After incubation, 10 μL of GNPs probe mixture was then added to the samples and negative control and incubated at 50 ºC for 20 min to allow aggregation of GNPs. 3 μL of sample was then deposited on the surface of TLC plate. The remaining of the sample was then measured using UV-vis spectrophotometer to record the peak absorbance wavelength.

For cross-reactivity test and screening clinical isolates of the first multiplexed group, 18 μL of multiplexed blocked amplicons of the 5 genes of each group or elution buffer was mixed with 3 μL of 10X MNAzyme buffer (0.1 M Tris-HCl, 0.5 M KCl, pH 8.3), 3 μL of 300 mM MgCl2, 3 μL of 5 MNAzyme mixtures of the 5 genes (4 μM) and 3 μL of 1 μM of 5 different DNA linkers. The mixture was incubated at 50 ºC for 1 hour. After incubation, both the positive and negative control mixtures were pipetted out into 5 different tubes (5 uL in each tube), 5 μL of 5 different GNPs probes was then added to the samples and negative control and incubated at 50 ºC for 20 min to allow aggregation of GNPs. 3 μL of sample was then deposited on the surface of TLC plate.

3.2.8 PCR

PCR reactions were set up separately for each antibiotic resistance gene by mixing 12.5 µL of 2x PCR master Mix (Thermo Fisher), 0.5 µL of 10 µM primer mix, 11 µL nuclease free water, and 1 µL of template DNA product extracted from bacterial clinical isolates. 1 µL of 10^5 copies/µL of synthetic DNA was used as a positive control, and 1 µL of nuclease free water as negative control. PCR included 40 seconds 95ºC initial denaturation step, and was carried out for 40 cycles with each cycle including 30 seconds 95ºC denaturation, 30 seconds primer melting step (51ºC for *ErmC*; 54ºC for *mecA*, *blaZ*, *tetK*, *tetM*, *acc6*; 58ºC for *vanA*, *vanB*, Aph3, *ermA*), and 30 seconds 72ºC polymerase extension. The reaction was terminated by 4 min 72ºC extension, and cooling of the product to 4ºC. 3 µL of the product were visualized on 3% agarose gel.

3.2.9 Antimicrobial susceptibility test using agar diffusion method

Eight different antibiotic discs were purchased from Bacterius LTC, US and used in this experiment: penicillin (10 units), oxacillin (1 µg), vancomycin (30 µg), tetracycline (30 µg), minocycline (30 µg), gentamicin (10 µg), kanamycin (30 µg) and erythromycin (15 µg). The procedure was done following CLSI antimicrobial susceptibility testing guideline [102]. Briefly, fresh cultures of *S. aureus* strains was prepared from single colony on fresh Luria agar (LA) plates. Plates were incubated at 37 ºC for 24 hr. Three to five colonies of each culture were then transferred to 1 ml of 0.85% NaCl solution and the turbidity of the solution was adjusted to 0.5 McFerland standard. A sterile cotton swab was immersed into the cell suspension and rotated firmly several times against the upper inside wall of the tube to remove excess fluid. The swab was then used to inoculate the surface of Muller Hinton agar plates (MHA) plates by spreading the swab over the agar surface. The desired antibiotic discs were applied to the surface of the MHA plates using sterile forceps. The plates were incubated at 35 ºC for 16 hours. After incubation the diameter of inhibition zone was measured and compared to the CLSI antimicrobial susceptibility testing guideline tables to determine the antibiotic susceptibility of the bacterial strains.

3.2.10 Statistical analysis

Data were statistically analyzed using GraphPad Prism 6 and Microsoft Excel 2013. The student t-test was used for hypothesis testing between data pairs.

3.3 Results and Discussion

3.3.1 Assay design

Ten different AR genes were selected to represent 5 different classes of antibiotics: *balZ* gene for penicillin resistance, *mecA* gene for oxacillin resistance, *vanA* and *vanB* genes for vancomycin resistance, *tetK* and *tetM* genes for tetracycline resistance, *tetM* gene for minocycline, *acc6* and *aph3iiia* genes for gentamicin and kanamycin resistance, and *ermA* and *ermC for* erythromycin resistance. These genes were selected based on their common presence in *S. aureus* strains. While there are many genes responsible for antibiotic resistance (AR) in *S. aureus,* choosing the two most common genes responsible for resistance in each antibiotic can achieve high detection sensitivity. Twenty-four research papers were analyzed for the prevalence of the AR genes that were selected in this study. These studies included about 2599 *S. aureus* isolates that were collected from different sources and different geographical regions. As shown in Table 3.1, the selected AR genes show high prevalence rates between 83 to 96%. Thus, by selecting the most prevalent AR genes we can avoid screening large number of AR genes while achieving high diagnostic sensitivity[108,186,187,199–219]. All the gene sequences were screened using BLAST to select the most conserved region. Then, the primers were designed for each conserved region to achieve high specificity and minimal cross reactivity. Figure 3.2 depicts the schematic and description of the assay. Genomic DNA was first extracted from bacterial cells, followed by isothermal amplification of AR genes by RPA at 37ºC. The purified amplicons were chemically denatured using NaOH[183]. This chemical denaturation step was used to overcome the limitation of thermal denaturation which requires heating devices. This makes the proposed diagnostic assay more feasible for remote testing locations. The denatured amplicons were then mixed with blocking strands and the solution was neutralized with HCl to allow hybridization of blocking stands with the sense strand of the target gene. The blocked amplicons were then mixed with MNAzyme solution to allow hybridization of blocked amplicons with the MNAzyme sensor arms, which triggers the catalytic activity of MNAzyme. Target-activated MNAzyme binds “linker DNA” and cleaves it. The cleaved linker DNA fails to crosslink the GNPs rendering them monodispersed, which results in a distinct red color. In the absence of the target, the linker DNA remains intact and hybridizes with DNA probes on the surface of GNPs to produce a dark purple color due to crosslinking of GNPs. DNA sequences of RPA primers, sense-strand of target DNA,

MNAzyme components, linker DNA, GNP probes, and blocking strands are presented in Table 3.2 and Table 3.3.

Table 3.1. Prevalence of the selected antibiotic resistance genes.

Antibiotic class	Antibiotic	AR genes	Prevalence (%)	References
B-lactam	Oxacillin	*mecA*	96	108,199–204
	Penicillin	*blaZ*	99.5	187,204–207
Glycopeptides	Vancomycin	*vanA & vanB*	97.8	208,210,220
Tetracyclines	Tetracycline	*tetK & tetM*	93.2	108,186,204,211–214
Aminoglycosides	Gentamicin	*Acc6 & aph3iiia*	83	204,211,215
Macrolides	Erythromycin	*ermA & ermC*	91.2	108,204,213,216–219

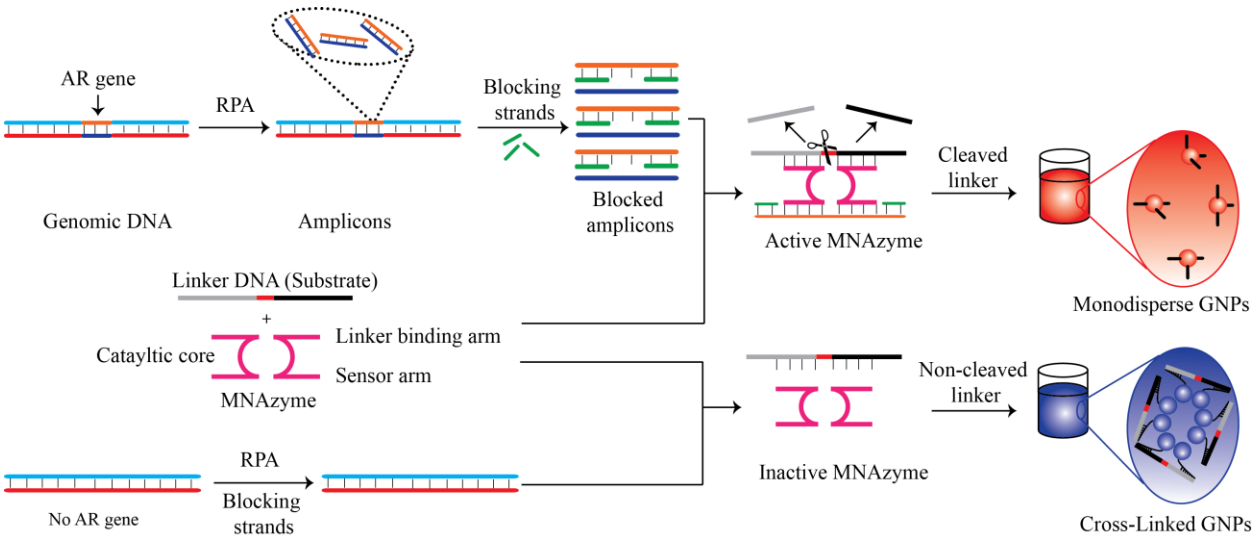

Figure 3.2. MNAzyme-GNPs assay description. Design of MNAzyme-GNPs assay. AR gene is amplified via RPA followed by chemical denaturation and blocking of amplicons from re-hybridization. MNAzyme is activated by blocked amplicons, which cleaves the linker DNA rendering GNPs monodispersed. In absence of AR gene the linker DNA remains intact due to inactive MNAzye hence, cause GNPs to aggregate. AR: antibiotic resistance, RPA: recombinase isothermal amplification.

Table 3.2. List of DNA sequences for the first group.

	blaZ (5' to 3')	*vanA* (5' to 3')	*tetK* (5' to 3')	*aph3* (5' to 3')	*ermA* (5' to 3')
FP	AAGATGATATAGTT GCTTATTCTCC	CAGTGCCGCGTTAG TTGTTG	CTGGAACCATGAGT GTTATTG	CGCGCGAGCTGTAT GATTT	AAGCGGTAAACCCC TCTGA
RP	TTATCACTATATGTC ATTGAAGCC	GGTCTGCGGGAACG GTTAT	TCAACCACATACTA AACTCAAC	CGGATGCAGAAGGC AATGT	CCAAAGCTCGTTGC AGATT
Target	AAGATGATATAGTT GCTTATTCTCCT ATTTTAGAAAAATA TGTAGGAAAAGATA TCACTTTAAAAGCA CTTATTG AGGCTTCAATGACA TATAGTGATAA	CAGTGCCGCGTTAG TTGTTGGCGAGGTG GACCAAATCAGGCT GCAGTACGGAATCT TTCGTATTCATCAGG AAGTCGAGCCGGAA AAAGGCTCTGAAAA CGCAGTT ATAACCGTTCCCGC AGACC	CTGGAACCATGAGT GTTATTGTTTTTGGT TATTTTGGTGGTTTT TTAGTGGATAGAAA AGGATCATTATTTGT TTTTATTTTAGGATC ATTGTCTATCTCTAT AAGTTTTTTAACTAT TGCATTTTTT GTTGAGTTTAGTATG TGGTTGA	CGCGCGAGCTGTAT GATTTTTTAAAGACG GAAAAGCCCGAAGA GGAACTTGTCTTTTC CCACGGCGACCTGG GAGACAGCAACATC TTTGTGAAAGATGG CAAAGTAAGTGGCT TTATTGATCTTGGGA GAAGCGGCAGGGCG GACAAGTGGTATG ACATTGCCTTCTGCA TCCG	AAGCGG TAAACCCCTC TGAGAATATA AAAGTGATTC AAACGGATAT TCTAAAATTT TCCTTCCCAA AACATATAAA CTATAAGATATATG GTAATA TTCCTTATAA CATCAGTACG GATATTGTCA AAAGAATTAC CTTTGAAAGT CAGGCTAAAT ATAGCTATCT TATCGTTGAG AAGGGATTTG CGAAAAGATT GCAAAATCTG CAACGAGCTTTGG
MNAzyme Left arm	GACACAAAGAAGGC TAGCTCTTTTCCTAC ATATTTTTCTA	GAATAGGTGCAGGC TAGCTACGAAAGAT TCCGTACTGCAG	CACGTGTTCTCAGGC TAGCTAAATAAAAA CAAATAATGATC	AATCCTATACAGGC TAGCTTCTTTCACAA AGATGTTGCTG	CAAGATCGCTAGGC TAGCTTCCGTACTGA TGTTATAAGGA
MNAzyme Right arm	AAGTGCTTTTAAAGT GATATACAACGATC TCTACGACT	GGCTCGACTTCCTGA TGAATACAACGATC GGAATTAAC	AGAGATAGACAATG ATCCTAACAACGAT ATGGTTTGCG	TAAAGCCACTTACTT TGCCAACAACGATC TGTCCAGCA	AGGTAATTCTTTTGA CAATAACAACGAAT AGTGTCACA
Linker DNA	GCGTCCCTCCTCGTA TAGTCGTAGAGARG RUTCTTTGTGTCTTC ATACAATTGCACT	GCCTTACTGCAACCC TGTTAATTCCGARGR UGCACCTATTCTCTC CCTGGTAGCTCG	ACATACATCGGCCA TTCGCAAACCATAR GRUGAGAACACGTG TAGCCTACTTTCCTC T	GAGTAACACCAATA ATTGCTGGACAGAR GRUGTATAGGATTT ACTACATGCCCTAC A	CGTCGCACTCACTCG TTGTGACACTATRGR UAGCGATCTTGTTG ACTGTAAGCCACC

GNPs probe 1	SS-- AAAAAAAAAATACG AGGAGGGACGC	SS-- AAAAAAAAAAGGGT TGCAGTAAGGC	SS-- AAAAAAAAAAATGG CCGATGTATGT	SS-- AAAAAAAAAATTAT TGGTGTTACTC	HS-- AAAAAAAAAACGAG TGAGTGCGACG
GNPs probe 2	AGTGCAATTGTATG AAAAAAAAAAA--SS	CGAGCTACCAGGGA GAAAAAAAAAA--SS	AGAGGAAAGTAGGC TAAAAAAAAAA--SS	TGTAGGGCATGTAG TAAAAAAAAAA--SS	GGTGGCTTACAGTC AAAAAAAAAAA--SH
BS #1	AAAT AGGAGAATAAGCAA CTATATCATCTT	CCTGATTTGGTCCAC CTCGCCAACAACTA ACGCGGCACTG	CTTTTCTATC CACTAAAAAA CCACCAAAAT AACCAAAAAC AATAACACTC ATGGTTCCAG	TCTCCC AGGTCGCCGT GGGAAAAGAC AAGTTCCTCT	ATATTACCAT ATATCTTATA GTTTATATGT TTTGGGAAGG AAAATTTTAG
BS #2	TTATCACTATATGTC ATTGAAGCCT CAAT	GGTCTGCGGGAACG GTTATAACTGCGTTT TCAGAGCCTTTTTCC	TCAACCACAT ACTAAACTCA ACAAAAAATG CAATAGTTAA AAAACTTAT	TCGGGCTTTT CCGTCTTTAA AAAATCATAC AGCTCGCGCG	AATATCCGTT TGAATCACTT TTATATTCTC AGAGGGGTTT ACCGCTT
BS #3	NA	NA	NA	CGGAT GCAGAAGGCA ATGTCATACC ACTTG	CCAAAGCTCG TTGCAGATTT TGCAATCTTT TCGCAAATCC
BS #4	NA	NA	NA	TCCGC CCTGCCGCTT CTCCCAAGAT CAA	CTTCTCAACG ATAAGATAGC TATATTTAGC CTGACTTTCAA

Table 3.3. List of DNA sequences for the first group.

	***mecA* (5' to 3')**	***vanB* (5' to 3')**	***tetM* (5' to 3')**	***acc6* (5' to 3')**	***ermC* (5' to 3')**
FP	AAGATATGAAGTGG TAAATGGT	CATGATGTGTCGGT AAAATCCG	GTGGAGCGATTACA GAATTAG	AGATTTGCCAGAAC ATGAA	AGTACAGAGGTGTA ATTTCG
RP	CTTACTGCCTAATTC GAGTG	TCCGTACATGGCTTC TTGCA	CTGGCGTGTCTATGA TGTT	CACACTATCATAAC CACTACC	ACAATTTTGCGTATT ATATCC
Target	AAGATATGAAGTGG TAAATGGT AATATCGACTTAAA ACAAGCAATAGAAT CATCAGATAACATTT TCTTTGCTAGAGTAG CACTCGAATTAGGC AGTAAG	CATGATGTGTCGGT AAAATCCGCAATAG AAATTGCTGCGAA CATTAATACTGAAA AATTCG ATCCGCACTA CATCGGAATTACAA AAAACGGCGTATGG	GTGGAGCGATTACA GAATTAGGAAGCGT GGACAAAGGTACAA CGAGGACGGATAAT ACGCTTTTAGAACGT CAGAGAGGAATTAC AATTCAGACAGGAA TAACCTCTTTTCAGT	AGATTTGCCAGAAC ATGAATTACACGAG GGCAAAAAAGAAGA TTGTTATTTAATGGA ATATAGATATGATG ATAATGCCACAAAT GTTAAGGCAATGAA ATATTTAATTGAGCA	AGT ACAGAGGTGT AATTTCGTAA CTGCCATTGA AATAGACCAT AAATTATGCA AAACTACAGA AAATAAACTTGTTG ATCACG

		AAGCTATGCAAGAA GCCATGTACGGA	GGGAAAATACGAAG GTG AACATCATAGACAC GCCAG	TTACTTTGATAATTT CAAAGTAGATAGTA TTGAAATAATC GGTAGTGGTTATGA TAGTGTG	ATAATTTCCA AGTTTTAAAC AAGGATATAT TGCAGTTTAA ATTTCCTAAA AACCAATCCT ATAAAATATA TGGTAATATA CCTTATAACA TAAGTACGGA TATAATACGC AAAATTGT
MNAzyme Left arm	GACACAAAGAAGGC TAGCTGATTCTATTG CTTGTTTTAAG	GAATAGGTGCAGGC TAGCT GAATTTTTCAGTATT AATGTT	CACGTGTTCTCAGGC TAGCTTCTGACGTTC TAAAAGCGTAT	AATCCTATACAGGC TAGCTAACATTTGTG GCATTATCATC	CAAGATCGCTAGGC TAGCTCAACAAGTTT ATTTTCTGTAG
MNAzyme Right arm	CAAAGAAAATGTTA TCTGATACAACGAT CTCTACGACT	ATTCCGATGTAGTGC GGATCACAACGATC GGAATTAAC	TGTCTGAATTGTAAT TCCTCACAACGATAT GGTTTGCG	ATTAAATATTTCATT GCCTTACAACGATCT GTCCAGCA	AACTTGGAAATTAT CGTGATACAACGAA TAGTGTCACA
Linker DNA	GCGTCCCTCCTCGTA TAGTCGTAGAGARG RUTCTTTGTGTCTTC ATACAATTGCACT	GCCTTACTGCAACCC TGTTAATTCCGARGR UGCACCTATTCTCTC CCTGGTAGCTCG	ACATACATCGGCCA TTCGCAAACCATAR GRUGAGAACACGTG TAGCCTACTTTCCTC T	GAGTAACACCAATA ATTGCTGGACAGAR GRUGTATAGGATTT ACTACATGCCCTAC A	CGTCGCACTCACTCG TTGTGACACTATRGR UAGCGATCTTGTTG ACTGTAAGCCACC
GNPs probe 1	SS-- AAAAAAAAAATACG AGGAGGGACGC	SS-- AAAAAAAAAAGGGT TGCAGTAAGGC	SS-- AAAAAAAAAAATGG CCGATGTATGT	SS-- AAAAAAAAAATTAT TGGTGTTACTC	HS-- AAAAAAAAAACGAG TGAGTGCGACG
GNPs probe 2	AGTGCAATTGTATG AAAAAAAAAAA--SS	CGAGCTACCAGGGA GAAAAAAAAAA--SS	AGAGGAAAGTAGGC TAAAAAAAAAA--SS	TGTAGGGCATGTAG TAAAAAAAAAA--SS	GGTGGCTTACAGTC AAAAAAAAAAA--SH
BS #1	TCGATATT ACCATTTACCACTTC ATATCTT	CGCAGCAAT TTCTATTGCG GATTTTACCG ACACATCATG	TATC CGTCCTCGTT GTACCTTTGT CCACGCTTCC TAATTCTGTA ATCGCTCCAC	ATATCTATAT TCCATTAAAT AACAATCTTC	TTTTGC ATAATTTATG GTCTATTTCA
BS #2	CTTACTGCCTAATTC GAGTG CTACTCTAG	TCCGT ACATGGCTTC TTGCATAGCT TCCATACGCC GTTTTTTGTA	CTGGCGTGTC TATGATGTTC ACCTTCGTAT TTTCCCACTG AAAAGAGGTT ATTCC	TTTTTTGCCC TCGTGTAATT CATGTTCTGG CAAATCT	ATGGCAGTTA CGAAATTACA CCTCTGTACT

BS #3	NA	NA	NA	CACACTATCA TAACCACTAC CGATTATTTC	ACAATTTTGCG TATTATATCC GTACTTATGT TATAAGGTAT ATTACCATAT
BS #4	NA	NA	NA	AATACTATCT ACTTTGAAAT TATCAAAGTA ATGCTCA	ATTTTATAGG ATTGGTTTTT AGGAAATTTA AACTGCAATA TATCCTTGTT TAA

3.3.2 Analytical sensitivity of detecting synthetic AR genes.

As mentioned in section 2.1, it has been shown that a standalone MNAzyme-GNPs assay can detect about $10^7 – 10^9$ synthetic DNA copies/µL[221]. However, this LOD is insufficient for clinical detection of AMR in *S. aureus,* which requires the sensitivity of 10^5 CFU/ml, which corresponds to 10^2 CFU/µL or DNA copies/µL[102,105]. Therefore, RPA was incorporated into MNAzyme-GNPs assay to significantly improve the detection limit of the system. This was done by comparing the analytical sensitivity of the assay with and without RPA. For the RPA condition, the 10 synthetic AR genes were serially diluted ($10^{11} – 10^0$ DNA copies/µL), and amplified using RPA. Both the amplified and non-amplified (i.e. serially diluted genes without RPA) targets were chemically denatured, blocked and added to the MNAzyme assay mixture to allow the cleavage process followed by the addition of GNPs probes for the signal readout. 3 µL of the samples were then deposited on TLC and observed for a color shift from purple to red as an indication for a positive signal. Data in Figure 3.3 shows that the RPA step significantly increased the analytical sensitivity for all genes by 8-9 order of magnitudes yielding a detection limit of 10^2-10^3 DNA copies/reaction (2-20 DNA copies/µL). This was indicated by the GNPs color shift from purple to red on the TLC plate and was confirmed quantitatively by measuring the peak absorbance wavelength using UV-Vis spectrophotometer Figure 3.4. Data shows that there is a significant difference in the peak absorbance wavelength at or greater than 10^2 DNA copies/reaction for *tetM*, *acc6*, *aph3iiia* and *ermA* genes (*P* value <0.0001 or <0.00001) and at or greater than 10^3 DNA copies/µL for all other genes (*P* value <0.0001 or <0.00001) when RPA is used. This confirms the need for RPA as a pre-amplification step in the assay to achieve clinically relevant limit of detection.

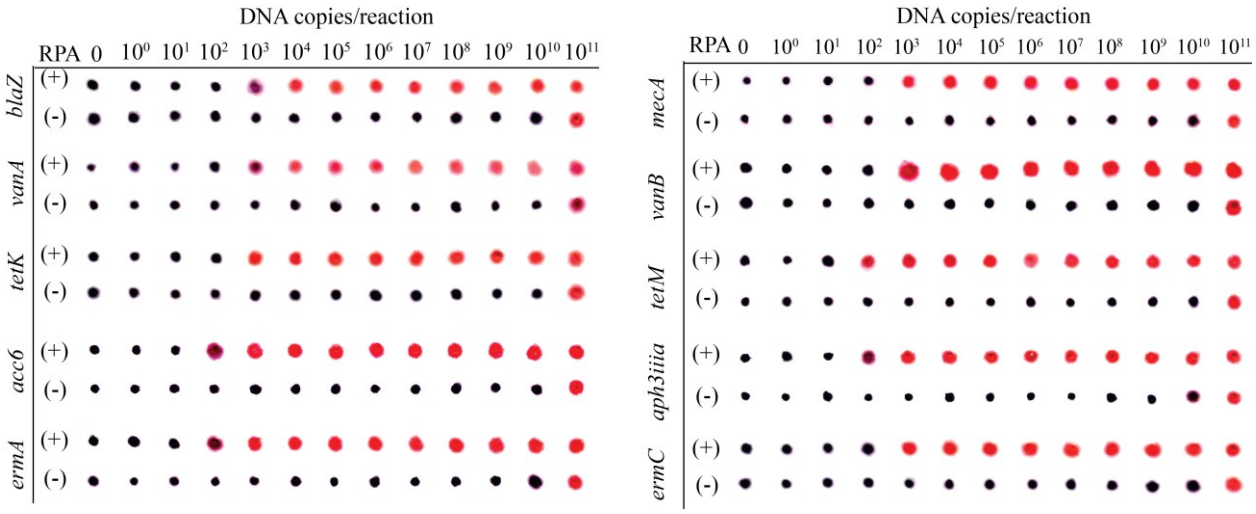

Figure 3.3.Analytical sensitivity of detecting AR genes with and without RPA. 10 synthetic AR genes were serially diluted, amplified via RPA and detected with MNAzyme-GNP assay. The assay results were compared to no RPA conditions. Spot images represent colorimetric readout on a TLC plate after adjusting for brightness and contrast on Image J.

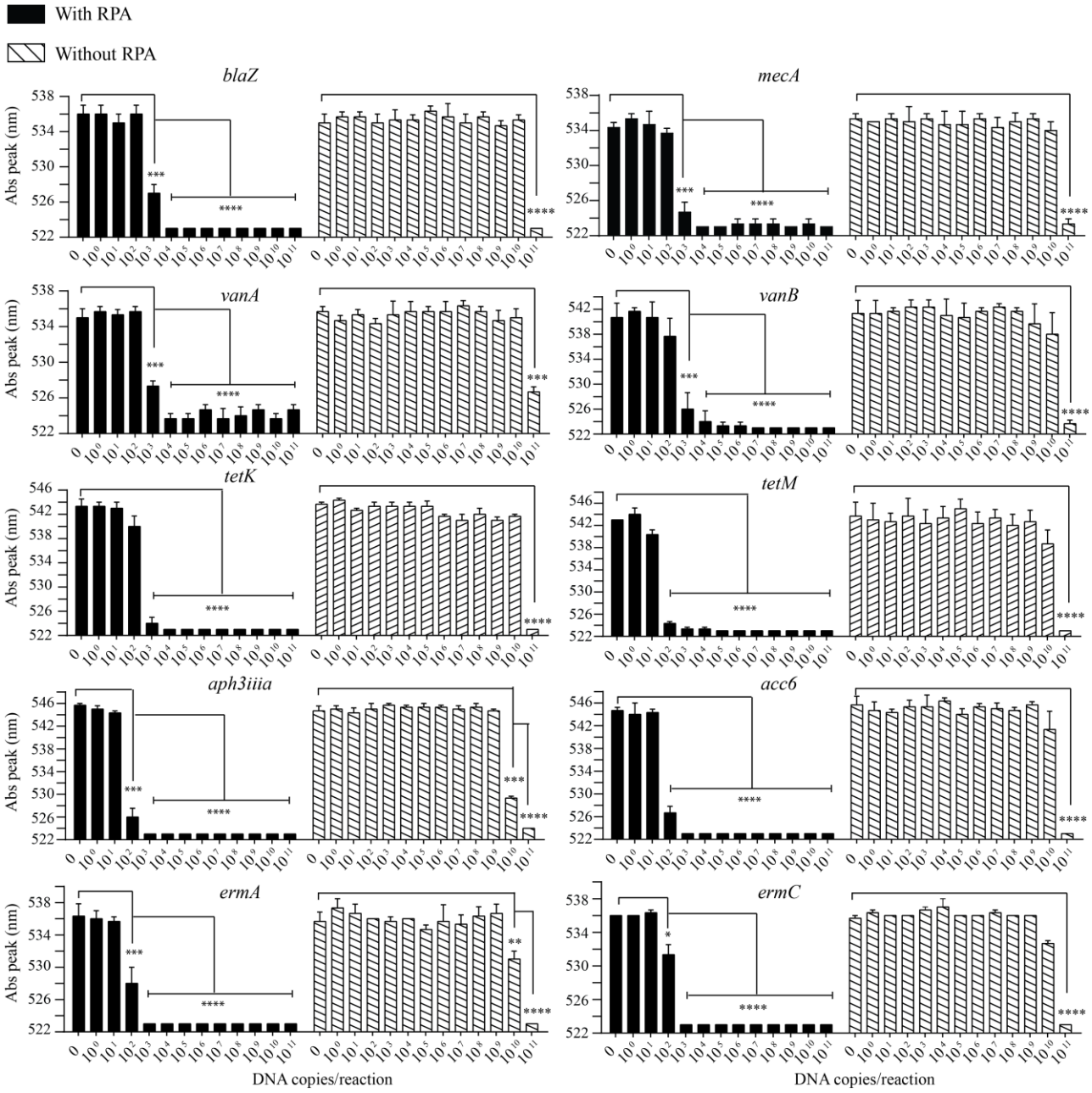

Figure 3.4.Quantitative measurement of analytical sensitivity of AR genes with and without RPA. Wavelength peak absorbance measurement reveals the analytical sensitivity of MNAzyme-GNPs assay at 10^2-10^3 DNA copies/reaction when RPA is used compared to 10^{11} DNA copies/reaction without RPA. Error bars denotes the standard deviation where n=3. (*p≤0.05, **p<0.001, ***p<0.0001 and ****p<0.00001).

3.3.3 Detection of multiple synthetic AR genes

The ability to identify multiple AR determinants is critical for detecting MDR bacteria, which will facilitate more accurate treatment decisions in a time effective manner. Hence, the ability of to detect multiple AR genes in parallel was demonstrated. AR genes were divided into 2 groups based on the gene size and the possibility of primers cross-reactivity. Group 1 included *blaZ*, *vanA*, *tetK*, *aph3iiia* and *ermA* genes, and group 2 included *mecA*, *vanB*, *tetM*, *acc6* and *ermC* genes. For each group, 5 synthetic AR genes were added simultaneously to our multiplexed RPA solution containing primers for *balZ*, *vanA*, *tetK*, *aph3iiia* and *ermA* for group 1, and *mecA*, *vanB*, *tetM*, *acc6* and *ermC* for group 2. The amplicons were blocked and added to MNAzyme solution containing mixture of the 5 MNAzymes for each group. This was followed by parallel signal readout by 5 different GNPs detection probes.

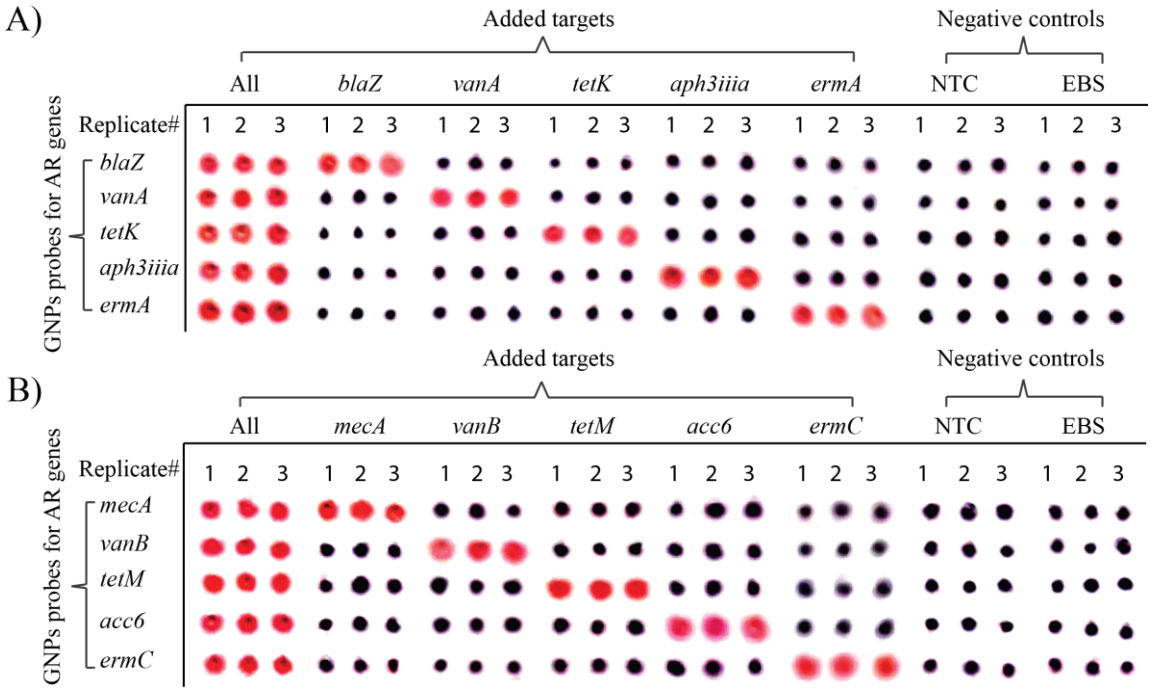

Figure 3.5.Cross-reactivity test for two Groups of AR genes. Synthetic AR gene(s) were added to the multiplexed RPA solution containing primers for (A) *balZ*, *vanA*, *tetK*, *aph3iiia*, and *ermA*, or (B) *mecA*, *vanB*, *tetM*, *acc6*, and *ermC*. Amplicons were detected with MNAzyme-GNP assay. "NTC" indicates no template control of multiplexed RPA reaction. "All" indicates that all AR genes of the group are added to multiplexed RPA reaction. "EBS" control is composed of elution buffer of DNA purification kit and blocking strands to test aggregation of GNPs. Spot images represent colorimetric readout on a TLC plate after adjusting for brightness and contrast on Image J.

Data in Figure 3.5 and Figure 3.6 shows that the assay successfully detected all AR genes simultaneously. This was indicated by the red color spots for "All" condition in which all genes were added simultaneously to the RPA reaction mixture. These red spots represent positive signals when compared to the purple color spots of the NTC condition. For NTCs, water was added instead of AR genes in the RPA reaction to check for any false-positive signals arising from the contamination of RPA reagents with AR genes or non-specific RPA products. Also, to examine any false-positive signals that could arise from improper aggregation of GNPs, "EBS" control composed of elution buffer of DNA purification kit and blocking strands was used. This control was mixed directly with MNAzyme assay components and transferred to GNP solutions to confirm proper aggregation of GNPs with inactive MNAzyme and intact linker DNA. Furthermore, we investigated the possibility of cross-reactivity in both RPA and MNAzyme reactions by incubating one of the five AR genes of each group in the multiplexed RPA reaction, and using the amplified products in the MNAzyme-GNPs assay. No cross-reactivity was observed for all conditions tested (Figure 3.5), and only the gene that was added to the multiplexed RPA reaction gave a positive signal. This confirms that the assay can selectively detect multiple AR genes without any cross-reactivity.

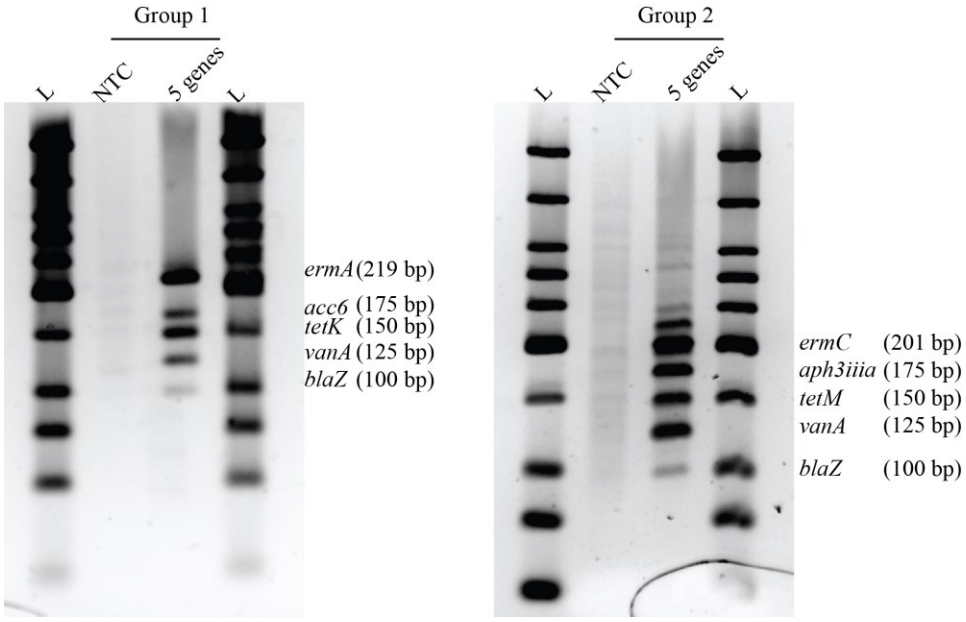

Figure 3.6.Multiplex RPA reaction using 5 AR genes simultaneously. Gel electrophoresis images show the presence of the amplified products of RPA of the 5 AR genes with marked different band sizes. (**L**: low molecular weight DNA ladder).

3.3.4 Validation of analytical sensitivity using clinical isolates.

DNA extracted from clinical isolates was used to validate the analytical sensitivity measured using synthetic DNA targets, and to confirm that a clinically relevant detection limit of $\leq 10^5$ CFU/ml can be achieved. First, three isolates of *S. aureus*: *S. aureus* ATCC BAA-44 (MRSA-44), *S. aureus* ATCC BAA-41 (MRSA-41) and *S. aureus* ATCC 29213 (MSSA) were screened for the presence of AR genes. Bacteria were grown at a high concentration of 10^7 CFU/ml, to ensure that negative detection of genes is not due to insufficient amount of target DNA. DNA was extracted from the three isolates and then screened for the presence of AR genes in a singleplex reaction. Both NTC and EBS controls were used to ensure correct interpretation of our results. Data in Figure 3.7 shows that MRSA-44 had the highest abundance of genes denoted by 5 AR genes: *blaZ*, *mecA*, *tetM*, *acc6* and *ermA* genes, followed by MRSA-41 which contained 3 AR genes: *balZ*, *mecA* and *ermA*, while MSSA contained only *blaZ* gene. The presence of these AR genes was confirmed by PCR (Figure 3.8), which detected the same genes in the three MRSA isolates. Afterwards, the analytical sensitivity was measured for the five AR genes that were present in MRSA-44 using serial dilutions of this bacteria (10^7-10^0 CFU/ml). Media without bacteria served as a negative control (i.e. 0 CFU/mL). Figure 3.9 shows detection limit of 10^2-10^3 CFU/ml, which corresponds to 2-20 DNA copies/µL. This limit of detection is similar to the analytical sensitivity measured with synthetic AR genes. This was also confirmed quantitatively by measuring the peak absorbance wavelength using UV-Vis spectrophotometer. Data in Figure 3.10 shows that there was a significant difference in the peak absorbance wavelength at or greater than 10^2 CFU/ml for *mecA* and *tetM* genes, and 10^3 CFU/ml for *balZ*, *acc6* and *ermA* genes (*P* value <0.0001 or <0.00001). These results confirm that the assay can detect AR genes in MRSA isolates at concentrations required for clinical applications.

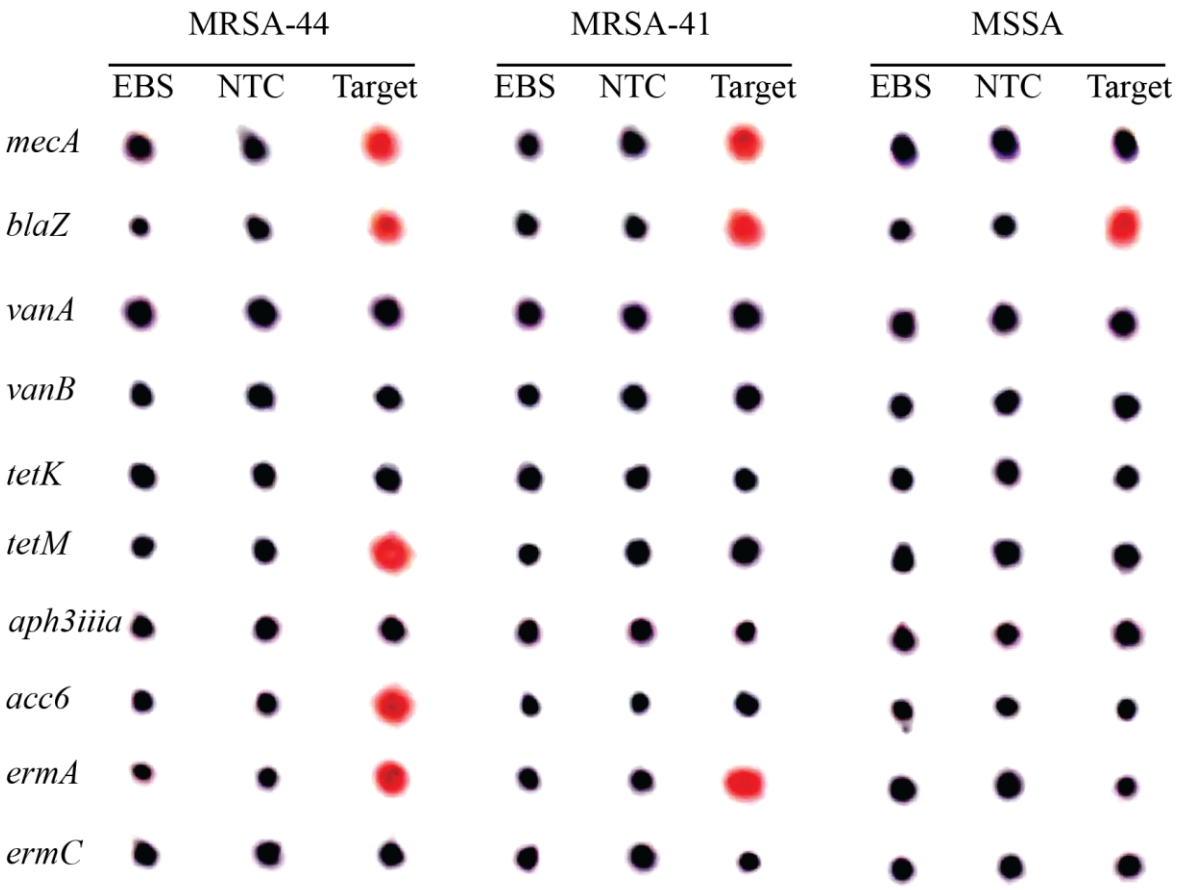

Figure 3.7.Screening clinical isolates for detection of AR genes using singleplex RPA and MNAzyme-GNPs assay. Three *S. aureus* strains (MSSA, MRSA-41, and MRSA-44) were screened to test for presence of the 10 AR genes. Spot images represent colorimetric readout on a TLC plate after adjusting for brightness and contrast on Image J. Red spots indicate the presence of genes while dark purple/blue spots indicate the absence of gene.

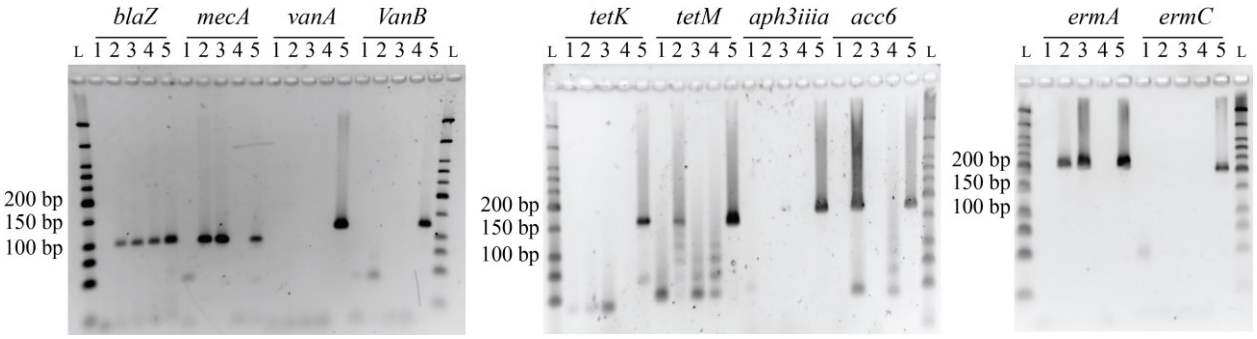

Figure 3.8.Detection of AR genes in bacterial strains using PCR. The gel electrophoresis images show the presence of AR genes in MRSA-44 (lane 2), MRSA-41 (lane 3) and MSSA (lane 4) strains. Synthetic AR genes (lane 5) was used as positive control while NTC (lane 1) was used as a negative control. (**L**: low molecular weight DNA ladder).

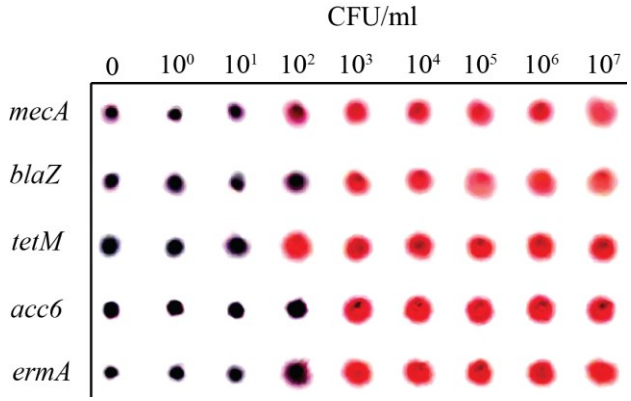

Figure 3.9.Analytical sensitivity of detecting AR genes from MRSA-44. MRSA-44 were serially diluted, the extracted DNA amplified via RPA and detected with MNAzyme-GNP assay. Spot images represent colorimetric readout on a TLC plate after adjusting for brightness and contrast on Image J.

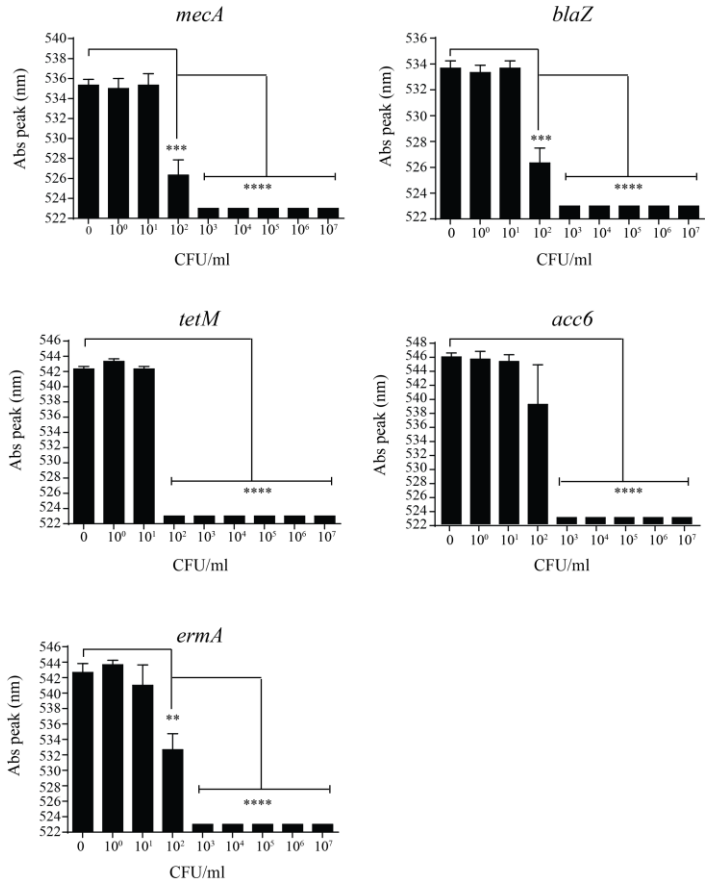

Figure 3.10. Measurement of analytical sensitivity of AR genes from MRSA-44. Wavelength peak absorbance measurement reveals the analytical sensitivity of MNAzyme-GNPs assay at 10^2-10^3 CFU/ml. Error bars denotes the standard deviation where n=3. ($0.1 \leq *p \leq 0.05$, $**p < 0.001$, $***p < 0.0001$ and $****p < 0.0001$).

3.3.5 Screening AR genes in MRSA isolates.

As a final step, the ability of the assay to detect multiple AR genes in parallel in the three *S. aureus* strains was investigated. Furthermore, the detection capability of the assay was compared to one of the most commonly used phenotypic assays. Extracted DNA was blocked and added to the multiplexed RPA and MNAzyme reactions as mentioned in the previous sections, followed by parallel colorimetric readout. Figure 3.11 A&B show that the assay detected the following AR genes: *balZ*, *mecA*, *tetM*, *acc6* and *ermA* genes in MRSA-44 strain, *balZ*, *mecA* and *ermA* genes in MRSA-41 strain and *balZ* gene in MSSA strain. These results perfectly match with the singleplex results obtained in Figure 3.7. Next, the results were compared to the agar diffusion method [102]. Figure 3.11C and Figure 3.12 show that MRSA-44 strain is resistant to penicillin, oxacillin, gentamicin, kanamycin, tetracycline and erythromycin, and intermediate resistant to minocycline. This is in agreement with the results of our assay, which detected the presence of *blaZ*, *mecA*, *tetM*, *acc6* and *ermA* genes. The data also shows that MRSA-41 strain is resistant to penicillin, oxacillin and erythromycin which corresponds to the presence of *blaZ*, *mecA* and *ermA* genes respectively, and MSSA strain is resistant to penicillin which corresponds to the presence of *blaZ* gene. Overall, MNAzyme-GNPs assay can detect multiple AR genes from MRSA isolates at 10^5 CFU/ml with the same predictive capability of phenotypic methods.

3.4 Conclusion

The work presented herein describes the development of a rapid diagnostic technique that can detect multiple AR determinants in parallel within 2 hours. In clinical practices, clinicians usually prescribe broad-spectrum antibiotics as initial therapy. Once, the antibiotic susceptibility test results are available an appropriate or narrow spectrum antibiotic is prescribed[104]. This time window between initial and definitive therapy is very critical. Previous studies have shown that the delay in the administration of appropriate antibiotics due to long diagnostic times of current clinical methods (24-72 hours) can lead to increased risk of patients mortality, higher costs due to prolonged hospitalization times and increased risk of AR development[104,222,223]. Therefore, the ability of MNAzyme-GNPs assay to provide the antibiotic susceptibility results much sooner than the current laboratory techniques can significantly improve the treatment outcomes, reduce health-care costs, and prevent emergence of AR. The assay demonstrated high analytical sensitivity of 10^2-10^3 CFU/ml, detection of 10 AR genes in parallel for profiling resistance to 5 antibiotic classes,

and produced results that matched standard laboratory techniques (e.g. PCR and agar diffusion methods, Table 3.4). Previously, it has been shown that the detection of multiple genes for diagnosis of a pathogen can increase the diagnostic sensitivity of an assay[177]. Similarly, two genes were used to test for resistance to the same antibiotic class, which demonstrated better predictive capability compared to using a single gene. For instance, the results for erythromycin resistance in MRSA-41 and 44 (Figure 3.11) showed absence of *ermC* gene. If only *ermC* gene was tested, the assay could have falsely predicted MRSA-41 and 44 to be susceptible to erythromycin. On the other hand, screening for both *ermA* and *ermC* genes correctly identified the resistance of MRSA-41 and 44 to erythromycin. Moreover, high detection selectivity was achieved through both RPA and MNAzyme-GNPs assay steps. This was confirmed with a cross-reactivity test that demonstrated selective amplification of the AR genes via RPA followed by selective activation of MNAzyme in response to the presence of specific amplification products.

In conclusion, MNAzyme-GNPs is simple, sensitive and instrument-free. This assay is also versatile and can be easily applied to detect different AR genes from different pathogens by simply modifying primer and MNAzyme sequences. Moreover, the ability of this assay to detect multiple antibiotic resistance genes can help minimizing the improper use of antibiotics and selecting for antibiotics that can effectively treat patients infected with bacterial pathogens.

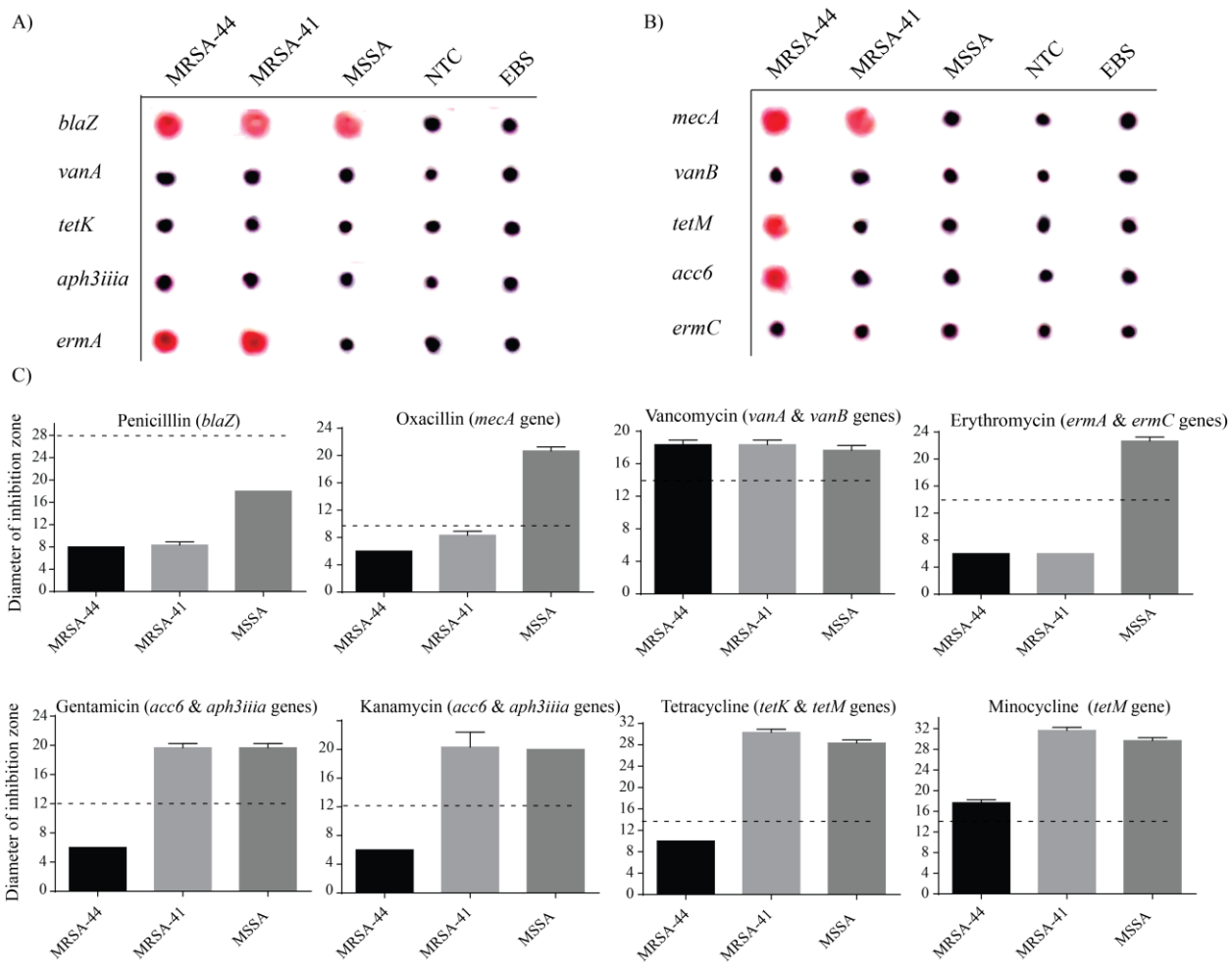

Figure 3.11. Screening clinical isolates for detection of multiple AR genes Three *Staphylococcus aureus* strains (MSSA, MRSA-41, and MRSA-44) were screened to test for presence of 10 AR genes. DNA extracted from 3 isolates were tested for the presence of (A) *balZ*, *vanA*, *tetK*, *aph3iiia*, and *ermA* genes, and (B) *mecA*, *vanB*, *tetM*, *acc6*, and *ermC* genes. "EBS" control is composed of elution buffer of DNA purification kit and blocking strands to test aggregation of GNPs. "NTC" indicates no template control of multiplexed RPA reaction. Spot images represent colorimetric readout on a TLC plate after adjusting for brightness and contrast on Image J. (C) Culture-based agar diffusion test. Bar graphs represent the diameter of inhibition zone, where the diameter below the horizontal dotted line indicates AR. Error bars represent standard deviation of the mean from experimental triplicates.

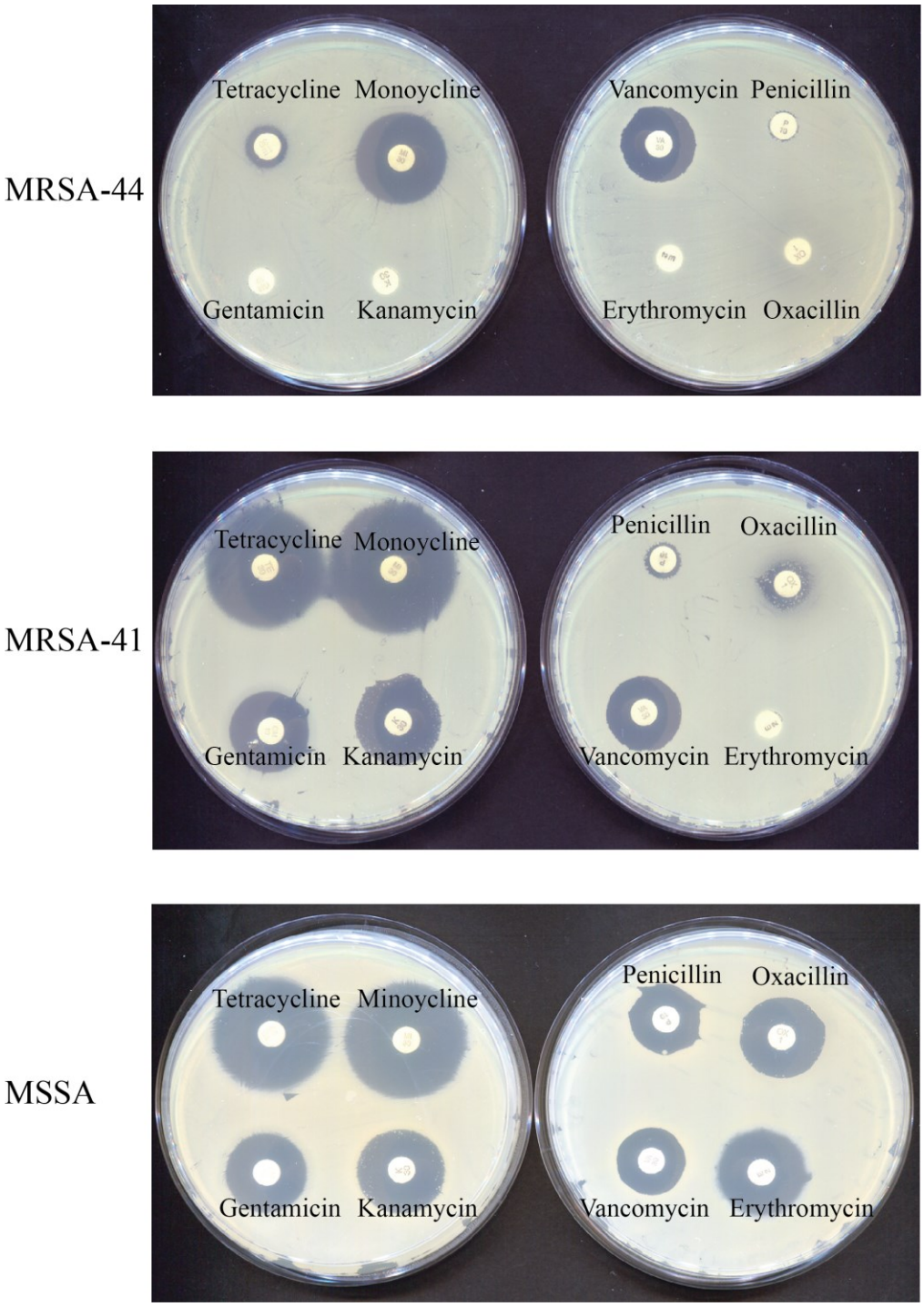

Figure 3.12.Antibiotic susceptibility assay using agar diffusion method. Photos show the susceptibility of MRSA-44, MRSA-41 and MSSA strains to antibiotics based on the diameter of inhibition zone.

Table 3.4. Comparison between MNAzyme-GNPs assay, PCR and agar diffusion method.

Antibiotic family	Antibiotic name	Resistance genes	Mz-GNPs assay			PCR			Agar diffusion method		
			MSSA	MRSA-41	MRSA-44	MSSA	MRSA-41	MRSA-44	MSSA	MRSA-41	MRSA-44
B-lactam	Penicillin	*balZ*	+	+	+	+	+	+	+	+	+
	Oxacillin	*mecA*	-	+	+	-	+	+	-	+	+
Glycopeptides	Vancomycin	*vanA*	-	-	-	-	-	-	-	-	-
		vanB	-	-	-	-	-	-			
Tetracyclines	Tetracycline/Monocycline	*tetK*	-	-	-	-	-	-	-	-	+
		tetM	-	-	+	-	-	+			
Aminoglycosides	Gentamicin/Kanamycin	*acc6*	-	-	+	-	-	+	-	-	+
		aph3iiia	-	-	-	-	-	-			
Macrolides	Erythromycin	*ermA*	-	+	+	-	+	+	-	+	+
		ermC	-	-	-	-	-	-			

.

Chapter 4
A versatile plasmonic thermogel for disinfection of antimicrobial resistant bacteria

4.1 Introduction

Delivery of effective antimicrobial therapeutics is crucial for successful treatment. Antibiotics are among the most common therapeutic agents that are used for treatment of bacterial infections. However, the rapid emergence of MDR among different bacteria made this treatment option very challenging, hence, the world might be moving to the post antibiotic era[114,160]. MDR superbugs are often hospital or community acquired sources of infection of the lungs, urinary tract, gastrointestinal tract, skin and soft tissue. These infections are also a significant economic burden. The clinical management of skin and soft tissue infections alone, for example, is estimated to surpass $4.8 billion/year in health care costs in the United States[224]. Complications associated with these infections are common, occurring in up to 25% of cases, and include bacteremia, endocarditis, and sepsis[225]. Taken together, there is an urgent need to develop effective alternative antimicrobial therapies for AMR infections.

At the correct temperature, heat can be used to destroy bacteria through disruption of the cell membrane, fatty acid melting, and protein denaturation[161]. Inorganic NPs offer fine control and homogenous distribution of heat over conventional heating probes, such as ultrasound, microwaves, and radiofrequency[162]. Hence, they can locally and selectively concentrate the heat to the infected areas without damaging the surrounding tissue. There are several types of heat-producing NPs including GNPs, magnetic NPs, carbon-based nanostructures, and porphysomes[164,226–228]. Typically, these particles are excited by light or magnetic fields and the resulting energy is converted into heat through atomic scale electronic and orientation transitions[229]. As mentioned in section 1.5.3, GNPs are the most common types of heat generating NPs that have been widely and extensively used in biomedical application. When GNPs are excited by light, the process is known as PTT. Previous studies demonstrated the capability of PTT using GNPs for selective killing of AMR bacteria *in vitro*[166,230–232]. However, there is a lack of the translation of this technique from *in vitro* to *in vivo*. Moreover, applying this technique for the treatment of microbial infections *in vivo* (wound and skin infections in particular) requires an appropriate dispersion medium of GNPs. Water is the most common and tradition dispersion

medium of GNPs. However, when an aqueous solution of GNPs is exposed to laser light, the heat generated by GNPs will cause water evaporation, followed by fast heat dissipation. This can result in uncontrolled heat delivery to the targeted area and low therapeutic efficacy. Therefore, there is a need to use a dispersion media that can preserve the heat generated by GNPs within it to achieve high therapeutic effect.

This chapter describes development of plasmonic thermogel that can potentially disinfect wounds contaminated with AR bacteria *in vivo* using PTT. A thermosensitive biocompatible polymer, n-vinyl poly caprolactam (PVCL) was used as a dispersion medium for GNPs. PVCL is a biocompatible polymer [233] that exhibits phase transition from sol to gel at 35 ^{o}C. When a solution of GNPs in PVCL is exposed to laser light, the heat produced by GNPs converts the polymer solution into gel, which can minimize water evaporation and trap the heat within it. This in effect will maintain the equilibrium temperature at the desired level during the course of treatment to ensure a consistent thermal effect. Therefore, it is hypothesized that this PTT method could be potentially used to disinfect AR bacteria when applied to experimentally infected wounds. To test the feasibility of this approach, Near-IR laser (NIR) at low power density for particle excitation was used to avoid damage to local tissues.

4.2 Materials and methods

4.2.1 Gold nanorods synthesis, functionalization and characterization

NRs were synthesized using a seed-mediated method described by Nikoobakht and El-Sayed and Gou and Murphy[234,235] with modifications. Briefly, the seed solution was prepared by adding 1.2 ml of 0.01 M sodium borohydride (Sigma-Aldrich, St. Louis, MO, USA) to 20 ml scintillation vial that contains 500 µL of 0.01 M gold chloride (Sigma-Aldrich, St. Louis, MO, USA) and 19.5 ml 0.1 M cetyl trimethylamonnium bromide (CTAB) (Sigma-Aldrich, St. Louis, MO, USA) under vigorous stirring. In a clean bottle, 49.5 ml of 0.01 M gold chloride was added to 950 ml of 0.1 M CTAB. To that, 5 ml of 0.01 M AgNO3 (Sigma-Aldrich, St. Louis, MO, USA) and 7 ml of 0.1 M ascorbic acid (Sigma-Aldrich, St. Louis, MO, USA) were added respectively under stirring. Finally, 20 ml of the above prepared seed solution were added and the entire solution was left overnight with constant stirring. The obtained NRs solution was then purified by centrifugation twice at 17000 g for 20 min and re-dispersed in deionized water to remove excess

CTAB. The CTAB-NRs were further characterized using UV–Vis spectrophotometer (Shimadzu, UV-1601PC) and zeta potential. For surface functionalization, 5 ml of the above concentrated CTAB-NRs solution was added to clean bottle containing a solution of m-PEG-SH (MW: 5000 Daltons, Laysan Bio) so that the final concentration of PEG was 0.5 mg/ml. The mixture was incubated at room temperature for 4 hours. PEG coated NRs (PEG-NRs) were further purified twice by centrifugation at 17000 g for 20 min to remove excess PEG and CTAB. PEG-NRs were further characterized using UV–Vis spectrophotometer, zeta potential (Nano-Zs) and TEM (Hitachi 7000).

4.2.2 Preparation and characterization of gold nanorods thermogel nanosol

21.5% w/v of PVCL (MW: ~176000 Daltons, PolySciTech Akina, Inc) solution was prepared by dissolving equivalent amount of polymer in 1x phosphate buffered saline buffer (1xPBS) at 4 °C overnight. This was followed by addition of the above prepared PEG-NRs to the polymer solution so that the final concentration of NRs and polymer was 5 nM and 20%, respectively. The NRs-PVCL solution was further characterized by UV-Vis spectrophotometric measurement and TEM.

4.2.3 Development of temperature profiles

The rise in temperature of 3 different solutions of the NRs was measured using an infrared (IR)-Camera (ICI 7320) for 20 min. First, 1.5 µL of 400 nM PEG-NRs were dispersed in 56.5 µL of 21.5% w/v PVCL, 1xPBS and 21.5% w/v PEG solutions respectively. 2 µL of 1xPBS was then added to all solutions so that the final volume was 60 µL. Then 50 µL of each solution was applied on the surface of 35 mm Petri dish followed by laser irradiation using 785 nm continuous wave diode laser (CW) as light source (0.65 W/cm^2) for 20 min. The rise in temperature (ΔT_f) was calculated as the difference between film temperature at time point t ($T_f(t)$) and initial film temperature (T0 ~ 18.5 ± 1.5) on the surface. Blank solutions of PVCL, PBS and PEG were used as non-heating controls.

4.2.4 Heat dissipation and water evaporation measurements

1.5 µL of 400 nM PEG-NRs was dispersed in 56.5 µL of 21.5% w/v PVCL and 1xPBS. 2 µL of 1xPBS was then added to all solutions so that the final volume was 60 µL. Then 50 µL of

each solution was applied on the surface of 35 mm Petri dish followed by laser irradiation at 0.65 W/cm^2 for NRs-PVCL and 1.5 W/cm^2 for NRs-PBS. After 10 min of exposure, the laser was turned off and the drop of temperature from the two solutions was measured as described above. For water evaporation measurement, 50 µL of each solution was weighed before and after laser exposure using analytical scale (METTLER TOLEDO, AL54, readability 0.0010), and the amount of evaporated water was calculated as:

$$\%\ of\ water\ evaporation = (W_b - W_a / W_b) \times 100$$

Where, Wb is the weight (g) of sample before laser exposure and Wa is the weight (g) of sample after laser exposure.

4.2.5 Antimicrobial effect of gold nanorods-thermogel in vitro

Three antibiotic resistant bacteria were used in this study. Ampicillin-resistant *E. coli* NEB 10 beta was obtained from Dr. Aaron Wheeler's lab (Chemistry Department, University of Toronto, Canada). MDR *Acinetobacter baumannii* and vancomycin resistance *Enterococcus faecalis* (VRE) ATCC51299 were obtained from Dr. Justin Nodwell's lab (Biochemistry Department, University of Toronto, Canada). Overnight cultures of *E. coli*, *A. baumannii* and *E. faecalis* bacteria were prepared by streaking small amount of the frozen bacterial stock on Luria agar (LA) plates and incubated at 37 °C. A single colony of each bacteria was inoculated in Luria broth (LB) medium and incubated at 37 °C while shaken (200 rpm). Fresh cultures were prepared in LB medium by adding 30 µL of overnight culture to 2.97 ml of LB media and incubating for another 3–4 hours at 37 °C while shaken or until the OD600 of the culture medium reached approximately 0.3–0.4 (logarithmic growth phase). The bacteria pellets were then collected by centrifugation at 3000 g for 10 min and then washed three times with sterile PBS. The pellets were re-suspended in an appropriate amount of sterile PBS buffer for further use. To test the antimicrobial effect of NRs-PVCL, 2 µL of bacterial cultures was added into 56.5 µL of 21.5% PVCL followed by addition of 1.5 µL of 400 nM PEG-NRs. The samples were then exposed to laser (0.65 W/cm^2) for 10, 20 and 40 min and up to 60 min for *E. faecalis*. The percentage of living cells was calculated by dividing (CFU/ml) of sample by CFU/ml of control (bacteria in PBS without any treatment). Briefly, 450 µL of PBS was added to the sample in the 35 mm Petri dish and then transferred to centrifuge tubes for further dilutions.

100 µL of each dilution were inoculated on LA plates. After 24 hours of incubation at 37 °C, colonies on the plates were counted and percentage of living cells was calculated as mentioned earlier. All the control experiments that were used to test the antimicrobial effect of NRs-PBS + Laser, laser without NRs and NRs without laser were conducted similarly.

4.2.6 Transmission electron microscopy for in vitro study

NRs-PVCL photothermal treated and non-treated bacterial cells were pelleted and washed thrice in PBS by centrifugation. Residual PBS was decanted. Cells were fixed in TEM fixative for 1 hour at room temperature, stained, and sliced onto a TEM grid for visualization using TEM (FEI Tecnai 20).

4.2.7 Surgical wound creation

CD-1 rat was used in this study due to similarities between the wound healing processes between the species [236,237]. The animals were anesthetized using isoflurane (5% induction, 2–3% maintenance) in 100% oxygen. Ketoprofen was administered as analgesic (5 mg/kg, SC, once daily for 2 d). For surgical preparation, the rat dorsum was shaved and a hair removing cream (Nair, Church and Dwight Canada Corp, Canada) was applied to ensure complete hair removal. The skin was disinfected by two successive swabs of 70% ethanol followed by betadine (Rougier Pharma, Canada) and a sterile drape was placed over the rat. A sterile 5 mm biopsy punch (Miltex Inc, USA) was used to make 2 circular full thickness wounds centered just cranial to the scapula. The skin was lifted using forceps and the tissue was excised using sterile scissors. A circular silicone splint (10 mm diameter) with 0.7 mm diameter opening (Grace Bio Labs, USA) was placed over each wound and anchored in place with 6-0 nylon sutures (Covidien, Canada) to prevent healing by wound contraction [238,239]. Wounds were then left untreated or experimentally infected and treated with the PTT technique as described below. Rats were monitored in recovery cages under heat lamps and returned to their home cages following recovery of purposeful movement and postural control.

4.2.8 Safety assessment of PTT technique

Following surgical wound creation (n = 6) as described above, 50 µl of NRs-PVCL solution was applied to the wound. The wound was exposed to diode laser (785 nm) at power

density 0.65 W/cm^2 for 40 min, and then covered with a transparent dressing (Tegaderm, JM healthcare, USA). Animals with untreated wounds served as controls. Some animals underwent wound treatment unilaterally, with the contralateral wound serving as control. Animals were euthanized after 72 hours, the tissue was excised, fixed in 10% neutral buffered formalin, embedded in paraffin wax, sectioned and stained with hematoxylin and eosin, and examined by a veterinary pathologist without knowledge of wound treatment. Tissues were scored on a scale of 1–4 across 4 parameters for inflammation and 8 for rate of healing.

4.2.9 Experimental wound infection

Three groups of animals (3 animals/group) were used. The first group comprised animals whose wounds were infected with *E. coli* NEB 10 beta strain (K12 strain) then treated as above using the thermogel and laser application. After laser application, animals were euthanized. The infected tissue was excised, homogenized using tissue homogenizer, serially diluted and plated on ampicillin containing LB agar media for bacteria count. The percentage of living cells was calculated by dividing CFU/ml of treated group by CFU/ml of non-treated group. The second and third groups served as controls. The second group was infected with bacteria and left untreated while the third group's wounds were neither infected nor treated. For the wound healing experiment three groups of animals (3 animals/group) were treated in the same manner as described above but were monitored for wound closure for up to 12 days.

4.2.10 Statistical analysis

Data were statistically analyzed using SPSS version 20, GraphPad Prism 6 and Microsoft Excel 2013. The student t-test was used for hypothesis testing between data pairs. One-way ANOVA followed by Post HOC Tukey was used for hypothesis testing in data sets with more than two means and one independent variable. Two-way ANOVA was used for hypothesis testing in data sets with more than two means and two independent variable.

4.3 Results and discussion

4.3.1 Preparation and characterization of NRs-PVCL nano-formulation

NRs were selected because they possess high absorption cross-section, high photo-thermal conversion efficacy, and are able to absorb light at between 700 and 1000 nm (a region of the

electromagnetic spectrum with low biological scattering and absorption)[229]. NRs were synthesized using CTAB method pioneered by the El-Sayed and Murphy labs with some slight modifications[234,235]. After synthesis, the surface of CTAB-NRs was modified with m-PEG-SH, which makes the particles more stable in aqueous buffer and reduces their cellular toxicity due to CTAB[240,241]. Figure 4.1 summarizes the characteristics of both CTAB and PEG-NRs. Further, the PEG-NRs were dispersed in a 20% w/v PVCL solution that exhibits a lower critical solution temperature (LCST) of 35 °C (Figure 4.2 and Figure 4.3).

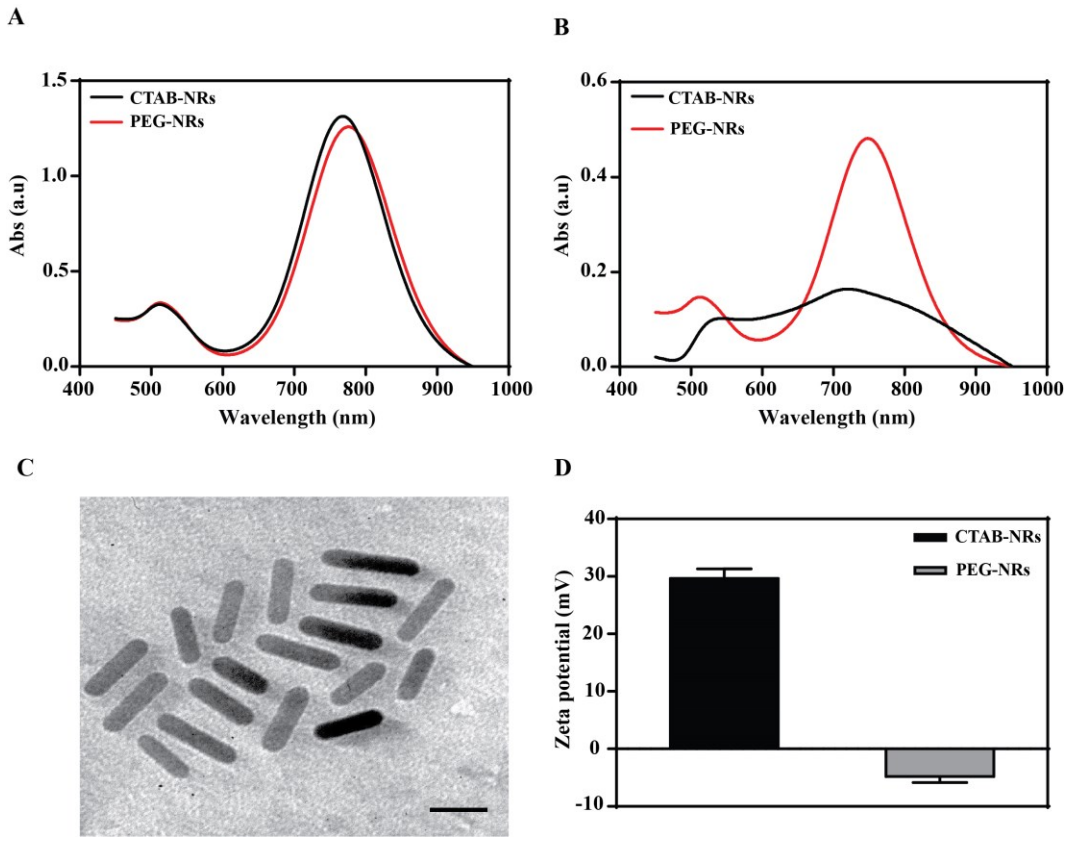

Figure 4.1. Gold nanorods characterization. (A) & (B) UV-Vis spectra of CTAB and PEG-NRs in deionized water and 1x PBS respectively. Both CTAB and PEG NRs are stable in water and have two absorbance peaks in the visible and NIR regions due to transverse and longitudinal surface plasmon resonance. However, CTAB-NRs tend to aggregate in PBS compared to PEG-NRs that showed more stability and dispersion in the same medium. (C) TEM image validates the shape and monodispersity of PEG-NRs with aspect ratio of 3.6 ±2 (scale bar denotes 20 nm). (D) Zeta potential measurement in HEPES buffer (pH = 7.4) reveals that CTAB-NRs exhibit positive surface charge while PEG-NRs exhibit slightly negative surface charge. Error bars represent standard deviation, where n = 3.

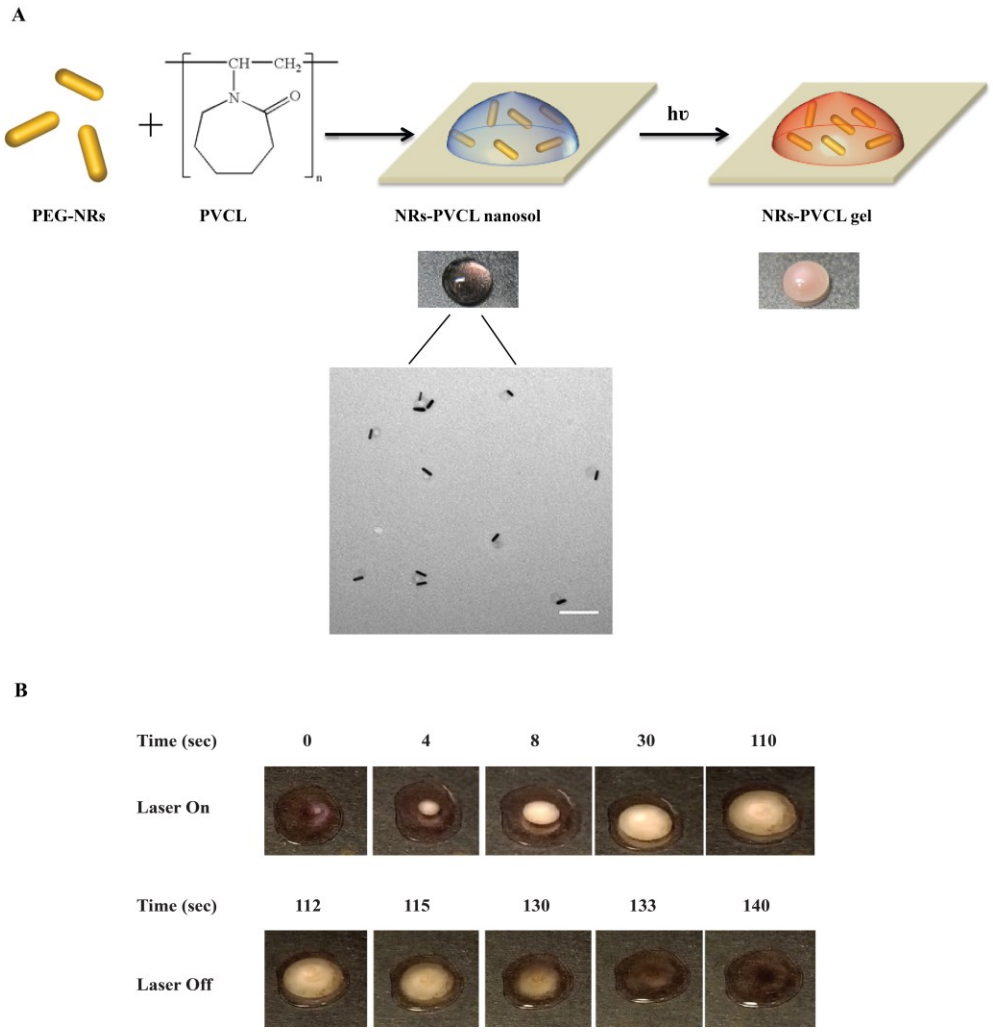

Figure 4.2.Characterization of gold nanorods thermogel. (A) Schematic of the proposed concept solution composed of PEG-NRs dispersed in biocompatible PVCL thermogel solution. Inset TEM image represents nanoscale dispersion of NRs embedded in PVCL thin film (scale bar denotes 100 nm). (B) Photos of NRs-PVCL solution. The upper panel shows that upon laser exposure, the PVCL exhibits phase transition from sol to gel while the lower panel shows that when the laser was turned off it converts back to liquid.

At low temperature, the polymer forms hydrogen bonds with water, which leads to polymer dissolution in water. However, when temperature increases to lower critical solution temperature, the hydrogen bonds start to break and an increase in the hydrophobic interactions between the polymer moieties become dominant. As a result, the polymer collapse and undergoes phase separation[242]. TEM image demonstrated homogeneous dispersion of NRs inside the PVCL solution (Figure 4.2). UV-Vis spectrophotometry confirmed the monodispersity and homogeneity of NRs-PVCL solution by showing two distinct absorbance peaks around 520 nm and 770 nm for the NRs transverse and longitudinal SP (Figure 4.3 A). The data further showed that the presence

of NRs in the solution did not affect the transition temperature of the PVCL polymer Figure 4.3 B & C. NRs-PVCL solution is liquid at temperature below 35 °C, however, when the solution is exposed to a 785 nm diode laser light, it heats to a temperature higher than 35 °C. As a result, the NRs-PVCL converts into gel state. When the laser is removed, the gel converts back into liquid state Figure 4.2 B&C.

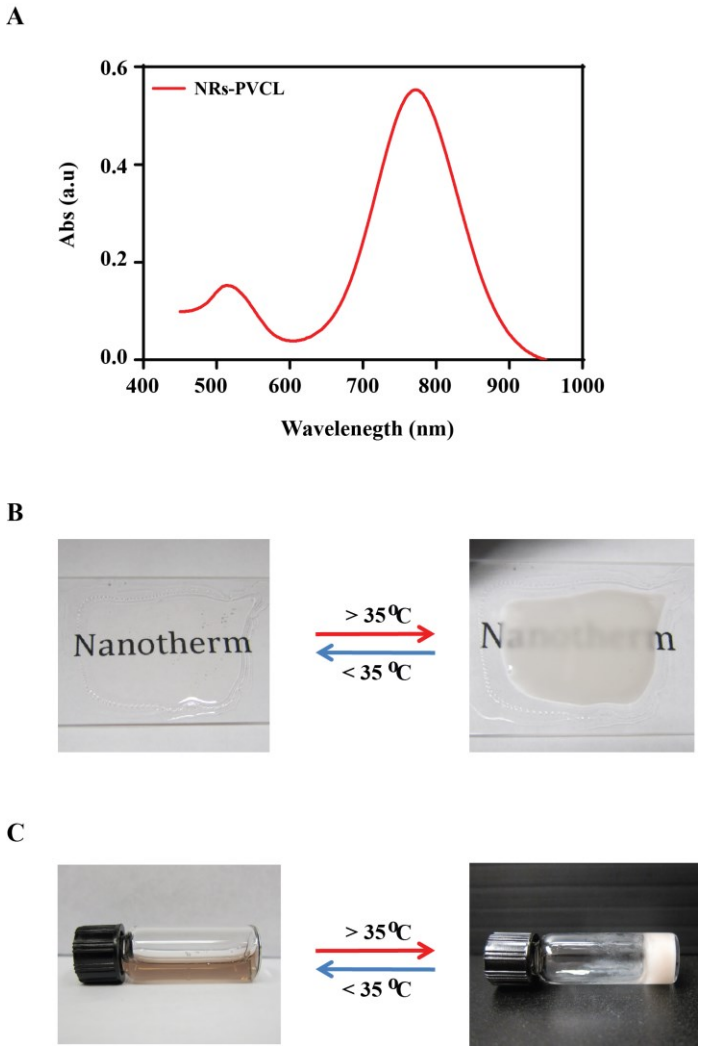

Figure 4.3. Characterization of nanorods-thermogel. (A) UV-Vis Spectrum of NRs in 20% PVCL shows two absorption peaks at 517 and 775 nm assigned to transverse and longitudinal plasmon resonance of NRs. (B) Reversible sol-to-gel transition of PVCL film with LCST >35 ºC. (C) The presence of NRs does not affect the LCST of the PVCL.

4.3.2 Thermal assessment of PVCL as a dispersion medium for GNRs

To test the ability of the NRs-PVCL thermogel to significantly increase the temperature on a surface in comparison to NRs in aqueous solution, film temperature profiles were developed. The aqueous solution for all experiments was PBS. Experiments were carried out by placing the solutions on the surface of a 35 mm Petri dish. The films were then excited with a 785 nm diode laser with an absorbance wavelength that closely matched the absorbance of the longitudinal axis of the NRs for 20 min at 0.65 W/cm^2. For film temperature measurements, a thermal camera was selected because the camera provides a more accurate measurement for surface temperature compared to thermocouples[243]. The emissivity for each individual sample was corrected relative to a reference sample (electrical black tape) with known near perfect emissivity of 0.95. A temperature difference parameter (ΔT_f) was calculated as the difference between the film temperature at time point t ($T_f(t)$) and initial film temperature (T_0) on the surface. After plotting temperature change over time, the data suggested that at the same concentration of NRs and volume of solution, both NRs-PBS and NRs-PVCL showed an initial increase in temperature followed by an equilibrium steady-state plateau. The blank solutions of PBS and PVCL (without NRs) did not show any change in temperature under laser excitation Figure 4.4.

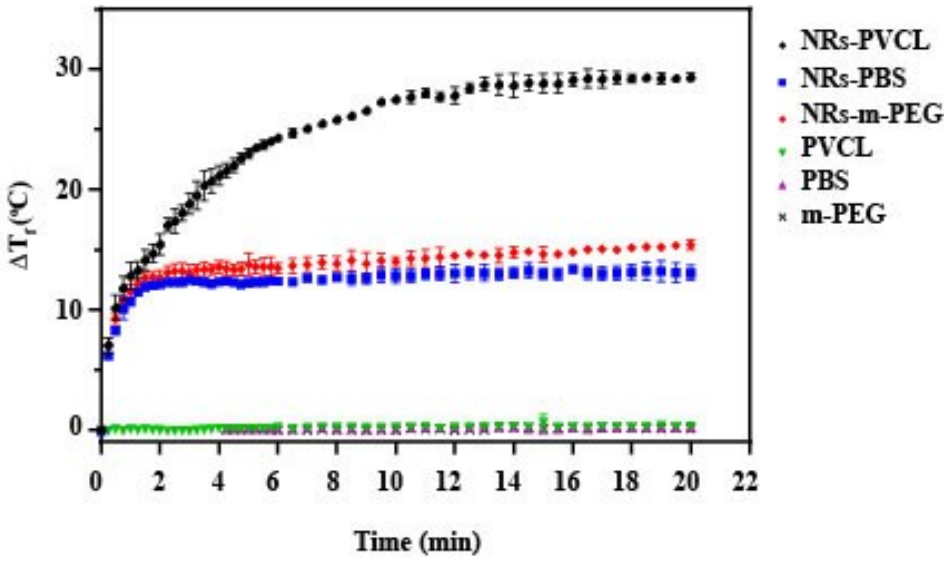

Figure 4.4. Temperature profiles. (A) Temperature elevation of NRs-PVCL, NRs-PBS and NRs-PEG solutions (at the same concentration of NRs) exposed to 785 nm CW diode laser (0.65 W/cm^2) as function of exposure time**.** Blank solution without NRs was used as negative control**.** Error bars represent standard deviation, where n = 3.

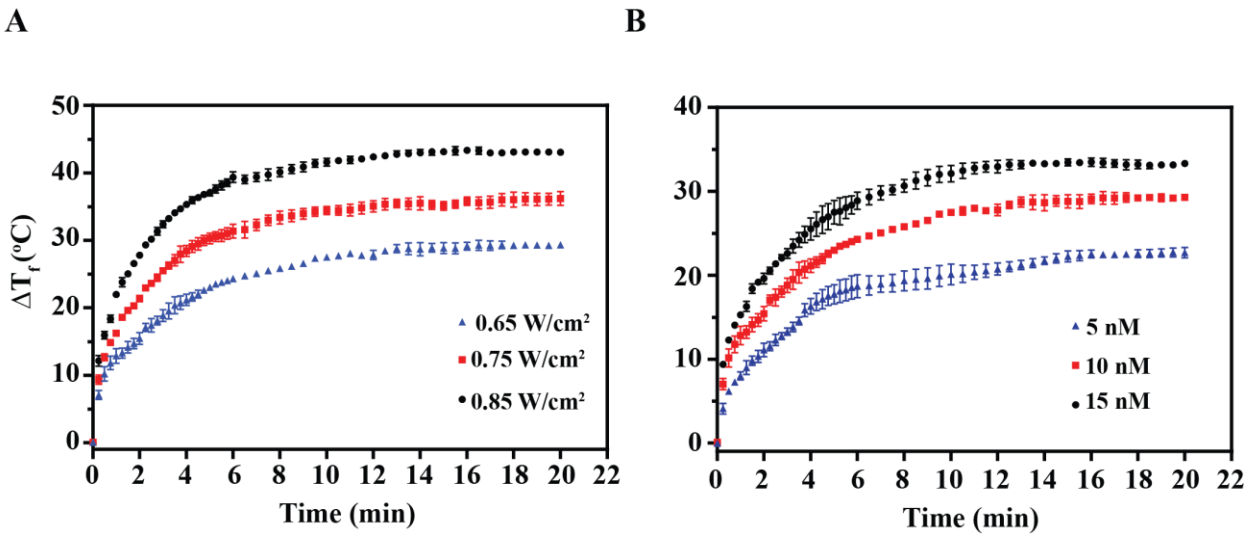

Figure 4.5. Controlling the heating process using NRs-PVCL through different key parameters. (A) Laser power and (B) concentration of NRs. As both the concentration and laser intensity increase, the temperature also increases. Error bars represent standard deviation, where n = 3.

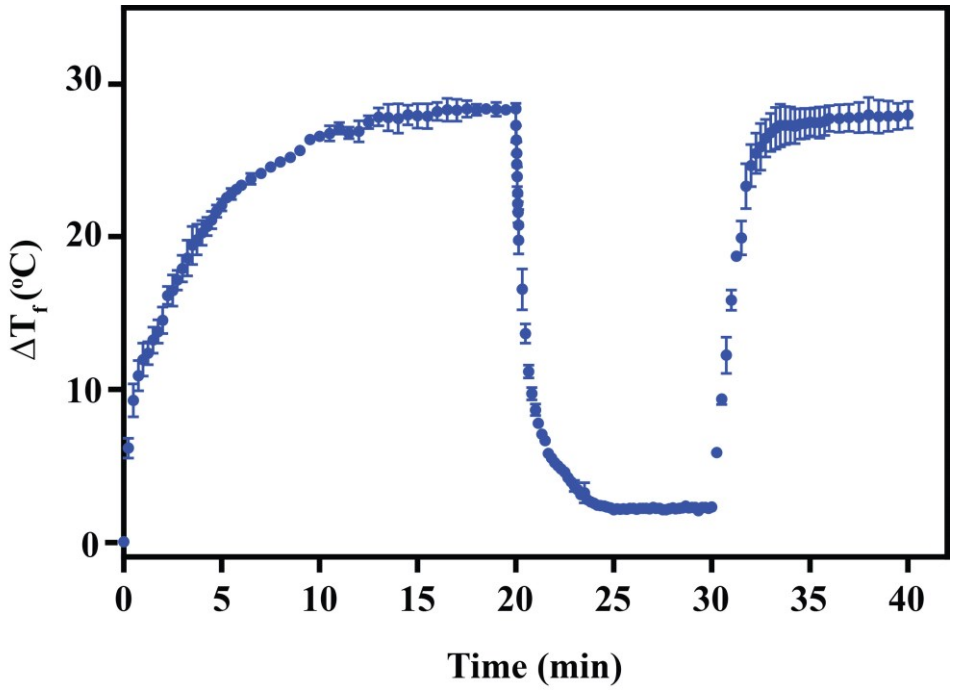

Figure 4.6. Re-cycling of NRs-PVCL. The NRs-PVCL thermogel can be re-cycled more than once as it can heat up with the same efficiency after the second radiation cycle. Error bars represent standard deviation, where n = 3.

A significantly higher equilibrium temperature increase of about 12 °C ± 2 °C was detected for NRs-PVCL thermogel ($\Delta T_f \approx 25$ °C ± 2 °C) compared to NRs-PBS solution ($\Delta T_f \approx 12$ °C ± 2 °C) (Figure 4.4). This data suggests that the temperature increase maintained by the NRs-PVCL gel was 2-fold higher than that obtained for the NRs-PBS solution ($P < 0.001$). Control samples containing NRs in non-thermogel polymer m-PEG exhibited no polymer transition (Figure 4.4) designated as NRs-m-PEG. In addition, the temperature of the film could be manipulated by altering the laser fluence (W/cm^2), the concentration of NRs, and the irradiation time (Figure 4.5). Additionally, NRs-PVCL nanocomposite can be cycled (Figure 4.6) on and off, which also suggests that gel can be used multiple times.

Two possible mechanisms were hypothesized to explain the difference in temperature of the NRs dispersed in the PVCL and PBS: (1) delayed heat dissipation resulting from sol-to-gel transition; and (2) water evaporation. If one considers the same initial heat generation rates due to the same number of NRs in both media, one can envision that the transition of surrounding medium from a liquid to a gel phase may influence the preservation of heat produced. One possible mechanism that could be responsible for the observed difference in temperature between NRs-PVCL thermogel and NRs-PBS solution is that the gel slows the dissipation of heat from NRs-PVCL solution. Thus, NRs-PVCL solution can reach higher equilibrium temperature. We examined this by measuring the temperature drop from an equal elevated temperature in both NRs-PVCL and NRs-PBS solutions. To do this, we raised the temperature of both solutions to the same value. This was achieved using different laser fluence for NR-PVCL (0.65 W/cm^2) versus NRs-PBS (1.5 W/cm^2) as the earlier data in Figure 4.4 showed that NRs-PVCL exhibited higher temperature than NRs-PBS under same laser fluence. After the temperature of the two solutions reached almost the same point at 10 min of laser exposure, the laser was turned off and the drop in temperature was measured over time. Data in Figure 4.7A shows that the heat dissipation rate from NRs-PBS was faster than that from NRs-PVCL with a time constant of 15.15 s versus 33.71 s, respectively ($P < 0.001$). This suggests that the PVCL offers a rigid medium that reduces heat dissipation. A second possible mechanism for the observed temperature difference is water evaporation. To measure the amount of water evaporation, the sample solution was weighed before and after laser exposure and then the amount of water evaporation was measured as a percentage and calculated according to the method described in 4.2.4. When NRs-PVCL and NRs-PBS

solutions were excited, the NRs generated heat, which caused the evaporation of water from both solutions. However, the amount of water evaporating from the NRs-PBS solution was significantly higher (80%) compared to NRs-PVCL (35%) ($P < 0.001$) (Figure 4.7B). This significant water loss can lead to a faster heat dissipation from the solution to the air. As a result, NRs-PBS solution heats to a lower equilibrium temperature. This suggests that both proposed mechanisms could be potentially involved in the temperature differences between the two solutions.

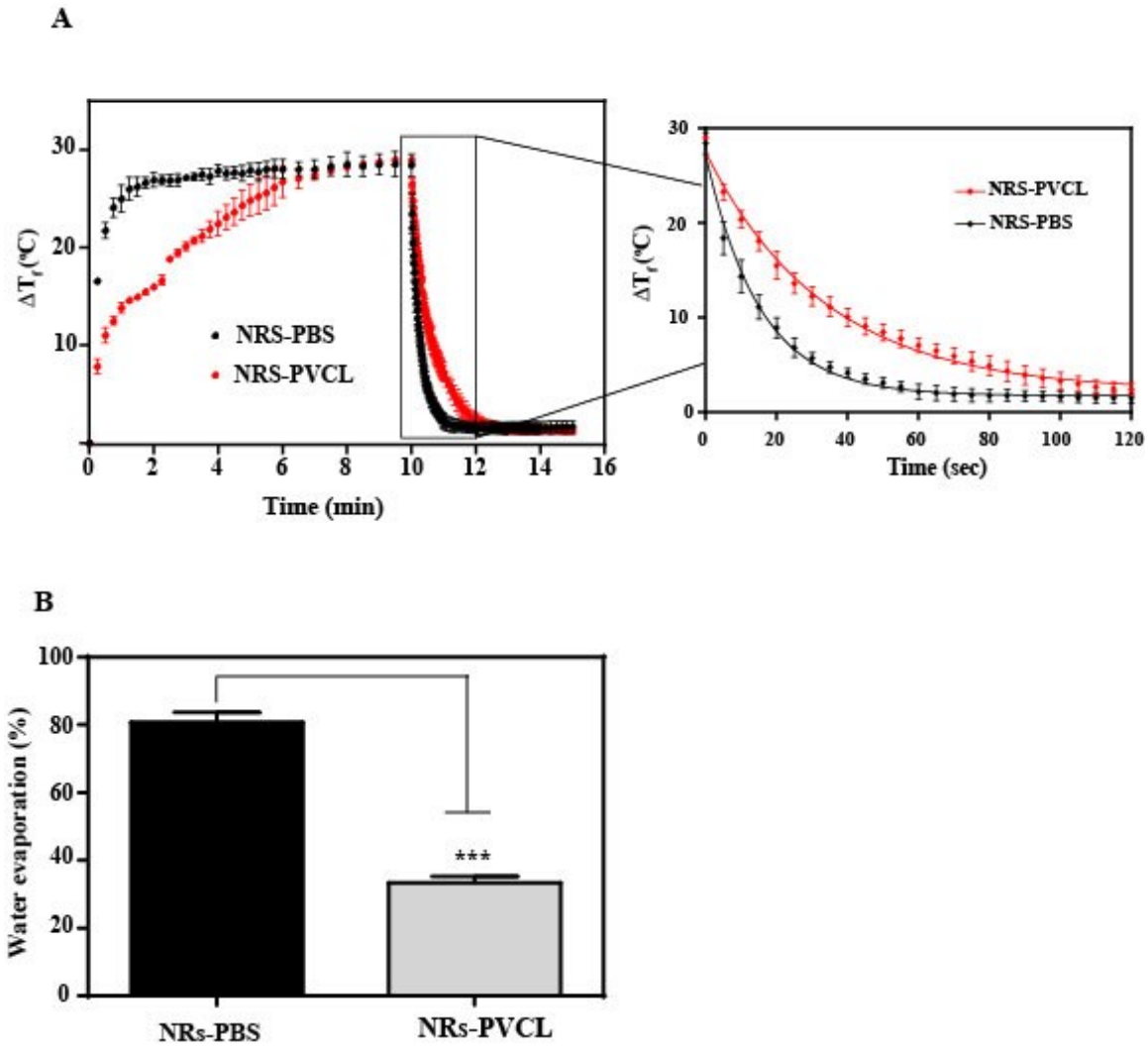

Figure 4.7. Heat dissipation and water evaporation from NRs-PVCL thermogel and NRs-PBS solution. (A) Heat dissipation. Magnified inset represents the heat dissipation rate from the two solutions as a function of time after laser was turned off. (B) Water evaporation from the two solutions after 10 min of laser exposure. Error bars represent standard deviation, where n = 3. ***$P < 0.001$.

4.3.3 Assessment of photothermal therapy technique on bacterial survival in-vitro

The thermal properties of the NRs-PVCL thermogel were investigated to determine if they could be applied to kill bacteria. Three AMR bacterial strains were investigated: *E. coli*, *A. baumannii*, and *E. faecalis*. These bacterial strains were selected because they are frequently associated with hospital acquired infections of skin and soft tissue, and the urinary and gastrointestinal tracts [244]. Figure 4.8A shows the schematic of the platform. First, all components of the platform were investigated for antimicrobial effect. In the absence of laser application, neither NRs-PBS nor NRs-PVCL solution applied on the top of contaminated area had antimicrobial effect (Figure 4.9 A&B). This was also confirmed for laser application of blank PBS and blank PVCL solutions (Figure 4.9C), leaving laser activated heating as the only possible antimicrobial mechanism. Following the control experiments, the effect of laser activated NRs-PVCL on both Gram-positive and Gram-negative AR bacteria was examined under various laser exposure times (10, 20, 40 and 60 min). Generally, the increase in exposure time resulted in improved antimicrobial efficacy against both gram-positive and gram-negative strains. For the Gram-negative strains (*E. coli* and *A. baumannii*), there was a significant decrease in cell viability of 96% and 94%, respectively, after 40 min of laser exposure ($P < 0.001$) (Figure 4.8 B&F). Although the Gram-positive strain (*E. faecalis*) was more heat tolerant, the data showed that there is a significant bactericidal effect ($P < 0.001$) of 65% and 50%, respectively, after 40 and 60 min of laser exposure (Figure 4.8C). The *E. coli* data suggests that the antimicrobial effect against *E. faecalis* can be enhanced by increasing the temperature via increasing laser power. The antimicrobial efficacy of the NRs-PVCL against *E. coli* was significantly enhanced by about 28% ($P < 0.05$) reaching 99% in 20 min after the laser power was increased from 0.65 to 0.85 W/cm^2 (Figure 4.8D). Imaging analysis using TEM showed that the outer membranes of the bacteria were damaged after thermal ablation, leading to loss of structural integrity of bacterial cell walls (Figure 4.8G and Figure 4.10). It has been shown that heat can melt fatty acids and denature proteins, which in effect results in rupture of cell membranes and subsequent bacterial death[161,245].

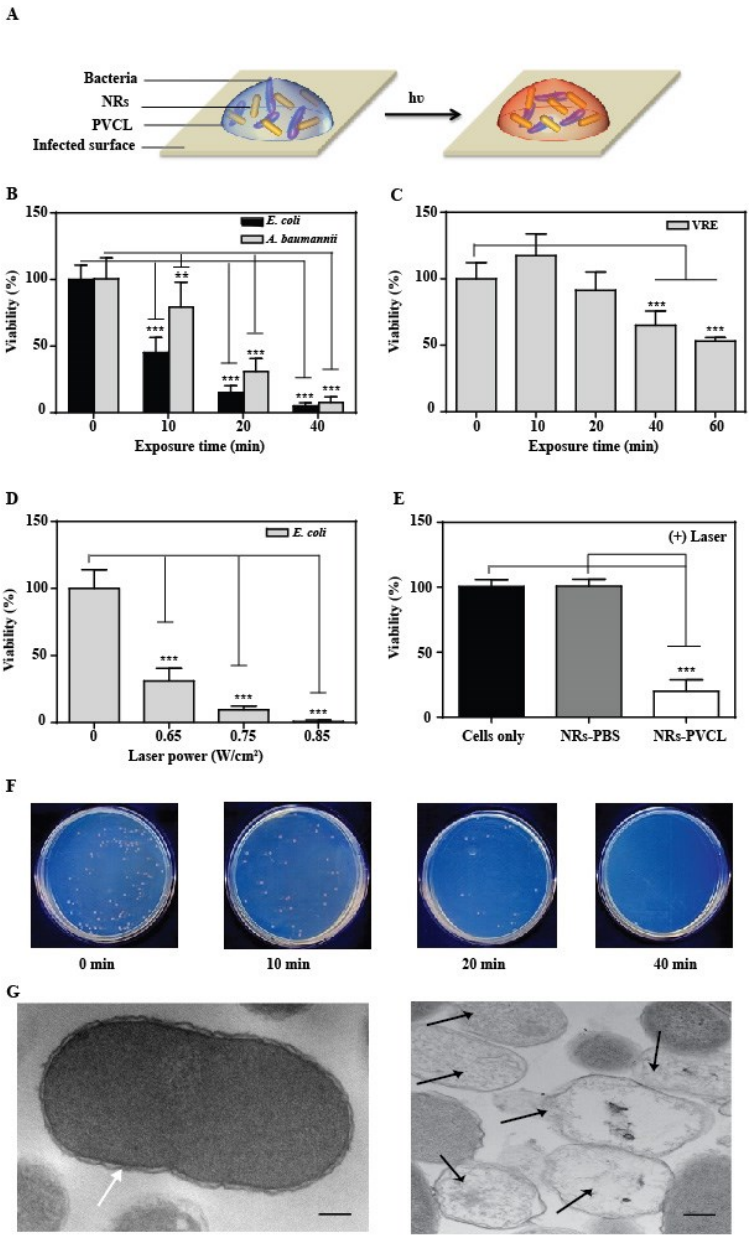

Figure 4.8. Photothermal effect of gold nanorods-thermogel on gram-negative and gram-positive bacteria. (A) Schematic representation of the antibacterial effect of NRs-PVCL (B) Anti-bacterial effect on gram-negative strains *E. coli* and *A. baumannii* and (C) on gram-positive strain *E. faecalis* after incubation with NRs-PVCL followed by laser irradiation (0.65 W/cm^2) for 10, 20, 40 and 60 min. (D) The enhancement of the anti-bacterial effect of PVCL-NRs on *E. coli* by increasing laser power. (E) Comparison between antibacterial effect of NRs-PVCL and NRs-PBS up on laser exposure for 20 min on *E. coli*. (F) Photos of *E. coli* colonies on Luria agar plates show the decrease in the colonies number as a function of exposure time to NRs-PVCL+Laser. (G) TEM image of *E. coli* cells that were exposed to NIR laser (0.65 W/cm^2) for 20 min. The image to the left shows the cells without treatment while the image to the right shows the cells after treatment. White Arrows indicate the areas of cell membrane while the black arrow indicates cell membrane disruption (Scale bars denote 160 nm). Error bars represent standard deviation, where n > 3. *$P < 0.05$, **$P < 0.01$, ***$P < 0.001$.

To compare to the current plasmonic NPs methods for killing bacteria [168–173], the killing efficiency of NRs-PVCL was compared to NRs-PBS after 20 min of laser exposure at 0.65 W/cm^2 on *E. coli*. Results showed that the NRs-PVCL method achieved 3-fold higher bactericidal activity compared to NR-PBS. The bacterial viability significantly ($P < 0.001$) decreased by about 75% using NRs-PVCL compared to NR-PBS, which did not show antibacterial effect (Figure 4.8E).

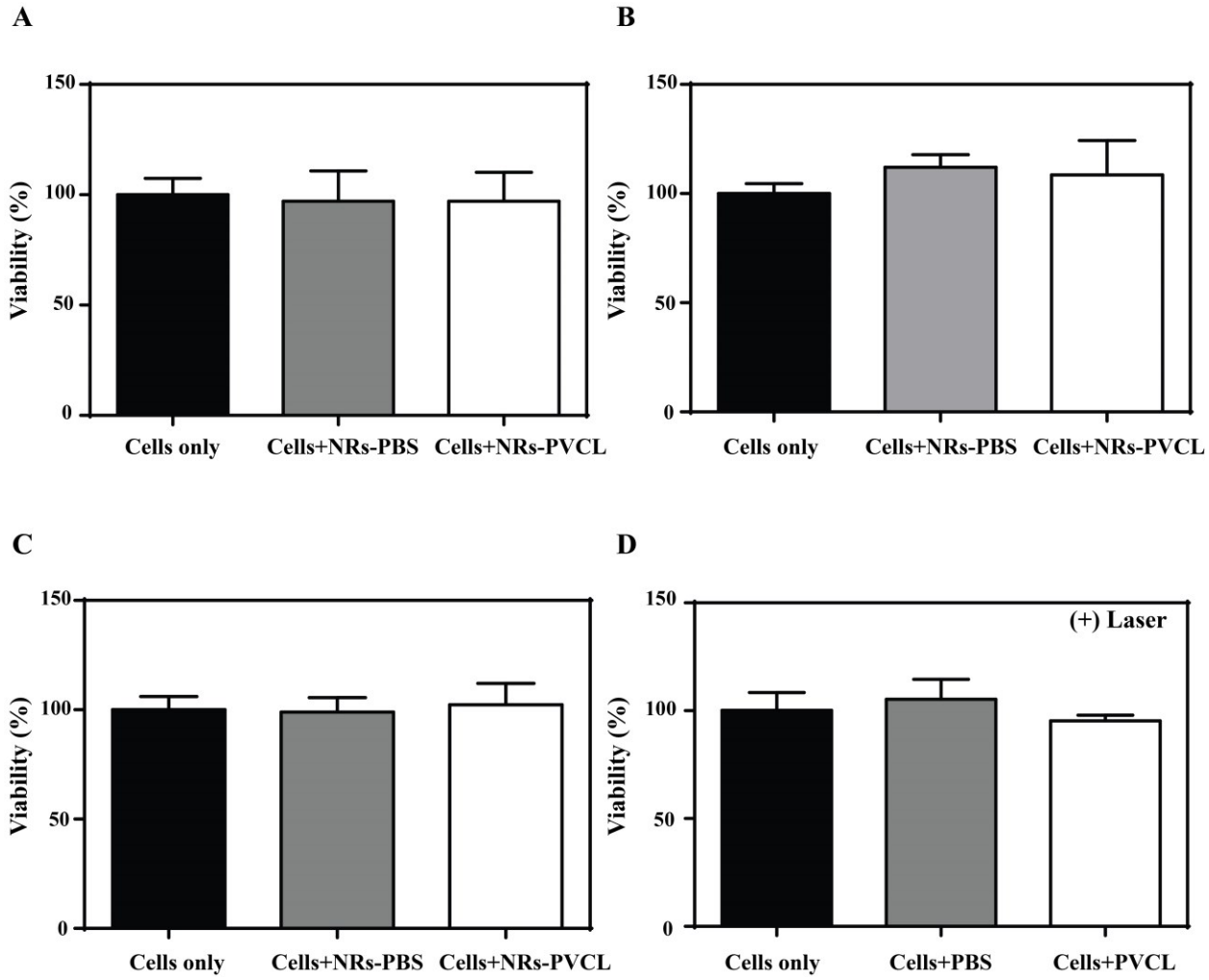

Figure 4.9. Effect of NRs-thermogel and NRs-PBS solution on bacteria (control experiment). (A) on *E. coli* (B) on *A. baumannii* and (C) on *E. faecalis.* Neither NRs-PVCL nor NRs-PBS had antibacterial effect on the bacterial strains. Error bars represent standard deviation, where n > 3. (D) Blank solutions of PVCL and PBS + laser that did not show any antibacterial effect against *E. coli*.

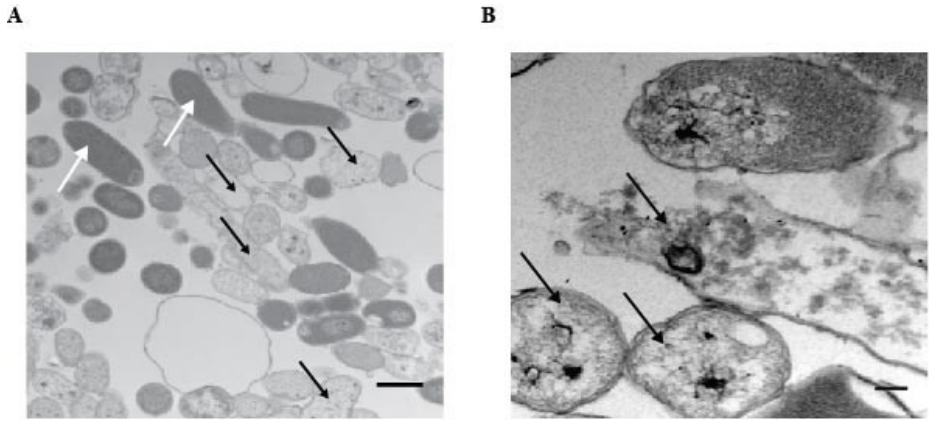

Figure 4.10. TEM images of *E. coli* cells that were exposed to NIR laser (0.65 W/cm^2) for 20 min. White Arrows indicate the healthy cells while the black arrows indicate dead and ruptured cells (scale bars denote 1000 nm for (A) and 200 nm for (B).

4.3.4 Safety assessment of photothermal therapy technique on skin and surrounding tissues

After the technique successfully achieved a significant antimicrobial effect against antimicrobial resistant bacteria *in vitro*, the feasibility and applicability of this technique was investigated *in vivo*. An infected excisional wound was used as an *in vivo* model to test the ability of the technique to decontaminate infected wounds. First, the safety of the laser-activated NRs-PVCL was evaluated prior to testing its ability to kill bacteria *in vivo* (Figure 4.11A for experimental design schematic). This was achieved by applying 50 µL of NRs-PVCL solution to an excisional wound created with a standard 5 mm biopsy punch on the dorsum of CD-1 rats. This was followed by laser exposure at 0.65 W/cm^2 for 40 min. Control animals with only wounds were left without any treatment. The animals were euthanized after 72 hours and tissue samples were collected and fixed in 10% neutral buffered formalin, embedded in paraffin, sectioned, and stained with hematoxylin and eosin prior to microscopic evaluation. Tissues were scored by a pathologist, without knowledge of animal treatment using a scale of 1–4 (0 = normal, 1 = <5% of section affected, 2 = 5–10% of section affected, 3 = >10–30% of section affected, and 4 = >30% of section affected) on 7 inflammation-related parameters (relative numbers of polymorphonuclear leukocytes, macrophages, and lymphocytes, degree of hemorrhage, presence of fibrin, edema, and necrosis) and 2 parameters related to rate of healing (presence of granulation tissue and degree of epithelial regrowth over the wound). There were no significant differences either in inflammation scores or in rate of healing scores between tissues taken from rats that had been subject to laser

application as part of the PTT and those that had not undergone laser application (Figure 4.11B and Table 4.1). Finally, there may be concerns of nanoparticles transporting through the skin. A previous study showed that the localization of NPs in the skin can be observed by changes in the skin color and the NPs can be imaged using bright field microscopy after resection and silver staining[246]. After NRs exposure to the skin, a change in the skin color and the histopathology did not show nanoparticles and thus, it is concluded that the NRs were not transported through the skin within the timeframe and concentration used in this study. Thus, these results suggest that this treatment method is safe for use on animals.

4.3.5 Assessment of photothermal therapy technique on bacterial survival in vivo

After establishing the safety of the PTT on the skin and surrounding tissues, the bactericidal effect was investigated using the same excisional wound model. This was done by applying 1–2 × 10^6 CFU of *E. coli* to an excisional wound for 30 min to allow bacteria to attach to the tissue [247]. This was followed by application of 50 μL of NRs-PVCL solution then laser exposure at 0.65 W/cm^2 for 40 min as previously described. Five minutes after treatment, animals were euthanized, wound tissues were excised, homogenized, and serially diluted for bacterial plate count. Five minutes timeframe was selected because the immune system of the rat can potentially start to attack and kill these surface applied bacteria after 5 min, which could affect the therapeutic evaluation of the PTT strategy. The results indicated that PTT using NRs-PVCL reduced the bacterial load by 98% ($P < 0.001$) compared to the untreated wounds (Figure 4.11C and Figure 4.12C). Moreover, the effect of this technique on the wound healing process was investigated. The technique did not inhibit the wound healing process as the treated wounds healed at the same rate as control wounds (Figure 4.12A). Interestingly, the infected wounds also healed at the same rate as control wounds. This could be due to the non-invasiveness of this strain of *E. coli,* which can be cleared by the immune system [247]. During the course of wound healing no weight loss was observed (Figure 4.12B), further demonstrating the safety of the technique. Further studies are needed to determine if AMR bacteria such as methicillin-resistant *Staphylococcus aureus* would be similarly susceptible to the bactericidal effects of the PTT technique described here. However, such studies would require specialized biosafety facilities

but these studies are required to establish the therapeutic effectiveness of NRs-PVCL treatment system.

4.4 Conclusion

In conclusion, the work described herein demonstrated that a combination of a thermosensitive biocompatible polymer and GNPs can significantly reduce the bacterial load *in vitro* and *in vivo*. The PTT technique successfully reduced the bacterial load *in vitro* by 94–96% for gram-negative bacteria and by 50% for gram-positive bacteria. This technique also, reduced the bacterial load in experimentally infected wounds by 98%.

Unlike antimicrobials or other chemotherapeutics (e.g. silver-based materials, mafenide acetate, mupirocin, and polysoporin (polymyxin *B*) in which the mechanism of bacterial killing is based on the binding of the drug to a specific target within or on the bacterial cell wall, the PTT technique does not depend on bacterial binding. Antimicrobial chemotherapeutics are also limited in the spectrum of bacteria against which they are effective, being classified as effective against gram-negative or gam-positive bacteria or both. Additionally, these agents have potentially serious risks following prolonged or incorrect use, such as cytotoxicity accompanied by a delay in wound healing and risk of antimicrobial resistance[248–257]. In contrast, the PTT technique demonstrates bactericidal activity against both gram-positive and gram-negative bacteria by means of physical destruction of bacterial cell components. This mechanism of action circumvents standard modes of AMR and may be applied without requirement for preliminary culture and sensitivity testing, speeding the onset of therapy. In addition, this technique has the following characteristics: i) is simple to prepare and apply; ii) does not affect the stability of the dispersed NPs; iii) can be excited by low laser power that can be provided by a hand held laser device; and iv) is safe and has minimal effect on surrounding tissue or the healing process. Finally, additional investigation is required to establish the efficacy of the PTT technique described on more common causes of skin and soft tissue infections, such as methicillin-resistant *S. aureus*.

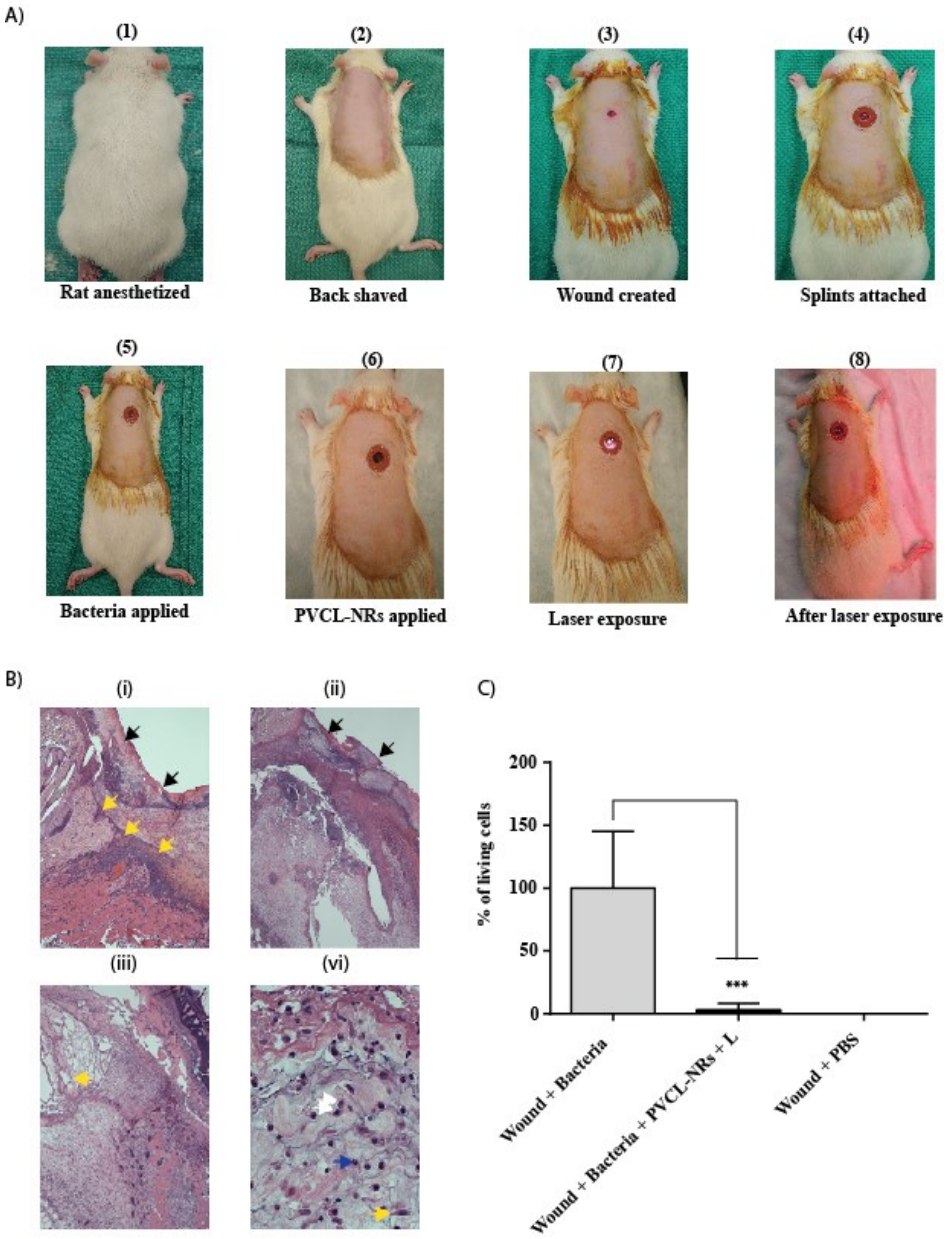

Figure 4.11. Evaluating the safety and the antibacterial effect of the PTT technique in vivo. (A) Schematic representation of the experimental design. B) Photomicrographs of the safety assessment of the PTT technique. Wounds treated with thermogel and laser (0.65W/cm^2 for 40 min) or control wounds without treatment. i) Control wound (x200) with serocellular crust (black arrows), moderate to marked mixed leukocytic infiltrate and re-epithelialization (yellow arrows) ii) Wound treated with thermogel and laser (x200) with serocellular crust (black arrows), moderate to marked mixed leukocytic infiltrate and loose granulation tissue in the mid to lower left of the image. iii) Control wound (x400) with granulation tissue subtending the wound bed with strands of fibrin (fine, thread-like pink strands, yellow arrow). iv) Wound treated with thermogel and laser (x400) with inflammatory cell infiltrate (macrophages, white arrows; and neutrophil, blue arrow), and evidence of early granulation (fibroblast, yellow arrow). (C) Antimicrobial effect of NR-PVCL and laser in infected wounds after 40 min of laser exposure at laser fluence of 0.65W/cm^2. Error bars represent standard deviation, where n = 3. ***P < 0.001.

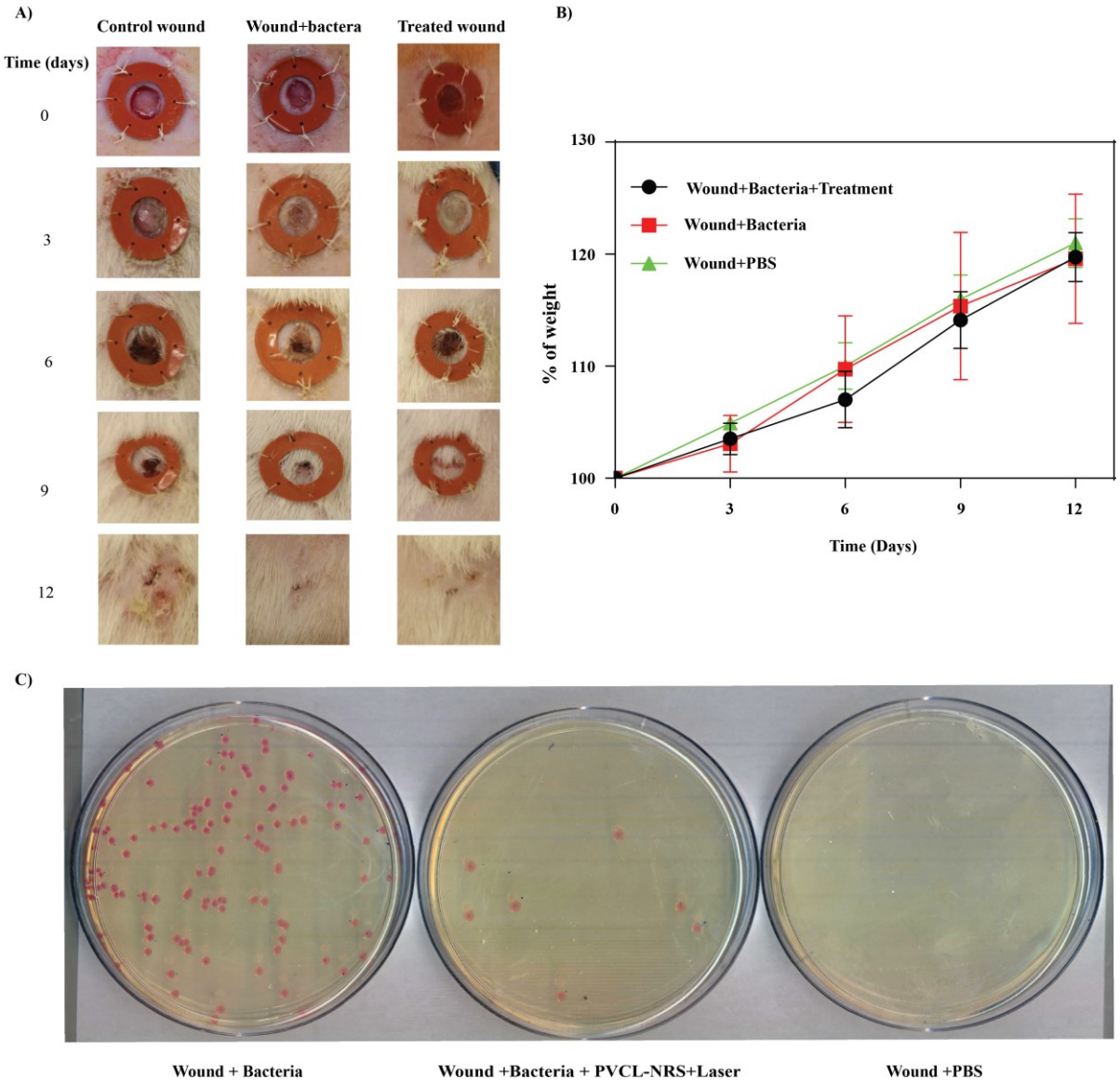

Figure 4.12. Safety assessment of PTT using NRs-PVCL on wound healing. A) Wound healing with and without treatment. The images show that the treated wounds heal at the same rate as control ones (n=3). B) Weight % due to thermogel treatment. No weight loss was observed for the treated and untreated animals. In contrast, all animals were gaining weight over time. C) Photos of *E. coli* colonies on Luria agar plates show the decrease in the colonies number due to NRs-PVCL+Laser treatment compared to the untreated wounds.

Table 4.1. Histology evaluation of wounds. (Yellow = treated wounds)

Rat #	Wound #	PMNs	Macrophg	Lymphcyte	Hemorr	Fibrin	Edema	Necrosis	Inflam Subscore	Granulation tissue	Epithelial regrowth	Healing subscore	Histo Comments
1	a	4	3	3	3	0	1	0	**14**	2	3	**5**	dense and thick serocellular crust, re-epithel~25%, hemorr w/in wound crater and subtending areas, min edema, no fibrin/necrosis, mild granuation, largely in crater and less around edges
	b	4	4	3	2	3	4	2	**22**	4	0	**4**	dense and thick serocellular crust, marked, loose granulation tissue, largely subtending crater admixed with patchy hemorrhage throughout, almost no re-epithelialization present, m/f areas of necrosis (largely muscle)
2	a	4	3	3	2	2	2	1	**17**	3	1	**4**	dense and thick serocellular crust, moderate loose granulation tissue, largely subtending crater admixed with patchy hemorrhage throughout, minimal re-epithelialization, focal area of necrosis (muscle)
	b	4	3	3	1	3	3	0	**17**	4	2	**6**	dense and thick serocellular crust, marked loose granulation tissue, largely subtending crater, mild re-epithelialization present
3	a	4	3	3	0	3	2	2	**15**	3	1	**4**	moderate serocellular crust, moderate loose granulation tissue, minimal re-epithelialization, multifocal areas of necrosis (muscle)
	b	4	3	3	2	2	3	1	**18**	2	0	**2**	dense and thick serocellular crust, moderate loose granulation tissue admixed with patchy hemorrhage throughout, no re-epithelialization, focal area of necrosis (muscle)
4	a	4	3	3	0	0	3	0	**13**	4	2	**6**	dense and thick serocellular crust, re-epithel~10%, mod edema, no fibrin/necrosis, marked granulation tissue
	b	4	3	3	1	0	2	0	**13**	4	3	**7**	dense and thick serocellular crust, marked dense granulation tissue, largely subtending crater, mod re-epithelialization present, no fibrin/necrosis
5	a	4	3	3	1	3	3	1	**17**	4	2	**6**	dense and thick serocellular crust, re-epithel~10%, mod edema, no fibrin/necrosis, marked granulation tissue
	b	4	3	2	1	3	4	1	**17**	4	2	**6**	dense and thick serocellular crust, re-epithel~10%, mod edema, no fibrin/necrosis, marked granulation tissue
6	a	4	3	3	0	4	4	0	**18**	3	1	**4**	dense and thick serocellular crust, re-epithel~5%, marked edema and fibrin, no necrosis, mod granulation tissue
	b	4	3	3	0	2	3	1	**15**	2	1	**3**	dense and thick serocellular crust, re-epithel~5%, marked edema and fibrin, no necrosis, mod granulation tissue

Chapter 5
Conclusions and Future work

5.1 Conclusions

The 20th century has witnessed a tremendous effort in the development and improvement of diagnostics and antimicrobials to combat and control infectious diseases. Rapid and early diagnosis of infectious pathogens will not only help prevent the transmission of pathogens, but will also enable healthcare-providers to provide appropriate treatment, thus improving the treatment outcomes, reducing health-care costs, and reducing the risk of AMR development [10,11,16,113]. Furthermore, delivering appropriate therapeutics is also a very important factor for successful disease management. The current advances in the field of nanotechnology has provided a new era of diagnostics and therapeutics development. GNPs are among the most common types of NPs that have been extensively used and have proven their versatility as potential candidates for disease bio-sensing and therapeutics. They can be easily synthesized with different shapes and sizes, and their surface can be easily modified with different ligands to perform different functions. The unique intrinsic bright color of these particles can be tuned by changing their size to detect presence or absence of an analyte providing an easy readout with the naked eye. Furthermore, when these particles are excited by light, the resulting energy is converted into heat. This makes GNPs potential candidates for thermal ablation. The work presented in this thesis described the development of simple yet effective platforms for combating infectious diseases and AMR in the context of theranostics using GNPs. In particular, the thesis focused on developing: i) POC diagnostic assay for accurate and rapid detection of infectious diseases and AMR, and ii) a versatile PTT for rapid treatment of wound infections associated with AMR bacteria.

In chapter 2, the integration of RPA or rt-RPA into MNAzyme-GNPs assay improved the analytical sensitivity of the assay by 6-orders of magnitude for the detection of HBV, and by 8-orders of magnitude for the detection of FluA. Over 90% clinical sensitivity and 95% clinical specificity were achieved when clinical specimens were screened using the colorimetric amplification system in a blinded manner. This system is potentially well-suited for rapid, cost-effective and sensitive diagnosis of viral diseases in POC settings since the entire assay can be performed within 2 hours, does not require expensive equipment, and can detect as low as 10^3 copies of genetic material.

In chapter 3, the RPA-MNAzyme-GNPs assay was used to detect and profile multiple AR determinants. Three different antibiotic resistant *S. aureus* strains were screened to demonstrate detection of multiple AR genes. This was achieved using multiplex RPA and MNAzyme reactions followed by parallel colorimetric signal readouts using different GNPs probes. The assay results of the three AR isolates were in agreement with PCR and culture results (gold standard methods). Furthermore, the MNAzyme-GNPs assay achieved analytical sensitivity of 10^2-10^3 DNA copies/reaction when synthetic DNA targets were used, and 10^2-10^3 CFU/ml when detecting antibiotic resistance genes in MRSA strains. The ability of MNAzyme-GNPs assay to provide comprehensive antibiotic susceptibility information can significantly improve the treatment outcomes, reduce health-care costs, and prevent emergence of AR.

In chapter 4, the use of a thermosensitive biocompatible polymer solution as a dispersion medium of NRs significantly improved their antimicrobial photo-thermal capability *in vitro* and *in vivo*. When the designated formulation was used in combination with laser excitation, a significant bacterial reduction of 96% and 65% was observed *in vitro* for AR gram-negative and gram-positive bacteria respectively. This technique also reduced the bacterial load in experimentally infected wounds by 98%. More importantly, this plasmonic thermogel can be prepared easily and applied to the wounds, can be excited by low laser power that can be provided by a hand-held laser device, safe for the operator, and does not have any adverse effects on the wound tissue or healing process.

5.2 Future work

This section highlights the potential future research studies that can facilitate the translation of these techniques to clinical settings.

[Study #1] Development of all-in-one portable device for assay automation.

A. Rationale and objective

The current MNAzyme-GNPs assay includes three major steps: nucleic acid extraction, amplification and signal readout using MNAzyme-GNPs assay. These steps involve the use of external devices (e.g. nucleic acid extraction device, water bath for incubation of MNAzyme reaction mixture and centrifuge for post RPA purification) and extensive pipetting and labor work.

Therefore, the objective of this future study will focus on the elimination of heating steps associated with the current MNAzyme reaction, avoidance of centrifugation step post-RPA while developing all-in-one portable device that can automate the whole process. This study will facilitate the translation of MNAzyme-GNPs assay to POC settings by developing a simple and portable device that can process and analyze samples with the push of a single button.

B. Envisioned experimental design

1). Elimination of heating step associated with MNAzyme reaction. One limitation of the current MNAzyme-GNPs assay is the requirement of high incubation temperature (~50 ^{o}C) for the optimum catalytic activity of MNAzyme, which requires a water bath or other heating devices. In recent studies, however, it was demonstrated that the incubation temperature of MNAzyme could be further reduced by using a cationic co-polymer that consists of a polycationic backbone and hydrophilic chain of dextran[258,259]. These studies showed that incorporation of this polymer into MNAzyme assay achieved high enzymatic activity over a wide range of temperature (25 – 50 ^{o}C). Therefore, incorporating this polymer into the MNAzyme-GNPs assay will potentially simplify the assay by eliminating the heating step, hence, making the device design more amendable for use in POC settings.

2). *Elimination of centrifugation step post RPA*. The current post-RPA purification step involves the use of spin-columns to collect amplified products while removing proteins used in the RPA reaction. This step can be simplified using proteinase K (Figure 5.1). Proteinase K can rapidly digest proteins involved in the RPA reaction[260] which avoids the need for centrifugation.

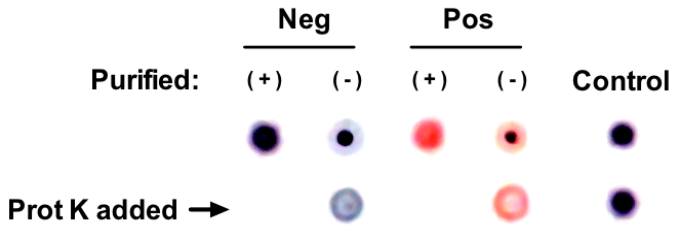

Figure 5.1. Post-RPA purification by Proteinase K. In this preliminary experiment, RPA products were compared with and without spin-column purification. Unpurified samples that produced aggregated spots at the core were mixed with Proteinase K for 15 min to prevent undesirable interaction between RPA proteins and DNA in MNAzyme-GNP assay.

3). *Design of all-in-one device for POC testing*. A portable all-in-one device that can automate the nucleic acid extraction for QDs barcode assay is currently under development in Chan's lab by a PhD student Pranav Kadhiresan. This device can also be adopted for MNAzyme-GNPs assay and it is intended to work as follow: 1) biological samples (e.g. blood, urine, serum…etc) will be collected from patients and added into an extraction unit that contains chemical cell lysis reagents, 2) the lysed sample will be then treated with binding buffer and passed through a filter column to trap the extracted nucleic acid, 3) DNA will be then eluted by pumping in an elution buffer, 4) the eluted DNA will be then pumped into a tube that contains RPA reagent for gene amplification, 5) the amplicons will be pumped into another reaction tube that contains proteinase K for sample purification, 6) the purified amplicons will be mixed with NaOH and blocking strands followed by HCl, 7) the blocked amplicons will be pumped into a tube that contains lyophilized MNAzyme and gold nanoparticle, 8) finally, a microinjector will be used to spot the GNPs onto TLC plate for visualization by the naked eye or smart phone (Figure 5.2).

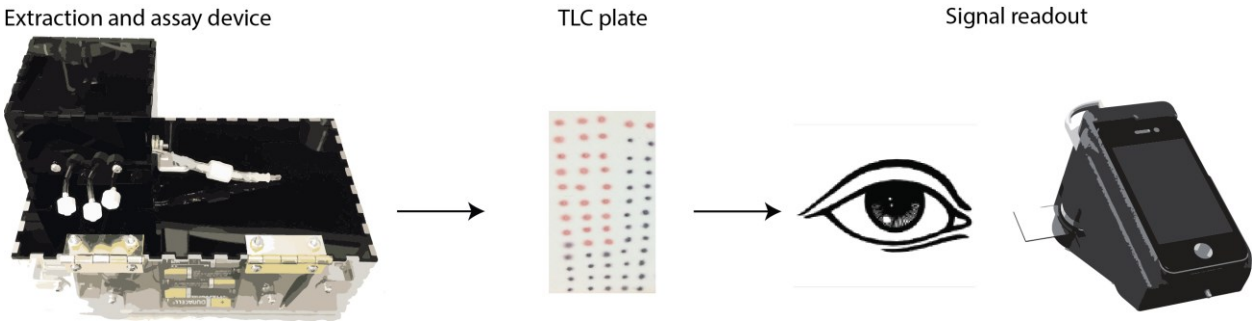

Figure 5.2. Envisioned point-of-care diagnostic device. The device uses a high flow rate 100 Series Williamson peristaltic pump in conjunction with an RV-SN2 10-way rotary valve to direct the required reagents from pre-loaded micro-centrifuge tubes into a Bio-Basic EZ-10 sample spin column. Eluate is directed into a scintillation vial by means of a low flow rate Takasago RP-Q1 peristaltic pump. Automation is controlled by an ATMega328 AVR Dev board and programmed using open-source Arduino IDE. Both peristaltic pumps are controlled by means of a DRV8835 dual motor shield, while the rotary valve stepper motor is controlled by means of an Autodriver L6470 motor control board. The described components are housed in a laser cut acrylic box. Adapted with permission from Pranav Kadhiresan..

[Study #2] MNAzyme-GNPs diagnostic device as a universal platform for detection of IDs and their AMR profiles

A. Rationale and objective

In chapter 2, the MNAzyme-GNPs assay successfully detected two viral diseases HBV and FluA in clinical samples. However, the versatility of this assay for diagnosing different diseases

and AR determinants in clinical samples needs to be verified. Therefore, the objective of this future study is to develop different disease and AR panels for parallel detection of multiple pathogens and profile their AR genes in clinical patient samples before the device is commercially available. The parallel detection will increase the outcome information of the assay and make it more comprehensive, versatile and therefore, suitable for POC testing.

B. Envisioned experimental design

1). Parallel detection of infectious pathogens. As a continuation of chapter 2, a panel of related sexually transmitted diseases (e.g. HBV, HCV and HIV), or respiratory viruses (FluA, FluB, RHV, and ADV) needs to be developed and tested. In a proof of concept experiment to test for possible cross-reactivity between specific MNAzymes of HBV and HCV, it was found that non-specific MNAzymes do not get activated (Figure 5.3) indicating the feasibility of the assay for parallel detection of related diseases. Furthermore, different panels for differentiation between infections caused by viruses and those caused by bacteria need to be developed. Respiratory tract infection for instance can be caused by Flu viruses which produces respiratory symptoms that are clinically similar to those caused by streptococci and mycoplasmas[74]. A clinical screening of viral and bacterial pathogens in parallel is therefore needed before initiation of treatment[12,74]. The outcome test results will then determine the specified AR panel to be tested. This in effect will reduce the unnecessary use of antibiotics for viral infections, the cost of treatment, and mitigate risk of AR development.

2). Parallel detection of AR genes. In a similar manner, panels of different AR genes for different pathogens need to be developed to demonstrate the versatility of the device to profile AR of different pathogens (e.g. bacteria, viruses and parasites) in clinical samples.

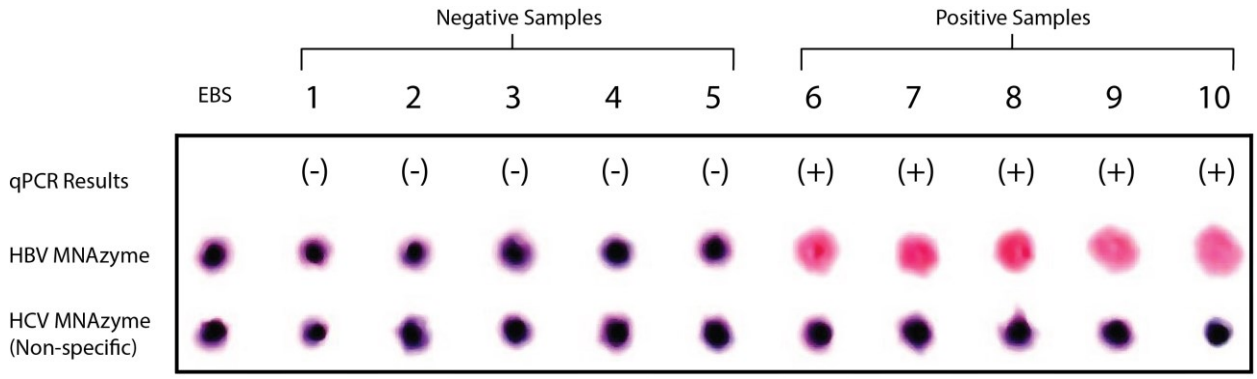

Figure 5.3. Cross-reactivity of MNAzyme-GNP assay. Five HBV-positive RPA products were incubated with specific HBV MNAzyme, and non-specific HCV MNAzyme.

[Study#3] MNAzyme assay for toleration of nucleic acid mutations

A. Rationale and objective

Nucleic acid based diagnostic assays can be influenced by mutations or sequence variations. It has been reported that viruses such as: HBV, HCV and HIV can exist as quasi-species due to mutation or variations in their genome sequences. These mutations could develop due to alteration at a single base pair or multiple base pairs[261]. Similarly, AR can also be acquired via mutation in chromosomal genes[65,262,263]. Currently our assay can only detect conserved genetic elements. Therefore, further testing is required to test the ability of MNAzyme-GNPs assay to tolerate or detect mutations.

B. Envisioned experimental design

Temperature is one of the key factors that influences hybridization of nucleic acids. For example, presence of mismatches can lower the melting temperature of nucleic acid strands. Therefore, using high incubation temperatures could result in false negative results due to inability of the target to hybridize with the MNAzyme sensor arm. This problem however, can be addressed by incorporation of cationic co-polymer[258,259] that activates MNAzyme over a wide range of temperatures. The incubation temperature of the assay can be then adjusted to a lower level than the melting temperature to allow hybridization between MNAzyme and the complementary mismatched target. On the other hand, it has been demonstrated that MNAzyme can be also used to detect single point mutations (SNPs). This has been demonstrated via truncation of the

MNAzyme sensor arm and incorporation of stabilizer arm[264]. In this context, the target sequence with a SNP hybridizes with the truncated arm of the MNAzyme, which activates the MNAzyme (Figure 5.4). Therefore, MNAzyme-GNPs assay can be adapted to tolerate or detect genetic mutations.

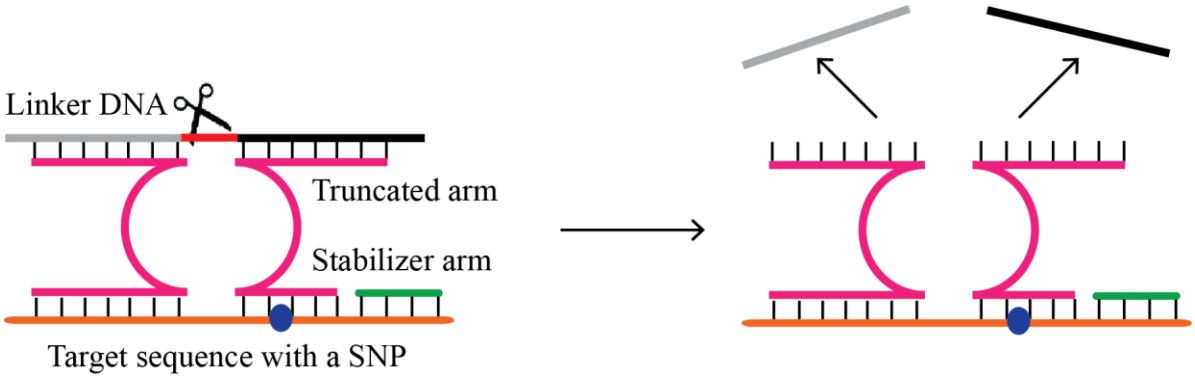

Figure 5.4. Truncated MNAzyme design for detection of SNPs. Truncated MNAzyme hybridizes with a target sequence that contains a SNP. The MNAzyme is activated in the presence of the stabilizer arm.

[Study #4] Development of photo-thermal wound bandage

A. Rational and Objective

In chapter 4, the ability of plasmonic thermogel to disinfect wounds contaminated with AR bacteria was reported. This concept was demonstrated in a flat wound model, where it was easy to apply the NRs-PVCL solution on the top of the wound. However, in order to bring this technique to clinical or health-care settings, the following challenges need to be addressed; need for a pipette or syringe to apply the solution onto the wound, difficulty in applying liquid solutions onto inclined or non-flat wounds, wash off of the thermogel solution by blood or wound fluids, and spill off of the solution due to uncontrolled or frequent movement of patients. Therefore, the objective of this future study is to develop a photo-thermal wound dressing or bandage that can be easily handled and attached to the wounds. This photo-thermal bandage will simplify the technique and make it user friendly.

B. Envisioned design

The NRs-thermogel bandage can be synthesized using an electrospinning method described by Abrigo el al [265]. A typical electrospinning setup is shown in Figure 5.5 and it consists of syringe pump and capillary needle, high voltage power supply, and a grounded collector. In this process, a high voltage is applied to the polymer solution at the tip of capillary needle and forms a charged jet. The jet is then dried and collected on the grounded collector in the form of nano/micrometric fibrous mesh[266,267]. In a similar manner, the photo-thermal bandage can be fabricated using electrospinning method. This bandage can be then attached to the infected wounds or other lesions, followed by laser irradiation, resulting in wound sterilization or disinfection (Figure 5.5).

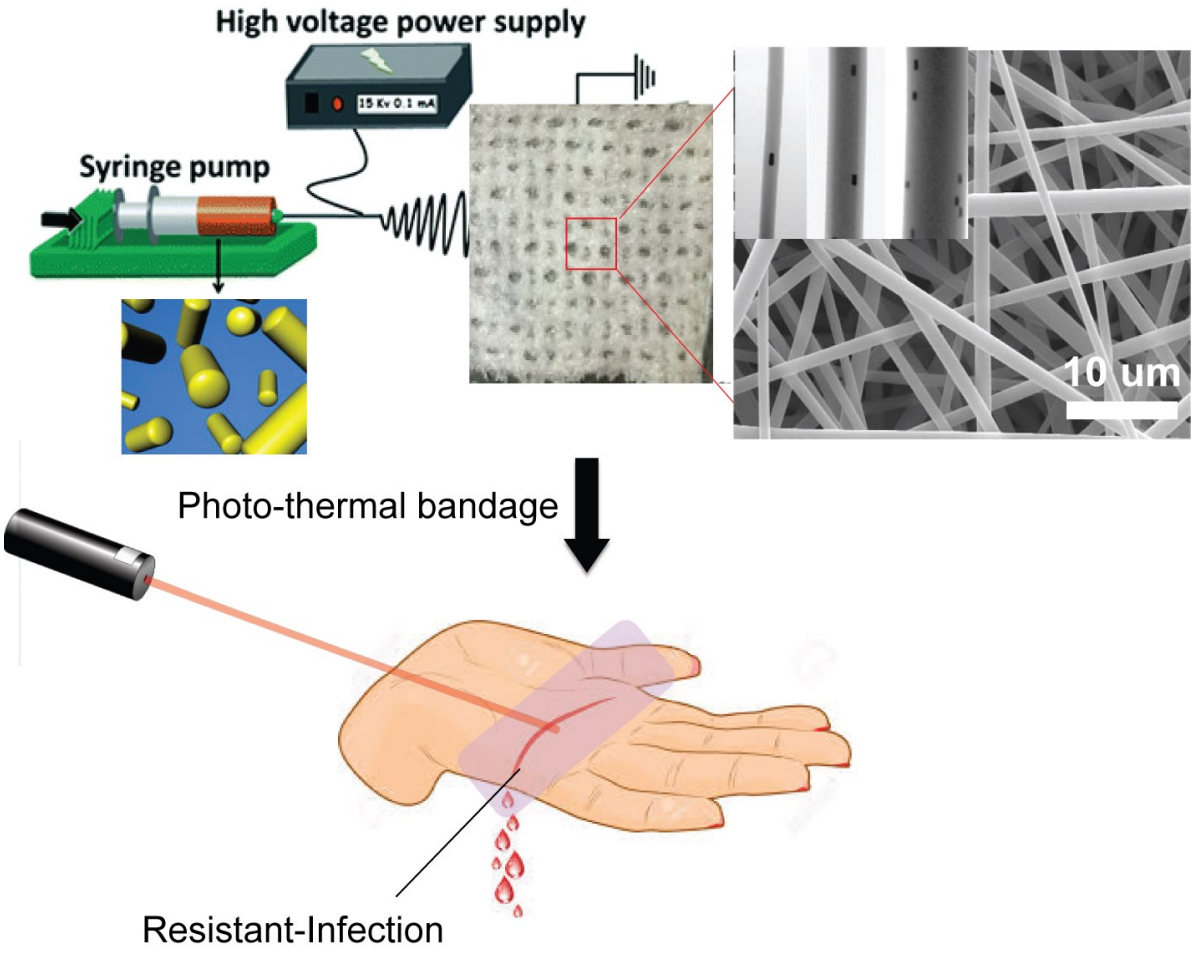

Figure 5.5. Concept of light-trigger wound dressing for disinfection of antibiotic resistance bacteria. NRs in thermogel solution is subjected to high voltage to make microfiber encapsulated with NRs. The resulting wound dressing can be attached onto wound infected area followed by laser exposure. Reproduced from ref [268]. Copyright 2016 with permission from Vahid Raeesi.

References

1. World Health Organization. http://www.who.int/topics/infectious_diseases/en/.

2. Woolhouse, M. E. J. & Gowtage-Sequeria, S. Host range and emerging and reemerging pathogens. *Emerg. Infect. Dis.* **11,** 1842–1847 (2005).

3. Taylor, L. H., Latham, S. M., Woolhouse, M. E. J., Lathamt, S. M. & Bush, E. Risk factors for human disease emergence. **356,** 983–989 (2013).

4. Hay, S. I. *et al.* Global mapping of infectious disease. *Philos. Trans. R. Soc. Lond. B. Biol. Sci.* **368,** 1–11 (2013).

5. Cleaveland, S., Laurenson, M. K. & Taylor, L. H. Diseases of humans and their domestic mammals: pathogen characteristics, host range and the risk of emergence. *Philos. Trans. R. Soc. Lond. B. Biol. Sci.* **356,** 991–9 (2001).

6. World Health Organization. http://www.who.int/mediacentre/factsheets/fs310/en/.

7. Sanders, J. W., Fuhrer, G. S., Johnson, M. D. & Riddle, M. S. The epidemiological transition: The current status of infectious diseases in the developed world versus the developing world. *Sci. Prog.* **91,** 1–37 (2008).

8. Turner, R. B. Epidemiology, pathogenesis, and treatment of the common cold. *Ann. allergy, asthma Immunol.* **78,** 531–540 (1997).

9. Gupta, I. & Guin, P. Communicable diseases in the South-East Asia Region of the World Health Organization: towards a more effective response. *World Heal. Organ. Bull. World Heal. Organ.* **88,** 199–205 (2010).

10. WHO. Urgently needed : rapid , sensitive , safe and simple Ebola diagnostic tests. *http://www.who.int/mediacentre/news/ebola/18-november-2014-diagnostics/en/ The* (2014).

11. Hauck, T. S., Giri, S., Gao, Y. & Chan, W. C. W. Nanotechnology diagnostics for infectious diseases prevalent in developing countries. *Adv. Drug Deliv. Rev.* **62,** 438–448

(2010).

12. Peeling, R. W. & Mabey, D. Point-of-care tests for diagnosing infections in the developing world. *Clin. Microbiol. Infect.* **16,** 1062–1069 (2010).

13. Pai, N. P., Vadnais, C., Denkinger, C., Engel, N. & Pai, M. Point-of-Care Testing for Infectious Diseases: Diversity, Complexity, and Barriers in Low- And Middle-Income Countries. *PLoS Med.* **9,** 1–7 (2012).

14. Sharma, S., Zapatero-Rodríguez, J., Estrela, P. & O'Kennedy, R. Point-of-Care diagnostics in low resource settings: Present status and future role of microfluidics. *Biosensors* **5,** 577–601 (2015).

15. Yu, A. C.-H. *et al.* Nucleic acid-based diagnostics for infectious diseases in public health affairs. *Front. Med* **6,** 173–86 (2012).

16. CDC. About Antibiotic Resistance. *http://www.cdc.gov/drugresistance/about.html* (2015).

17. Neu, H. C. Crisis in Antibiotic Resistance. *Science (80-.).* **257,** 1064–1073 (1992).

18. O'Neill, J. Antimicrobial Resistance : Tackling a crisis for the health and wealth of nations. *Rev. Antimicrob. Resist.* 1–20 (2014).

19. Monto, A. S. Viral respiratory infections in the community: Epidemiology, agents, and interventions. *Am. J. Med.* **99,** 66–69 (1995).

20. Gibson, G. J., Loddenkemper, R., Lundback, B. & Sibille, Y. Respiratory health and disease in Europe: the new European Lung White Book. *Eur. Respir. J.* (2013). doi:10.1183/09031936.00105513

21. Stover, C. S. & Litwin, C. M. The Epidemiology of Upper Respiratory Infections at a Tertiary Care Center: Prevalence, Seasonality, and Clinical Symptoms. *J. Respir. Med.* **2014,** (2014).

22. Denny, F. W. The Clinical Impact of Human Respiratory Virus Infections. *Am. J. Respir. Crit. Care Med.* **152,** S4–S12 (1995).

23. Gwaltney, J. M. Clinical Significance and Pathogenesis of Viral Respiratory Infections. *Am. J. Med.* **112,** 13S–18S (2002).

24. Taubenberger, J. K. & Kash, J. C. Influenza virus evolution, host adaptation, and pandemic formation. *Cell Host Microbe* **7,** 440–451 (2010).

25. Johnson, N. P. A. S. & Mueller, J. Updating the accounts: global mortality of the 1918-1920 'Spanish' Influenza Pandemic. *Bull. Hist. Med.* **76,** 105–115 (2002).

26. Centers for Disease Control and Prevention (CDC). Types of Influenza Viruses. *https://www.cdc.gov/flu/about/viruses/types.htm*

27. Al-Tawfiq, J. A. *et al.* Surveillance for emerging respiratory viruses. *Lancet Infect. Dis.* **14,** 992–1000 (2014).

28. Vemula, S. *et al.* Current Approaches for Diagnosis of Influenza Virus Infections in Humans. *Viruses* **8,** 1–15 (2016).

29. Centers for Disease Control and Prevention (CDC). Bloodborne pathogens and workplace sharps injuries. *https://www.cdc.gov/niosh/stopsticks/bloodborne.html* (2010).

30. WHO. Hepatitis B. *http://www.who.int/mediacentre/factsheets/fs204/en/* (2016).

31. WHO. Hepatitis C. *http://www.who.int/mediacentre/factsheets/fs164/en/* (2016). doi:10.1016/j.mpmed.2011.06.007

32. WHO. Global Burden of Disease (GBD) for Hepatitis C. *J. Clin. Pharmacol.* **44,** 20–29 (2004).

33. Averhoff, F. M., Glass, N. & Holtzman, D. Global burden of hepatitis C: considerations for healthcare providers in the United States. *Clin. Infect. Dis.* **55,** 10–15 (2012).

34. WHO. HIV/AIDS WHO. *http://www.who.int/immunization/topics/hiv/en/index1.html*

35. Shao, Y. & Williamson, C. The HIV-1 epidemic: Low- to middle-income countries. *Cold Spring Harb. Perspect. Med.* **2,** (2012).

36. UNAIDS. The Gap Report. (2013).

37. Kania, D. *et al.* Combining rapid diagnostic tests and dried blood spot assays for point-of-care testing of human immunodeficiency virus, hepatitis B and hepatitis C infections in burkina faso, west africa. *Clin. Microbiol. Infect.* **19,** E533–E541 (2013).

38. White, B. & Seaton, R. A. Complicated skin and soft tissue infections: literature review of evidence for and experience with daptomycin. *Infect. Drug Resist.* **4,** 115–27 (2011).

39. Janda, J., Abbott, S. & Brenden, R. Overview of the Etiology of Wound Infections with Particular Emphasis on Community-Acquired Illnesses. *Eur. J. Clin. microbilogy Infect. Dis.* **16,** 189–201 (1997).

40. Vincent Ki, C. R. Bacterial skin and soft tissue infections in adults : A review of their epidemiology , pathogenesis , diagnosis , treatment and site of care. *Can. J. Infect. Dis. Med. Microbiol.* **19,** (2008).

41. Emori, T. G. & Gaynes, R. P. An Overview of Nosocomial Infections , Including the Role of the Microbiology Laboratory. *Clin. Microbiol. Rev.* **6,** 428–442 (1993).

42. Giacometti, A. *et al.* Epidemiology and Microbiology of Surgical Wound Infections. *J. Clin. Microbiol.* **38,** 918–922 (2000).

43. Eron, L. J. *et al.* Managing skin and soft tissue infections : expert panel recommendations on key decision points Edited by. *J. Antimicrob. Chemother.* **52,** i3–i7 (2003).

44. Patel, N. P., Granick, M. S. & Kanakaris, N. K. Comparison of Wound Education in Medical Schools in the United States , United Kingdom , and Germany. *Eplasty* 61–67 (2008).

45. HALEY, R. W. *et al.* THE EFFICACY OF INFECTION SURVEILLANCE AND CONTROL PROGRAMS IN PREVENTING NOSOCOMIAL INFECTIONS IN US HOSPITALS In the acute-care hospitals in the United complicated the 37 . 7 million admissions , for a nationwide infection rate of 5 . 7 nos- ocomial inf. *Am. J. Epidemiol.* **121,** 182–205 (1985).

46. Edwards, R. & Harding, K. G. Bacteria and wound healing Colonisation Contamination. *Curr. Opin. Infect. Dis.* **17,** 91–96 (2004).

47. Dryden, M. S. Complicated skin and soft tissue infection. *J. Antimicrob. Chemother.* **65 Suppl 3,** iii35-44 (2010).

48. Robson, M. C., Mannari, R. J., Smith, P. D. & Payne, W. G. Maintenance of wound bacterial balance. *Am. J. Surg.* **178,** 399–402 (1999).

49. Gilbert, P. & Allison, D. Principles of Microbial Pathogenicity and Epidemiology. *Hugo Russell's Pharm. Microbiol. 7th ed. Blackwell Sci. Ltd, Massachusetts – USA,* 103–114 (2004).

50. Guo, S. & Dipietro, L. a. Factors affecting wound healing. *J. Dent. Res.* **89,** 219–29 (2010).

51. Bisno, A. L. & Stevens, D. STREPTOCOCCAL INFECTIONS OF SKIN AND SOFT TISSUES. *N. Engl. J. Med.* 240–245 (1996).

52. Amagai, M., Matsuyoshi, N., Wang, Z. H., Andl, C. & Stanley, J. R. Toxin in bullous impetigo and staphylococcal scalded-skin syndrome targets desmoglein 1. *Nat. Med.* **6,** 1275–7 (2000).

53. Nichols, R. L. & Florman, S. Clinical presentations of soft-tissue infections and surgical site infections. *Clin. Infect. Dis.* **33,** 84–93 (2001).

54. Kingsley, A. The Wound Infection Continuum and Its Application to Clinical Practice. *Ostomy wound mangement* **49,** 1–7 (2003).

55. Filius, P. M. G. & Gyssens, I. C. Impact of increasing antimicrobial resistance on wound management. *Am. J. Clin. Dermatol.* **3,** 1–7 (2002).

56. Guan, X. *et al.* Laboratory diagnosis, clinical management and infection control of the infections caused by extensively drug resistant gram-negative bacilli: A Chinese consensus statement. *Clin. Microbiol. Infect.* **22,** S15–S25 (2016).

57. WHO. Antimicrobial resistance. *http//www.who.int/mediacentre/factsheets/fs194/en/ Key*

58. Pillay, D. & Zambon, M. Antiviral drug resistance. *BMJ* **317,** 3–5 (1998).

59. Strasfeld, L. & Chou, S. Antiviral Drug Resistance: Mechanisms and Clinical Implications. *Infect. Dis. Clin. North Am.* **24,** 413–437 (2010).

60. CDC. Updated Interim Recommendations for the Use of Antiviral Medications in the Treatment and Prevention of Influenza for the 2009-2010 Season. *https://www.cdc.gov/H1N1flu/recommendations.htm*

61. Abbas, Z. & Siddiqui, A. R. Management of hepatitis B in developing countries. *World J. Hepatol.* **3,** 292–299 (2011).

62. Sosa, A. bal de J. *et al.* Antimicrobial Resistance in Developing Countries. *Springer New York Dordr. Heidelb.* 1–554 (2010).

63. Wright, G. D. Bacterial resistance to antibiotics : Enzymatic degradation and modification. *Adv. Drug Deliv. Rev.* **57,** 1451–1470 (2005).

64. Davies, J. & Wright, G. D. Bacterial resistance to aminoglycoside antibiotics. *Trends Microbiol.* 234–240 (1997).

65. Lambert, P. A. Bacterial resistance to antibiotics : Modified target sites. *Adv. Drug Deliv. Rev.* **57,** 1471–1485 (2005).

66. Kumar, A. & Schweizer, H. P. Bacterial resistance to antibiotics : Active efflux and reduced uptake. *Adv. Drug Deliv. Rev.* **57,** 1486–1513 (2005).

67. Andersson, D. I. & Hughes, D. Antibiotic resistance and its cost : is it possible to reverse resistance ? *Nat. Rev. Microbiol.* **8,** 260–271 (2010).

68. Kumar, N. Antimicrobial Resistance in Developing Countries Global Trends. *http://www.who.int/phi/implementation/NKGanguly_India.pdf?ua=1*

69. Klein, E., Smith, D. L. & Laxminarayan, R. Hospitalizations and Deaths Caused by

Methicillin-Resistant Staphylococcus aureus, 1999-2005. *Emerg. Infect. Dis.* **13,** 1840–1846 (2007).

70. Mediavilla, J. R. *et al.* Colistin- and Carbapenem-Resistant Escherichia coli Harboring mcr-1 and blaNDM-5 , Causing a Complicated Urinary Tract Infection in a Patient from the United States. *MBio* **7,** 5–8 (2016).

71. O'Neill, J. Rapid Diagnostics: Stopping Unnecessary Use of Antibiotics. *Rev. Antimicrob. Resist.* 1–36 (2015).

72. Misawa, S. Rapid diagnosis of infectious diseases; features and limitations of the microscopic examination of clinical specimens. *J. Assoc. Rapid Method Autom. Microbiol.* **10,** 121–131 (1999).

73. *Bergey's Manual of Systematic Bacteriology second edition*. *Springer-Verlag New York Inc.* (Springer, 2010). doi:10.1007/978-0-387-68572-4

74. Washington, J. A. *Medical Microbiology 4th edition: Principles of Diagnosis*. (Galveston (TX): University of Texas Medical Branch at Galveston, 1996).

75. Christiansen, B. C., Jessen, T. E., Nielsen, C. & Staun-Olsen, P. False Negative Anti-HIV1/ HlV2 ELlSAs in Acute HIV-2 Infection. *VoxSanguinis* **70,** 144–147 (1996).

76. Archana, S. & Marfatia, Y. S. Laboratory diagnosis of HIV. *Indian J Sex Transm Dis* **29,** 42–45 (2008).

77. Ghosh, M., Nandi, S., Dutta, S. & Saha, M. K. Detection of hepatitis B virus infection: A systematic review. *World J. Hepatol.* **7,** 2482–2491 (2015).

78. Supran, E., Boxall, E., Craske, J., Vandervelde, E. M. & Gardner, P. S. Enzyme-linked immunosorbent assay (ELISA) for the detection of hepatitis Be antigen and antibody: report of a field trial. *J. Clin. Pathol.* **36,** 581–585 (1983).

79. Swellam, M., Mahmoud, M. S. & Ali, A. A.-F. Diagnosis of hepatitis C virus infection by enzyme-linked immunosorbent assay and reverse transcriptase-nested polymerase chain

reaction: a comparative evaluation. *IUBMB Life* **63,** 430–434 (2011).

80. Barrera, J. M. Diagnostic tests for hepatitis C virus infection. *Nephrol. Dial. Transplant.* **15,** 15–18 (2000).

81. Ndao, M. Diagnosis of Parasitic Diseases: Old and New Approaches. *Interdiscip. Perspect. Infect. Dis.* 1–15 (2009). doi:10.1155/2009/278246

82. Galikowska, E. *et al.* Specific detection of Salmonella enterica and Escherichia coli strains by using ELISA with bacteriophages as recognition agents. *Eur. J. Clin. Microbiol. Infect. Dis.* **30,** 1067–1073 (2011).

83. Gan, S. D. & Patel, K. R. Enzyme immunoassay and enzyme-linked immunosorbent assay. *J. Invest. Dermatol.* **133,** 1–3 (2013).

84. Hu, J. *et al.* Advances in paper-based point-of-care diagnostics. *Biosens. Bioelectron.* **54,** 585–597 (2014).

85. Yetisen, A. K., Akram, M. S. & Lowe, C. R. Paper-based microfluidic point-of-care diagnostic devices. *Lab Chip* **13,** 2210–2251 (2013).

86. Posthuma-Trumpie, G. A., Korf, J. & Van Amerongen, A. Lateral flow (immuno)assay: Its strengths, weaknesses, opportunities and threats. A literature survey. *Anal. Bioanal. Chem.* **393,** 569–582 (2009).

87. Rohrman, B. A., Leautaud, V., Molyneux, E. & Richards-Kortum, R. R. A Lateral Flow Assay for Quantitative Detection of Amplified HIV-1 RNA. *PLoS One* **7,** 1–8 (2012).

88. Tangpukdee, N., Duangdee, C., Wilairatana, P. & Krudsood, S. Malaria diagnosis: A brief review. *Korean J. Parasitol.* **47,** 93–102 (2009).

89. Vidal, J. E. & Boulware, D. R. Lateral Flow Assay for Cryptococcal Antigen: an Important Advance To Improve the Continuum of Hiv Care and Reduce Cryptococcal Meningitis-Related Mortality. *Rev. Inst. Med. Trop. Sao Paulo* **57,** 38–45 (2015).

90. Suria, M., Afendy, M., Azlina, N. M. & Zamri, I. Lateral flow assay strip for detection of

Escherichia coli O157 : H7. *Int. Food Res. J. 22(6)* **22,** 2587–2593 (2015).

91. Zhao, Y. *et al.* Rapid multiplex detection of 10 foodborne pathogens with an up-converting phosphor technology-based 10-channel lateral flow assay. *Sci. Rep.* **6,** 1–8 (2016).

92. Roberts, J. R. Urine Dipstick Testing: Everything You Need to Know. *Emerg. Med. News* 24–27 (2007). doi:10.1097/01.EEM.0000279130.93159.d9

93. Wang, S. Q., Chinnasamy, T., Lifson, M. A., Inci, F. & Demirci, U. Flexible Substrate-Based Devices for Point-of-Care Diagnostics. *Trends Biotechnol.* **34,** 909–921 (2016).

94. Espy, M. J. *et al.* Real-Time PCR in Clinical Microbiology : Applications for Routine Laboratory Testing. *Clin. Microbiol. Rev.* **19,** 165–256 (2006).

95. Yang, S. & Rothman, R. E. PCR-based diagnostics for infectious diseases: Uses, limitations, and future applications in acute-care settings. *Lancet Infect. Dis.* **4,** 337–348 (2004).

96. WHO. Establishment of laboratory in developing countries. *http://apps.searo.who.int/PDS_DOCS/B4745.pdf* (2011).

97. Center for Disease Control and Prevention. Antibiotic resistance threats in the united states. (2013).

98. Jorgensen, J. H. & Ferraro, M. J. Antimicrobial Susceptibility Testing : A Review of General Principles and Contemporary Practices. *Med. Microbiol.* **49,** 1749–1755 (2009).

99. Mothershed, E. A. & Whitney, A. M. Nucleic acid-based methods for the detection of bacterial pathogens : Present and future considerations for the clinical laboratory. *Clin. Chim. acta* **363,** 206–220 (2006).

100. Deshpande, A. *et al.* A rapid multiplex assay for nucleic acid-based diagnostics. *J. Microbiol. Methods* **80,** 155–163 (2010).

101. Deshpande, A. & White, P. S. Multiplexed nucleic acid-based assays for molecular

diagnostics of human disease. *Expert Rev. Mol. Diagn.* 645–659 (2012).

102. CLSI. *Performance Standards for Antimicrobial Susceptibility Testing ; Seventeenth Informational Supplement*. **27,** (2007).

103. Marlowe, E. M. & Bankowski, M. J. Conventional and molecular methods for the detection of methicillin-resistant Staphylococcus aureus. *J. Clin. Microbiol.* **49,** 53–56 (2011).

104. Leekha, S., Terrell, C. L. & Edson, R. S. General principles of antimicrobial therapy. *Mayo Clin. proceedings.* **86,** 156–67 (2011).

105. Andrews, J. M. Determination of minimum inhibitory concentrations. *J. Antimicrob. Chemother.* **48,** 5–16 (2001).

106. CLSI. *Performance standards for antimicrobial susceptibility testing ; twenty-first informational supplement*. **31,** (2011).

107. Deshpande, A. & White, P. S. Multiplexed nucleic acid-based assays for molecular diagnostics of human disease. *Expert Rev. Mol. Diagn.* **12,** 645–59 (2012).

108. Strommenger, B., Kettlitz, C., Werner, G. & Witte, W. Multiplex PCR Assay for Simultaneous Detection of Nine Clinically Relevant Antibiotic Resistance Genes in Staphylococcus aureus. *J. Clin. Microbiol.* **41,** 4089–4094 (2003).

109. Malhotra-kumar, S., Lammens, C., Piessens, J. & Goossens, H. Multiplex PCR for Simultaneous Detection of Macrolide and Tetracycline Resistance Determinants in Streptococci. *Antimicrob. Agents Chemother.* **49,** 4798–4800 (2005).

110. Ágoston Ghidána, Csaba Jeneya, Csaba L. Maródia, K. C. and F. R. PCR detection of the vanA gene in a vancomycin-resistant Enterococcus faecalis clinical isolate from Hungary. *J. Antimicrob. Chemother.* **46,** 325–327 (2000).

111. Colom, K., Pe, J. & Larin, E. Simple and reliable multiplex PCR assay for detection of bla TEM , bla SHV and bla OXA À 1 genes in Enterobacteriaceae. *FEMS Microbiol. Lett.*

223, 147–151 (2003).

112. Laxminarayan, R. Antibiotic effectiveness: Balancing conservation against innovation. *Science (80-.).* **345,** 1299–1301 (2014).

113. The TDR Diagnostics Evaluation Expert Panel. Evaluation of diagnostic tests for infectious diseases: general principles. *Nat. Rev. Microbiol.* **6,** S17–S29 (2010).

114. WHO. Antimicrobial Resistance: Global Report on Surveillance. *http//www.who.int/drugresistance/documents/surveillancereport/en/ Overv.* 2014 (2014).

115. Betty Y.S. Kim, James T. Rutka, and W. C. W. C. Nanomedicine. *new Engl. J. o f Med.* **363,** 2434–2443 (2010).

116. Eustis, S. & El-Sayed, M. Why gold nanoparticles are more precious than pretty gold: noble metal surface plasmon resonance and its enhancement of the radiative and nonradiative properties of nanocrystals of different shapes. *Chem. Soc. Rev.* **35,** 209–17 (2006).

117. Dreaden, E. C., Alkilany, A. M., Huang, X., Murphy, C. J. & El-Sayed, M. A. The golden age: gold nanoparticles for biomedicine. *Chem. Soc. Rev.* **41,** 2740–79 (2012).

118. Link, S. & El-sayed, M. A. Shape and size dependence of radiative , non-radiative and photothermal properties of gold nanocrystals. *Int. Rev. Phys. Chem.* **19,** 409–453 (2000).

119. Schaming, D. & Remita, H. Nanotechnology: from the ancient time to nowadays. *Found. Chem.* **17,** 187–205 (2015).

120. Reineke, J. *Nanotoxicity Methods and Protocols*. (Human Press, 2012). doi:10.1007/978-1-62703-002-1

121. Jain, P. K., Huang, X., El-Sayed, I. H. & El-Sayed, M. a. Noble metals on the nanoscale: optical and photothermal properties and some applications in imaging, sensing, biology, and medicine. *Acc. Chem. Res.* **41,** 1578–86 (2008).

122. Yang, Z., Kang, S. & Zhou, R. Nanomedicine: de novo design of nanodrugs. *Nanoscale* **6,**

663–77 (2014).

123. Huang, X., Neretina, S. & El-Sayed, M. a. Gold Nanorods: From Synthesis and Properties to Biological and Biomedical Applications. *Adv. Mater.* **21,** 4880–4910 (2009).

124. Huang, X., Ivan, H. E.-S. & El-Sayed, M. A. in *Cancer Nanotechnology* (eds. Grobmyer, S. R. & Moudgil, B. M.) **624,** 163–175 (Springer, 2010).

125. Zeng, S., Baillargeat, D., Ho, H.-P. & Yong, K.-T. Nanomaterials enhanced surface plasmon resonance for biological and chemical sensing applications. *Chem. Soc. Rev.* **43,** 3426–52 (2014).

126. Radwan, S. H. & Azzazy, H. M. E. Gold nanoparticles for molecular diagnostics. *Expert Rev. Mol. Diagn.* **9,** 511–524 (2009).

127. Sperling, R. A., Gil, P. R., Zhang, F., Zanella, M. & Parak, W. J. Biological applications of gold nanoparticles. *Chem. Soc. Rev.* **37,** 1909–30 (2008).

128. Bunz, U. H. F. & Rotello, V. M. Gold nanoparticle-fluorophore complexes: Sensitive and discerning 'noses' for biosystems sensing. *Angew. Chemie - Int. Ed.* **49,** 3268–3279 (2010).

129. Zayats, M., Baron, R., Popov, I. & Willner, I. Biocatalytic growth of Au nanoparticles: From mechanistic aspects to biosensors design. *Nano Lett.* **5,** 21–25 (2005).

130. Zhao, W., Brook, M. A. & Li, Y. Design of gold nanoparticle-based colorimetric biosensing assays. *ChemBioChem* **9,** 2363–2371 (2008).

131. Saha, K., Agasti, S. S., Kim, C., Li, X. & Rotello, V. M. Gold nanoparticles in chemical and biological sensing. *Chem. Rev.* **112,** 2739–79 (2012).

132. Verma, M. S., Rogowski, J. L., Jones, L. & Gu, F. X. Colorimetric biosensing of pathogens using gold nanoparticles. *Biotechnol. Adv.* **33,** 666–680 (2015).

133. Wu, W.-H. *et al.* Aptasensors for rapid detection of Escherichia coli O157:H7 and Salmonella typhimurium. *Nanoscale Res. Lett.* **7,** 658–665 (2012).

134. Liu, Y. *et al.* Colorimetric detection of influenza A virus using antibody-functionalized gold nanoparticles. *Analyst* **140,** 3989–3995 (2015).

135. Pandey, S. K., Suri, C. R., Chaudhry, M., Tiwari, R. P. & Rishi, P. A gold nanoparticles based immuno-bioprobe for detection of Vi capsular polysaccharide of Salmonella enterica serovar Typhi. *Mol. Biosyst.* **8,** 1853–60 (2012).

136. Sung, Y. J. *et al.* Novel antibody/gold nanoparticle/magnetic nanoparticle nanocomposites for immunomagnetic separation and rapid colorimetric detection of Staphylococcus aureus in milk. *Biosens. Bioelectron.* **43,** 432–439 (2013).

137. Paul, A. M. *et al.* Bioconjugated Gold Nanoparticle Based SERS Probe for Ultrasensitive Identification of Mosquito-Borne Viruses Using Raman Fingerprinting. *J. Phys. Chem. C* **119,** 23669–23675 (2015).

138. Li, X. X., Cao, C., Han, S. J. & Sim, S. J. Detection of pathogen based on the catalytic growth of gold nanocrystals. *Water Res.* **43,** 1425–1431 (2009).

139. Garner, A. L., Fullagar, J. L., Day, J. A., Cohen, S. M. & Janda, K. D. Development of a high-throughput screen and its use in the discovery of Streptococcus pneumoniae immunoglobulin A1 protease inhibitors. *J. Am. Chem. Soc.* **135,** 10014–10017 (2013).

140. Liu, R. *et al.* Metallic nanoparticles bioassay for Enterobacter cloacae P99 beta-lactamase activity and inhibitor screening. *Analyst* **135,** 1031–6 (2010).

141. Jiang, T. *et al.* Colorimetric screening of bacterial enzyme activity and inhibition based on the aggregation of gold nanoparticles. *Chem. Commun. (Camb).* 1972–1974 (2009). doi:10.1039/b818853j

142. Chan, W.-S., Tang, B. S. F., Boost, M. V, Chow, C. & Leung, P. H. M. Detection of methicillin-resistant Staphylococcus aureus using a gold nanoparticle-based colourimetric polymerase chain reaction assay. *Biosens. Bioelectron.* **53,** 105–11 (2014).

143. Deng, H. *et al.* Long genomic DNA amplicons adsorption onto unmodified gold nanoparticles for colorimetric detection of Bacillus anthracis. *Chem. Commun.* 51–53

(2012). doi:10.1039/c2cc37037a

144. Jung, C., Chung, J. W., Kim, U. O., Kim, M. H. & Park, H. G. Real-time colorimetric detection of target DNA using isothermal target and signaling probe amplification and gold nanoparticle cross-linking assay. *Biosens. Bioelectron.* **26,** 1953–1958 (2011).

145. Thaxton, C. S., Georganopoulou, D. G. & Mirkin, C. A. Gold nanoparticle probes for the detection of nucleic acid targets. *Clin. Chim. Acta* **363,** 120–126 (2006).

146. Kalidasan, K., Neo, J. L. & Uttamchandani, M. Direct visual detection of Salmonella genomic DNA using gold nanoparticles. *Mol. Biosyst.* **9,** 618–21 (2013).

147. Pylaev, T. E. *et al.* Colorimetric and dynamic light scattering detection of DNA sequences by using positively charged gold nanospheres: a comparative study with gold nanorods. *Nanotechnology* **22,** 1–11 (2011).

148. Mancuso, M., Jiang, L., Cesarman, E. & Erickson, D. Multiplexed colorimetric detection of Kaposi's sarcoma associated herpesvirus and Bartonella DNA using gold and silver nanoparticles. *Nanoscale* **5,** 1678–86 (2013).

149. Carter, J. R., Balaraman, V., Kucharski, C. a, Fraser, T. S. & Fraser, M. J. A novel dengue virus detection method that couples DNAzyme and gold nanoparticle approaches. *Virol. J.* **10,** 201 (2013).

150. Zagorovsky, K. & Chan, W. C. W. A Plasmonic DNAzyme Strategy for Point-of-Care Genetic Detection of Infectious Pathogens. *Angew. Chem. Int. Ed. Engl.* 1–5 (2013). doi:10.1002/anie.201208715

151. Xing, Y. *et al.* A colorimetric method for H1N1 DNA detection using rolling circle amplification. *Analyst* **138,** 3457–3462 (2013).

152. Veigas, B., Pedrosa, P., Couto, I., Viveiros, M. & Baptista, P. V. Isothermal DNA amplification coupled to Au- nanoprobes for detection of mutations associated to Rifampicin resistance in Mycobacterium tuberculosis. *J. Nanobiotechnology* 1–6 (2013).

153. Gill, P., Alvandi, A. H., Abdul-Tehrani, H. & Sadeghizadeh, M. Colorimetric detection of Helicobacter pylori DNA using isothermal helicase-dependent amplification and gold nanoparticle probes. *Diagn. Microbiol. Infect. Dis.* **62,** 119–124 (2008).

154. Piepenburg, O., Williams, C. H., Stemple, D. L. & Armes, N. A. DNA Detection Using Recombination Proteins. *PLoS Biol.* **4,** 1115–1121 (2006).

155. Mollasalehi, H. & Yazdanparast, R. Non-crosslinking gold nanoprobes for detection of nucleic acid sequence-based amplification products. *Anal. Biochem.* **425,** 91–95 (2012).

156. Nagatani, N. *et al.* Detection of influenza virus using a lateral flow immunoassay for amplified DNA by a microfluidic RT-PCR chip. *Analyst* **137,** 3422 (2012).

157. Niazi, A., Jorjani, O. N., Nikbakht, H. & Gill, P. A nanodiagnostic colorimetric assay for 18S rRNA of leishmania pathogens using nucleic acid sequence-based amplification and gold nanorods. *Mol. Diagnosis Ther.* **17,** 363–370 (2013).

158. Tang, J., Zhou, L., Gao, W., Cao, X. & Wang, Y. Visual DNA microarrays for simultaneous detection of human immunodeficiency virus type-1 and Treponema pallidum coupled with multiplex asymmetric polymerase chain reaction. *Diagn. Microbiol. Infect. Dis.* **65,** 372–378 (2009).

159. Veigas, B., Machado, D., Couto, I. & Viveiros, M. Au-nanoprobes for detection of SNPs associated with antibiotic resistance in Mycobacterium tuberculosis. *Nanotechnology* **21,** 1–7 (2010).

160. Cohen, M. L. Epidemiology of Drug Resistance : Implications for a Post-Antimicrobiai Era. *Science (80-.).* **257,** 1050–1055 (1992).

161. Mrozik, A. & Łabużek, S. Cytoplasmatic Bacterial Membrane Responses to Environmental Perturbations. *Polish J. Environ. Stud.* **13,** 487–494 (2004).

162. Habash, R. W. Y., Bansal, R., Krewski, D. & Alhafid, H. T. Thermal therapy, part 2: hyperthermia techniques. *Crit. Rev. Biomed. Eng.* **34,** 491–542 (2006).

163. Gou, Liangran *et al.* Combinatorial Photothermal and Immuno Cancer Therapy Using CHitosan-Coated Hollow Copper Sulfide Nanoparticles. *ACS Nano* **8,** 5670–5681 (2014).

164. Qin, Z. *et al.* Significantly improved analytical sensitivity of lateral flow immunoassays by using thermal contrast. *Angew. Chem. Int. Ed. Engl.* **51,** 4358–61 (2012).

165. Yang, J. *et al.* Spatially confined fabrication of core-shell gold nanocages@Mesoporous silica for near-infrared controlled photothermal drug release. *Chem. Mater.* **25,** 3030–3037 (2013).

166. Dickerson, E. B. *et al.* Gold nanorod assisted near-infrared plasmonic photothermal therapy (PPTT) of squamous cell carcinoma in mice. *Cancer Lett.* **269,** 57–66 (2008).

167. Dreaden, E. C., Mackey, M. a, Huang, X., Kang, B. & El-Sayed, M. a. Beating cancer in multiple ways using nanogold. *Chem. Soc. Rev.* **40,** 3391–404 (2011).

168. Norman, R. S., Stone, J. W., Gole, A., Murphy, C. J. & Sabo-attwood, T. L. Targeted Photothermal Lysis of the Pathogenic Bacteria , Pseudomonas aeruginosa , with Gold Nanorods. *Nano Lett.* **8,** 302–306 (2008).

169. Kuo, W.-S., Chang, C.-N., Chang, Y.-T. & Yeh, C.-S. Antimicrobial gold nanorods with dual-modality photodynamic inactivation and hyperthermia. *Chem. Commun. (Camb).* 4853–5 (2009). doi:10.1039/b907274h

170. Khan, S. A., Singh, A. K., Senapati, D., Fan, Z. & Ray, P. C. Bio-conjugated popcorn shaped gold nanoparticles for targeted photothermal killing of multiple drug resistant Salmonella DT104. *J. Mater. Chem.* **21,** 17705 (2011).

171. Zhu, Y., Ramasamy, M. & Yi, D. K. Antibacterial Activity of Ordered Gold Nanorod Arrays. *ACS Appl. Mater. Interfaces* **6,** 15078–15085 (2014).

172. Castillo-martínez, J. C. *et al.* Antibacterial and Antibiofilm Activities of the Photothermal Therapy Using Gold Nanorods against Seven Different Bacterial Strains. *J. Nanomater.* **2015,** 1–7 (2015).

173. Kim, C.-B., Yi, D. K., Kim, P. S. S., Lee, W. & Kim, M. J. Rapid photothermal lysis of the pathogenic bacteria, Escherichia coli using synthesis of gold nanorods. *J. Nanosci. Nanotechnol.* **9,** 2841–5 (2009).

174. Zharov, V. P., Mercer, K. E., Galitovskaya, E. N. & Smeltzer, M. S. Photothermal nanotherapeutics and nanodiagnostics for selective killing of bacteria targeted with gold nanoparticles. *Biophys. J.* **90,** 619–27 (2006).

175. Mabey, D., Peeling, R. W., Ustianowski, A. & Perkins, M. D. Tropical infectious diseases: Diagnostics for the developing world. *Nat. Rev. Microbiol.* **2,** 231–240 (2004).

176. Drain, P. K. *et al.* Diagnostic point-of-care tests in resource-limited settings. *Lancet Infect. Dis.* **14,** 239–249 (2014).

177. Kim, J., Biondi, M. J., Feld, J. J. & Chan, W. C. W. Clinical Validation of Quantum Dot Barcode Diagnostic Technology. *ACS Nano* **10,** 4742–4753 (2016).

178. Hill, H. D., Vega, R. a & Mirkin, C. a. Nonenzymatic Detection of Bacterial Genomic DNA Using the Bio Bar Code Assay DNA . These blockers bind to specific regions of the target rehybridizing , which allows the particle probes to bind . *Anal. Chem.* **79,** 9218–9223 (2007).

179. Daher, R. K., Stewart, G., Boissinot, M., Boudreau, D. K. & Bergeron, M. G. Influence of sequence mismatches on the specificity of recombinase polymerase amplification technology. *Mol. Cell. Probes* **29,** 116–121 (2015).

180. Chan, W. C. W. *et al.* Patients, Here Comes More Nanotechnology. *ACS Nano* **10,** 8139–8142 (2016).

181. Borysiak, M. D. *et al.* Translating diagnostic assays from the laboratory to the clinic: analytical and clinical metrics for device development and evaluation. *Lab Chip* **16,** 1293–1313 (2016).

182. Abd El Wahed, A. *et al.* Recombinase Polymerase Amplification Assay for Rapid Diagnostics of Dengue Infection. *PLoS One* 1–17 (2015).

doi:10.1371/journal.pone.0129682

183. Rouer, E. Direct neutralization of alkaline-denatured plasmid DNA in sequencing protocol by the sequencing reagent itself. *Nucleic Acids Res.* **22,** 4844 (1994).

184. Ma, M., Wang, H., Yu, Y., Zhang, D. & Liu, S. Detection of antimicrobial resistance genes of pathogenic Salmonella from swine with DNA microarray. *J. Vet. Diagnostic Investig.* **167,** 161–167 (2007).

185. Maynard, C. *et al.* Antimicrobial resistance genes in enterotoxigenic Escherichia coli O149:K91 isolates obtained over a 23-year period from pigs. *Antimicrob. Agents Chemother.* **47,** 3214–21 (2003).

186. Xu, J. *et al.* Phenotypic and Genotypic Antimicrobial Resistance Traits of Foodborne Staphylococcus aureus Isolates from Shanghai. *J. Food Sci.* **79,** 635–642 (2014).

187. Haveri, M., Suominen, S., Rantala, L. & Pyo, S. Comparison of phenotypic and genotypic detection of penicillin G resistance of Staphylococcus aureus isolated from bovine intramammary infection. *Vet. Microbiol.* **106,** 97–102 (2005).

188. Allen, H. & Donato, J. Call of the wild: antibiotic resistance genes in natural environments. *Nat. Rev. …* **8,** 251–259 (2010).

189. Sabath, L. D. Mechanisms of resistance to beta-lactam antibiotics in strains of Staphylococcus aureus. *Ann.Intern.Med.* **97,** 339–344 (1982).

190. Veigas, B., Fernandes, A. R., Baptista, P. V, Dutta, N. K. & Hopkins, J. AuNPs for identification of molecular signatures of resistance. *Front. Microbiol.* **5,** 1–11 (2014).

191. Storhoff, J. J., Lucas, A. D., Garimella, V., Bao, Y. P. & Müller, U. R. Homogeneous detection of unamplified genomic DNA sequences based on colorimetric scatter of gold nanoparticle probes. *Nat. Biotechnol.* **22,** 883–887 (2004).

192. Ramesh, Ramakrishnan Wesley, B. *et al.* Sensitive Assay for Identification of Methicillin-Resis- tant Staphylococcus aureus, Based on Direct Detection of Genomic DNA by Use of

Gold Nanoparticle Probes. *Clin. Chem.* **50,** 1949–1952 (2004).

193. Valiadi, M. *et al.* Simple and rapid sample preparation system for the molecular detection of antibiotic resistant pathogens in human urine. *Biomed. Microdevices* **18,** 1–10 (2016).

194. Keays, M. C., O'Brien, M., Hussain, A., Kiely, P. A. & Dalton, T. Rapid Identification of Antibiotic Resistance Using Droplet Microfluidics. *Bioengineered* **7,** 79–87 (2016).

195. Fridkin, S. K. *et al.* Methicillin-Resistant Staphylococcus aureus Disease in Three Communities. *new Engl. J. o f Med.* **352,** 1436–1444 (2005).

196. Conly, J. M. & Johnston, B. L. The emergence of methicillin-resistant Staphylococcus aureus as a community-acquired pathogen in Canada. *Can. J. Infect. Dis.* **14,** 249–51 (2003).

197. Enright, M. C. *et al.* The evolutionary history of methicillin-resistant Staphylococcus aureus (MRSA). *Proc. Natl. Acad. Sci. U. S. A.* **99,** 7687–92 (2002).

198. Hiramatsu, K., Cui, L., Kuroda, M. & Ito, T. The emergence and evolution of methicillin-resistant Staphylococcus aureus. *Trends Microbiol.* **9,** 486–493 (2001).

199. Asghar, A. Molecular characterization of methicillin-resistant Staphylococcus aureus isolated from tertiary care hospitals. *Pakistan J. Med. Sci.* **30,** 698–702 (2014).

200. Elhassan, M. M., Ozbak, H. A., Hemeg, H. A., Elmekki, M. A. & Ahmed, L. M. Absence of the mec A Gene in Methicillin Resistant Staphylococcus aureus Isolated from Different Clinical Specimens in Shendi City , Sudan. *Biomed. Res. Int.* **2015,** 1–5 (2015).

201. Martineau, F. *et al.* Correlation between the Resistance Genotype Determined by Multiplex PCR Assays and the Antibiotic Susceptibility Patterns of Staphylococcus aureus and Staphylococcus epidermidis. *Antimicrob. Agents Chemother.* **44,** 231–238 (2000).

202. Sajith, K. A., Shetty, P. J., Lakshmi, S. Y., Chidambaram, A. & Ranganathan, R. Detection of mecA genes of Methicillin-Resistant Staphylococcus aureus by Polymerase Chain Reaction. **1,** 64–68 (2012).

203. Petinaki, E., Arvaniti, A., Dimitracopoulos, G. & Spiliopoulou, I. Detection of mecA , mecR1 and mecI genes among clinical isolates of methicillin-resistant staphylococci by combined polymerase chain reactions. *J. Antimicrob. Chemother.* **47,** 297–304 (2001).

204. Duran, N., Ozer, B., Duran, G. G., Onlen, Y. & Demir, C. Antibiotic resistance genes & susceptibility patterns in staphylococci. *Indian J. od Med. Res.* **135,** 389–396 (2012).

205. Pereira, L. A., Harnett, G. B., Hodge, M. M., Cattell, J. A. & Speers, J. Real-Time PCR Assay for Detection of blaZ Genes in Staphylococcus aureus Clinical Isolates. *J. Clin. Microbiol.* **52,** 1259–1261 (2014).

206. Richter, S. S. *et al.* Detection and Prevalence of Penicillin-Susceptible Staphylococcus aureus in the United States in 2013. *J. Clin. Microbiol.* **54,** 812–814 (2016).

207. Yang, F. *et al.* Prevalence of blaZ gene and other virulence genes in penicillin-resistant Staphylococcus aureus isolated from bovine mastitis cases in Gansu , China. *Turkish J. Vet. Anim. Sci.* **39,** 634–636 (2015).

208. Saadat, S., Solhjoo, K. & Kazemi, A. VanA and VanB Positive Vancomycin-resistant Staphylococcus aureus Among Clinical Isolates in Shiraz, South of Iran. *Oman Med. J.* **29,** 335–339 (2014).

209. Thati, V., Shivannavar, C. T. & Gaddad, S. M. Vancomycin resistance among methicillin resistant Staphylococcus aureus isolates from intensive care units of tertiary care hospitals in Hyderabad. *Indian J Med.Res.* **134,** 704–708 (2011).

210. Okolie, C. E., Cockayne, A., Wooldridge, K. & James, R. Development and validation of a new diagnostic PCR assay for vanA gene encoding vancomycin resistance in Staphylococcus aureus. *Int. J. Appl. Microbiol. Biotechnol. Res.* **2,** 1–10 (2014).

211. Emaneini, M. *et al.* Distribution of genes encoding tetracycline resistance and aminoglycoside modifying enzymes in Staphylococcus aureus strains isolated from a burn center. *Ann. Burns Fire Disasters* **26,** 76–80 (2013).

212. Schmitz, F.-J. *et al.* Resistance to tetracycline and distribution of tetracycline resistance

genes in European Staphylococcus aureus isolates. *J Antimicrob Chemother* **47,** 239–240 (2001).

213. Sekiguchi, J. *et al.* Spread of Erythromycin- , Tetracycline- , and Aminoglycoside-Resistant Genes in Methicillin-Resistant Staphylococcus aureus Clinical Isolates in a Kumamoto Hospital. *Jpn. J. Infect. Dis.* **56,** 133–137 (2003).

214. Ullah, F. *et al.* Investigation of the Genetic Basis of Tetracycline Resistance in Staphylococcus aureus from Pakistan. *Trop. J. Pharm. Res.* **11,** 925–931 (2012).

215. Schmitz, F., Fluit, A. C., Gondolf, M., Beyrau, R. & Lindenlauf, E. The prevalence of aminoglycoside resistance and corresponding resistance genes in clinical isolates of staphylococci from 19 European hospitals. 253–259 (1999).

216. Westh, H., Hougaard, D. M., Vuust, J. & Rosdahl, V. T. Prevalence of erm gene classes in erythromycin-resistant Staphylococcus aureus strains isolated between 1959 and 1988. *Antimicrob. Agents Chemother.* **39,** 369–373 (1995).

217. Khan, S., Nawaz, M., Khan, A. & Cerniglia, C. Simultaneous detection of erythromycin-resistant methylase genes ermA and ermC from Staphylococcus spp . by multiplex-PCR. *Mol. Cell. Probes* **13,** 381–387 (1999).

218. Schmitz, F. *et al.* Prevalence of macrolide-resistance genes in Staphylococcus aureus and Enterococcus faecium isolates from 24 European university hospitals. *J. Antimicrob. Chemother.* **45,** 891–894 (2000).

219. Lim, J.-A. *et al.* Prevalence of resistance to macrolide, lincosamide and streptogramin antibiotics in Gram-positive cocci isolated in a Korean hospital. *J. Antimicrob. Chemother.* **49,** 489–495 (2002).

220. Thati, V., Shivannavar, C. T. & Gaddad, S. M. Vancomycin resistance among methicillin resistant Staphylococcus aureus isolates from intensive care units of tertiary care hospitals in Hyderabad. 704–708 (2011).

221. Zagorovsky, K. & Chan, W. C. W. A plasmonic DNAzyme strategy for point-of-care

genetic detection of infectious pathogens. *Angew. Chemie - Int. Ed.* **52,** 3168–3171 (2013).

222. Ibrahim, E. H., Sherman, G., Ward, S., Fraser, V. J. & Kollef, M. H. The influence of inadequate antimicrobial treatment of bloodstream infections on patient outcomes in the ICU setting. *Chest* **118,** 146–155 (2000).

223. Kollef, M. H., Sherman, G., Ward, S. & Fraser, V. J. Inadequate Antimicrobial Treatment of Infections *. *Chest* **115,** 462–474 (1999).

224. Suaya, J. A. *et al.* Incidence and cost of hospitalizations associated with Staphylococcus aureus skin and soft tissue infections in the United States from 2001 through 2009. *BMC Infect. Dis.* **14,** 1–8 (2014).

225. Suaya, J. A., Eisenberg, D. F., Fang, C. & Miller, L. G. Skin and Soft Tissue Infections and Associated Complications among Commercially Insured Patients Aged 0 – 64 Years with and without Diabetes in the U . S . *PLoS One* **8,** 1–8 (2013).

226. Wu, M., Deokar, A. R., Liao, J., Shih, P. & Ling, Y. Graphene-Based Photothermal Agent for Rapid and E ff ective Killing of. *ACS Nano* **7,** 1281–1290 (2013).

227. Robinson, J. T. *et al.* Ultrasmall reduced graphene oxide with high near-infrared absorbance for photothermal therapy. *J. Am. Chem. Soc.* **133,** 6825–6831 (2011).

228. Pu, K. *et al.* Semiconducting polymer nanoparticles as photoacoustic molecular imaging probes in living mice. *Nat. Nanotechnol.* **9,** 233–9 (2014).

229. Qin, Z. & Bischof, J. C. Thermophysical and biological responses of gold nanoparticle laser heating. *Chem. Soc. Rev.* **41,** 1191–217 (2012).

230. Bagley, A. F., Hill, S., Rogers, G. S. & Bhatia, S. N. Plasmonic Photothermal Heating of Intraperitoneal Tumors through the Use of an Implanted Near-Infrared Source. *ACS Nano* **7,** 8089–8097 (2013).

231. Cheng, F.-Y., Chen, C.-T. & Yeh, C.-S. Comparative efficiencies of photothermal

destruction of malignant cells using antibody-coated silica@Au nanoshells, hollow Au/Ag nanospheres and Au nanorods. *Nanotechnology* **20,** 425104 (2009).

232. You, J.-O., Guo, P. & Auguste, D. T. A drug-delivery vehicle combining the targeting and thermal ablation of HER2+ breast-cancer cells with triggered drug release. *Angew. Chem. Int. Ed. Engl.* **52,** 4141–6 (2013).

233. Vihola, H., Laukkanen, A., Valtola, L., Tenhu, H. & Hirvonen, J. Cytotoxicity of thermosensitive polymers poly(N-isopropylacrylamide), poly(N-vinylcaprolactam) and amphiphilically modified poly(N-vinylcaprolactam). *Biomaterials* **26,** 3055–64 (2005).

234. Nikoobakht, B. & El-sayed, M. A. Preparation and Growth Mechanism of Gold Nanorods (NRs) Using Seed-Mediated Growth Method. *Chem. Mater.* 1957–1962 (2003).

235. Gole, A. & Murphy, C. J. Seed-Mediated Synthesis of Gold Nanorods : Role of the Size and Nature of the Seed. *Chem. Mater.* **16,** 3633–3640 (2004).

236. Dorsett-Martin, W. a. & Wysocki, A. B. in *Sourcebook of Models for Biomedical Research* 631–638 (2008). doi:10.1007/978-1-59745-285-4

237. Dorsett-Martin, W. A. Rat Models of Skin Wound Healing: Areview. *Wound Repair Regen.* **12,** 591–599 (2004).

238. Dunn, L. *et al.* Murine model of wound healing. *J. Vis. Exp.* e50265 (2013). doi:10.3791/50265

239. Wang, X., Ge, J., Tredget, E. E. & Wu, Y. The mouse excisional wound splinting model, including applications for stem cell transplantation. *Nat. Protoc.* **8,** 302–9 (2013).

240. Alkilany, A. M. *et al.* Cellular uptake and cytotoxicity of gold nanorods: molecular origin of cytotoxicity and surface effects. *Small* **5,** 701–8 (2009).

241. Grabinski, C. *et al.* Effect of gold nanorod surface chemistry on cellular response. *ACS Nano* **5,** 2870–9 (2011).

242. Qiu, Y. & Park, K. Environment-sensitive hydrogels for drug delivery. *Adv. Drug Deliv.*

Rev. **64,** 49–60 (2012).

243. Lucier, R. D. I Guess If I Really Wanted to Measure Surface Temperature , I Would Just Use a Thermocouple : Understanding the Challenges of Surface Temperature Measurements. *InfraMation 2011 Proc.* 1–12 (2011).

244. World Health Organization. Prevention of hospital-acquired infections. World Health Organization. Prevention of hospital-acquired infections. *WHO/CDC/EPH/2002.12* (2002).

245. Katsui, N. *et al.* Heat-induced blebbing and vesiculation of the outer membrane of Escherichia coli. *J. Bacteriol.* **151,** 1523–31 (1982).

246. Sykes, E. a., Dai, Q., Tsoi, K. M., Hwang, D. M. & Chan, W. C. W. Nanoparticle exposure in animals can be visualized in the skin and analysed via skin biopsy. *Nat. Commun.* **5,** 1–8 (2014).

247. Hamblin, M. R., O'Donnell, D. A., Murthy, N., Contag, C. H. & Hasan, T. Rapid control of wound infections by targeted photodynamic therapy monitored by in vivo bioluminescence imaging. *Photochem. Photobiol.* **75,** 51–57 (2002).

248. Monafo, W. W. & Freedman, B. Topical therapy for burns. *Surg. Clin. North Am.* **67,** 133–145 (1987).

249. Holder, I. A. & Boyce, S. T. Assessment of the potential for microbial resistance to topical use of multiple antimicrobial agents. *Wound Repair Regen.* **7,** 238–243 (1999).

250. Coombs, C. J. *et al.* Do burn patients have a silver lining? *Burns* **18,** 179–184 (1992).

251. Leitch, I. O., Kucukcelebi, A. & Robson, M. C. Inhibition of wound contraction by topical antimicrobials. *Aust. N. Z. J. Surg.* **63,** 289–293 (1993).

252. McHugh, G. L., Moellering, R. C., Hopkins, C. C. & Swartz, M. N. Salmonella typhimurium resistant to silver nitrate, chloramphenicol, and ampicillin. *Lancet* **1,** 235–240 (1975).

253. Bridges, K., Kidson, A., Lowbury, E. J. & Wilkins, M. D. Gentamicin- and silver-resistant pseudomonas in a burns unit. *Br. Med. J.* **1,** 446–449 (1979).

254. Hendry, A. T. & Stewart, I. O. Silver-resistant Enterobacteriaceae from hospital patients. *Can. J. Microbiol.* **25,** 915–921 (1979).

255. Herruzo-Cabrera, R., Garcia-Torres, V., Rey-Calero, J. & Vizcaino-Alcaide, M. J. Evaluation of the penetration strength, bactericidal efficacy and spectrum of action of several antimicrobial creams against isolated microorganisms in a burn centre. *Burns* **18,** 39–44 (1992).

256. Patel, J. B., Gorwitz, R. J. & Jernigan, J. a. Mupirocin resistance. *Clin. Infect. Dis.* **49,** 935–41 (2009).

257. Simor, A. E. *et al.* Mupirocin-resistant, methicillin-resistant Staphylococcus aureus strains in Canadian hospitals. *Antimicrob. Agents Chemother.* **51,** 3880–6 (2007).

258. Gao, J., Shimada, N. & Maruyama, A. MNAzyme-catalyzed nucleic acid detection enhanced by a cationic copolymer. *Biomater. Sci.* **3,** 716–720 (2015).

259. Saito, K., Shimada, N. & Maruyama, A. Cooperative enhancement of deoxyribozyme activity by chemical modification and added cationic copolymer. *Sci. Technol. Adv. Mater.* **17,** 437–442 (2016).

260. EBELING, W. *et al.* Proteinase K from Tritirachium album Limber. *Eur. J. Biochem.* **47,** 91–97 (1974).

261. Bartholomeusz, A. & Schaefer, S. Hepatitis B virus genotypes: Comparison of genotyping methods. *Rev. Med. Virol.* **14,** 3–16 (2004).

262. Fluit, A. D. C., Visser, M. R. & Schmitz, F. Molecular Detection of Antimicrobial Resistance. *Clin. Microbiol. Rev.* **14,** 836–871 (2001).

263. Blair, J. M. A., Webber, M. A., Baylay, A. J., Ogbolu, D. O. & Piddock, L. J. V. Molecular mechanisms of antibiotic resistance. *Nat. Rev. Microbiol.* **13,** 42–51 (2014).

264. Mokany, E., Bone, S. M., Young, P. E., Doan, T. B. & Todd, A. V. MNAzymes, a versatile new class of nucleic acid enzymes that can function as biosensors and molecular switches. *J. Am. Chem. Soc.* **132,** 1051–1059 (2010).

265. Abrigo, M., Kingshott, P. & McArthur, S. L. Electrospun polystyrene fiber diameter influencing bacterial attachment, proliferation, and growth. *ACS Appl. Mater. Interfaces* **7,** 7644–7652 (2015).

266. Zahedi, P., Rezaeian, I., Ranaei-Siadat, S. O., Jafari, S. H. & Supaphol, P. A review on wound dressings with an emphasis on electrospun nanofibrous polymeric bandages. *Polym. Adv. Technol.* **21,** 77–95 (2010).

267. Abrigo, M., McArthur, S. L. & Kingshott, P. Electrospun nanofibers as dressings for chronic wound care: Advances, challenges, and future prospects. *Macromol. Biosci.* **14,** 772–792 (2014).

268. Raeesi, V. Photo-thermal nanosystems for diseased cell treatment. *PhD thesis, Univ. Toronto* (2016).